JSTR
ASEAN Journal of Scientific and Technological Reports
Vol. 26 No. 1, January - March 2023

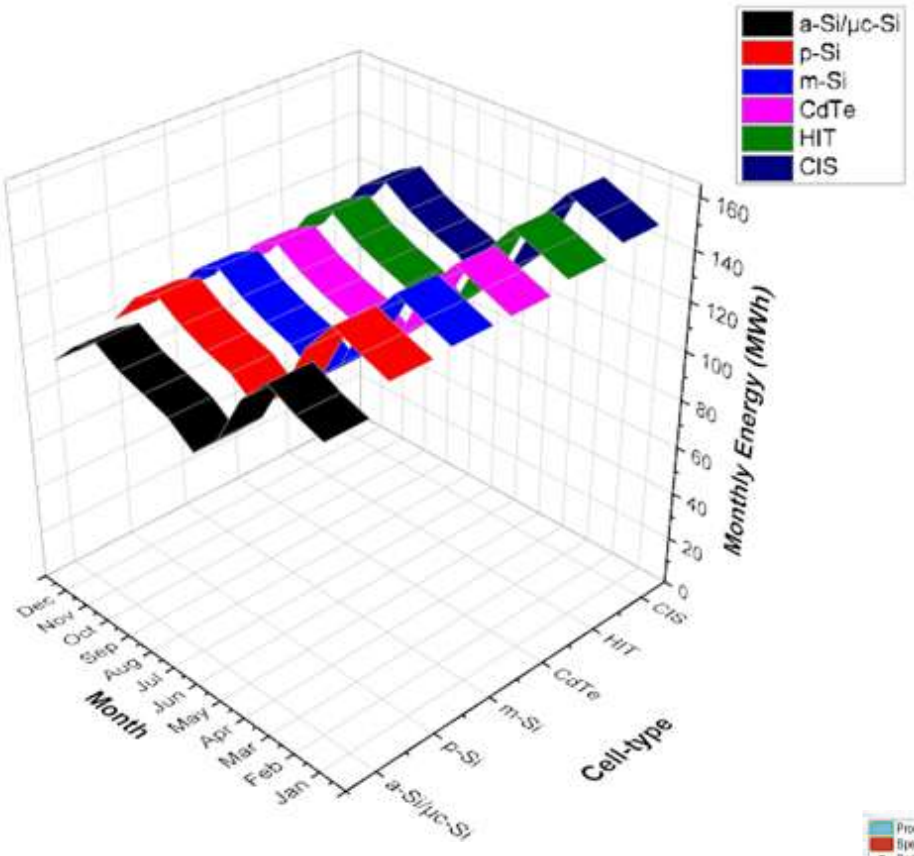

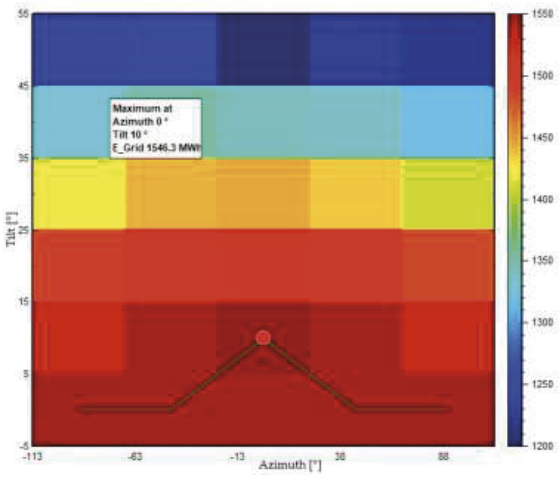

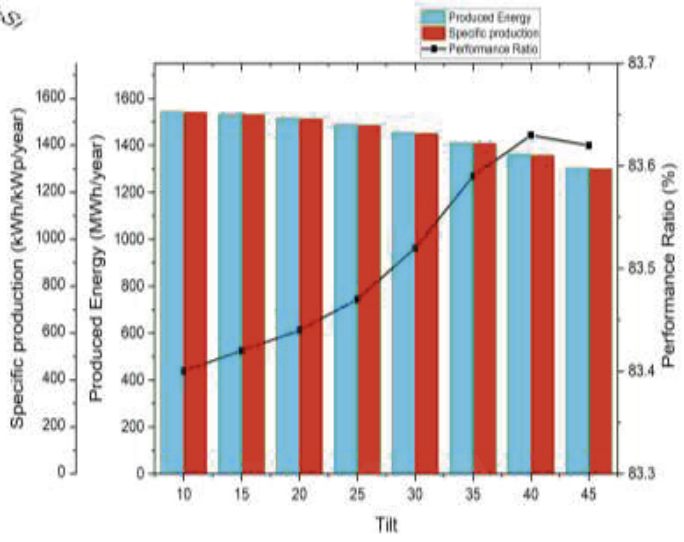

ISSN 2773-8752 (online)
https://ph02.tci-thaijo.org/index.php/tsujournal/issue/view/16949

ASEAN Journal of Scientific and Technological Reports (AJSTR)

Contact Us Research and Development Institute Thaksin University
222 M. 2 Ban-Prao sub-district, Pa-Pra-Yom district, Phatthalung province, Thailand
Tel. 0 7460 9600 # 7242 , E-mail: aseanjstr@tsu.ac.th

Editorial

The ASEAN Journal of Scientific and Technological Reports (AJSTR) Vol. 26 No. 1 (January-March 2023) ISSN 2773-8752 Published 8 worth-reading research articles. Experts from various universities and institutions reviewed and answered these exciting research articles. We sincerely hope some research papers will help guide and motivate our active researchers in ASEAN to produce and create more valuable research shortly. The AJSTR has served our energetic readers and customers on an international level.

This issue details the energy and char from Thailand biomass by gasification, yeast-Fermented Acacia mangium Leaf as a feed for Japanese Quails, the strategies to grow chilies with a high yield of capsaicin, frequency analysis of high amplitude δ scuti star V593 Lyr, the convective heat transfer of an alternating cross-section flattened tube with different twist angles, properties of biochar from coconut waste and application in agriculture, a techno-economic assessment of solar PV rooftop system applied in Thailand, and the effect of nutrients on pre-harvest periods and quality in hydroponic lettuce.

The AJSTR and an editorial team are ready to organize, manage, publish, and deliver all good quality articles written in well-organized English to the world of academic society.

Assoc. Prof. Dr. Sompong
O-Thong
Journal Editor-in-Chief

List of Contents

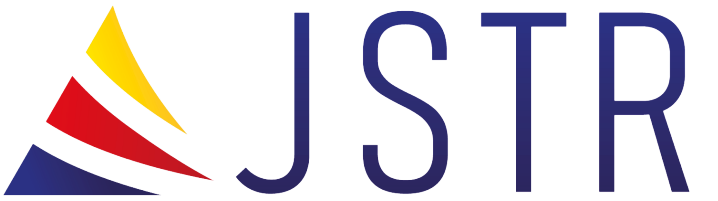

ASEAN Journal of Scientific and Technological Reports

JSTR
ASEAN Journal of Scientific and Technological Reports

Research article

Preliminary Experimental of Biomass Gasification Process with Open Core Throat Less Downdraft Gasifier

Woranuch Jangsawang[1*]

[1] Department of Energy Engineering, Faculty of Industrial Technology, Phranakhon Rajabhat University, Bangkok, 10220, Thailand
* Correspondence: Email: woranuch@pnru.ac.th

Citation:
Jangsawang, W.; Preliminary Experimental of Biomass Gasification Process with Open Core Throat Less Downdraft Gasifier. *ASEAN J. Sci. Tech. Report.* **2023**, *26*(1), 1-10. https://doi.org/10.55164/ajstr.v26i1.247166.

Article history:
Received: August 1, 2022
Revised: December 29, 2022
Accepted: January 20, 2023
Available online: March 9, 2023

Publisher'sNote:
This article is published and distributed under the terms of the Thaksin University.

Abstract: Gasification has been considered a promising approach to converting biomass into useful gaseous products. Downdraft gasifiers are famous for engine applications and used for thermal applications. The product gas has to meet the individual requirements of different end users or applications. The downdraft gasifier based on open core throat less design has been developed according to its suitability for small-sized biomass. The preliminary experiment investigated gasifying characteristics by studying the temperature distribution within the gasifier. This study used three kinds of biomass: Eucalyptus wood chip, Mimosa wood twig, and wood pellet. The results showed that the temperature distribution within the gasifier for each zone corresponds with the character of the gasifying process within the downdraft gasifier. Moreover, the temperature profiles for a gasifying process for all three biomass tests were in the same pattern. The maximum temperature was in the combustion zone (T_3). The maximum temperature at the combustion zone for the Eucalyptus wood chip is the highest compared with the maximum temperature at the combustion zone of the Mimosa wood twig and wood pellet. The temperature at the combustion zone (T_3) of the Eucalyptus wood chip, Mimosa wood twig, and the wood pellet were 838, 783, and 620 °C, respectively. The temperature at the combustion zone results in the temperature at the reduction zone. The average temperature at the reduction zone for gasifying all three biomass feeds ranges from 470-514 °C. While the temperature at the pyrolysis zone and the gas exit are not significantly different for all three biomass feeds. These results showed that the reaction within the gasifier could carry out continuously with a suitable temperature in each zone as per the design.

Keywords: Gasification; Open Core Throat Less; Downdraft; Preliminary Experimental; Temperature Distribution.

1. Introduction

Biomass is one of the most potent organic materials on the earth, produced by photosynthesis reaction in green plants in the presence of sunlight. It stores solar energy in its chemical bond as chemical energy [1], which can be further evolved by breaking down the bonds [2]. However, the bulky and inconvenient form of biomass is a major barrier to its wide applications. This motivates the conversion of solid biomass into liquid and the conversion process [3]. Thermochemical conversion, including combustion, gasification, and pyrolysis, can break down the chemical bond in biomass to release the stored energy. Combustion can directly release energy by the primary bond breaking of biomass. At the same time, gasification and

pyrolysis can transfer the energy into secondary products, which are likely ideal for fueling the furnace and the engine [4]. Gasification is one of the thermochemical conversion processes that has been considered a promising approach to converting biomass into useful gaseous products. Based on the advantages of energy efficiency and ease of application, gasification is the best choice for exploding energy from biomass [5]. The biomass gasification process converts biomass into producer gas consisting of methane, hydrogen, carbon monoxide, carbon dioxide, nitrogen, and other minor components. Although gasification technologies have been developed over a century, their commercial successes on a large scale are still limited [6]. A biomass gasification plant's economic and technological successes depend on the trouble-free operation of all system components over long periods [3]. The key success factors for the gasification process depend on several factors, such as fuel properties, gasifier design, operation, and gas cleaning. The main biomass property was considered an energy source, such as moisture content, calorific value, fixed carbon and volatiles proportions, ash content, alkali metal content, and cellulose/lignin ratio [7]. Gasification and combustion are closely related to thermochemical processes but have an important difference. Gasification packs energy into chemical bonds in the product gas; combustion breaks those bonds to release the energy. The gasification process adds hydrogen to and strips carbon away from the hydrocarbon feedstock to produce gases with a higher hydrogen-to-carbon ratio. At the same time, combustion oxidizes the hydrogen and carbon into the water and carbon dioxide, respectively. A typical biomass gasification process may include the following steps: drying, thermal decomposition or pyrolysis, partial combustion of some gases, vapors, and char, and gasification of decomposed products. Gasification requires a gasifying medium such as air, oxygen, or steam to rearrange the molecular structure of the feedstock to convert the solid feedstock into gases or liquids. Biomass is first heated (dried) and then undergoes thermal degradation or pyrolysis. The pyrolysis products (i.e., gas, solid, and liquid) react among themselves and with the gasifying medium to form the final gasification product. The thermal energy necessary for drying, pyrolysis, and endothermic reactions comes from a certain amount of exothermic combustion reactions allowed in the gasifier. Gasifiers are classified mainly based on their gas-solid contacting mode and gasifying medium. Based on the gas-solid contacting mode, gasifiers are divided into three principal types: fixed bed, fluidized bed, and entrained flow bed. There is an appropriate range of applications for each: the fixed bed type is used for smaller units (< 10 MW_{th}); the fluidized bed type is more appropriate for intermediate units (5-100 MW_{th}); entrained flow reactors are used for large capacity units (> 50 MW_{th}) [8]. The fixed bed gasifier has been the traditional process used for gasification, operated at temperatures around 1000 degree Celsius. Depending on the airflow direction, the fixed bed gasifiers are classified as updraft, downdraft, or cross draft [9]. Downdraft gasifiers are characterized by a co-current air or gas and fuel flow. In downdraft, with or without a throat gasifier, tar and other products off pyrolysis pass through the high-temperature oxidation zone of the reactor, where they are subsequently burnt or cracked. Thus, the producer gas from a downdraft gasifier contains very less tar (less than 1 % [10]. Therefore, downdraft gasifiers are also popular for engine applications and thermal applications. However, these gasifiers are highly fuel specific [11-14]. There are various methods for using producer gas produced from the gasification process. However, the product gas has to meet the individual requirements of different end users or applications. The end use of the gas determines the degree of clean-up required and can be achieved by either hot or cold gas cleaning. The benefit of hot gas cleaning is that more energy is gained from the gas. Still, the process poses significant technical simpler and produces wastewater contaminated with tar, likely posing a disposal problem [10]. Applying the product gas directly through the combustion process to produce heat for cooking or drying generally does not use a gas cleaning system. However, using a gasifier with no gas cleaning system for cooking if it still has tar or particulate in the product gas makes the pot dirty with the suit and causes a barrier for using a gasifier. Thus, primary treatments such as optimizing biomass feedstock properties and designing and operating the gasifier [15] are first implemented to remove unwanted products and contaminants in the product gas. Secondary treatments, such as a downstream cleaning system based on physical (scrubber, filters) or catalytic strategies, must be incorporated for end applications and environmental regulations [16]. Although mostly, the gasifier sizing will be designed based on suggestion information from the previous inventors. Thus, the new gasifiers that have been developed need to

investigate the results based on the references from the theoretical review before using gasifiers. Thus, this paper aims to investigate the temperature distribution within the gasifier to confirm that the reaction within the gasifier can carry out continuously with a suitable temperature in each zone.

2. Materials and Methods

2.1 Downdraft Gasifier

The Gasifier system developed and presented in this paper was designed based on the downdraft gasification process. The design and calculation of the gasifier have followed the design methodology for sizing the Imbert-type downdraft gasifier. The Imbert gasifier is the most used type of downdraft gasifier. The downdraft gasifier based on open core throat less design has been developed according to its suitability for small-sized biomass [17-19]. The main objective of developing this gasifier is to produce the producer gas that is cleaner for cooking applications to solve the disadvantage of using producer gas for cooking the particle or soot attached to the pot. The gas cleaning system, in conjunction with the gasifier, was developed. Thus, the gasifier system has been developed and comprises three main parts; gasifier, gas cleaning system, and cooking gas stove.

The gasifier was designed based on an open core throat less downdraft gasifier with biomass fuel feeding in batches. The maximum biomass fuel consumption rate is 15 kg/hr. Based on the function of each part within the gasifier, the gasifier can divide into three parts: fuel hopper, reaction chamber, and ash pit. The fuel hopper contains and fills biomass fuel; it lies at the top of the gasifier. The maximum fuel loading is about 15 kg/batch. The reaction chamber was designed with a diameter of 234 millimeters and an inner height of 356 millimeters. The reaction chamber was fabricated with 2 millimeter-thick steel plate. The ash pit is the part for collecting the ash from the reaction process within the reaction chamber. A pictorial drawing of an open core throat less downdraft gasifier showed in Figure 1.

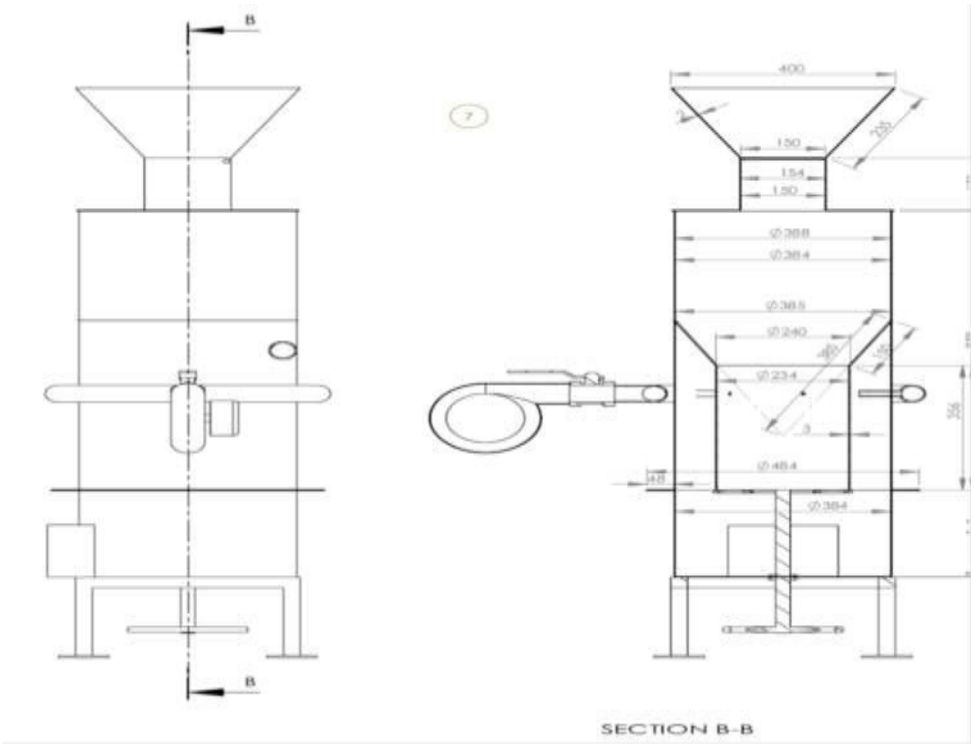

Figure 1. Open core throat less downdraft gasifier

A gas cleaning system has been developed to clean the producer gas produced from gasification. The main objective of developing the open core throat less gasifier is to use it for cooking applications. Thus the

gas cleaning equipment will be suitable for eliminating particles and tar in the producer gas. The producer gas will pass through four steps of the gas cleaning equipment in series. Four gas cleaning steps comprise cyclone, venturi scrubber, coarse bag house filter, and fine bag house filter. The producer gas from the gasifier will pass through the cyclone to separate the solid particle from the gaseous stream by vortex separation. After the gaseous stream passes through the cyclone, it will pass through the venturi scrubber to separate the tar and particles from the gaseous stream and reduce the producer gas's temperature. Then the gaseous stream will pass through two bag house filters in series, coarse bag house filter and fine bag house filter, to make cleaner producer gas before use—bag house filter made by filling with sawdust. Fine bag house filter will fill with sawdust denser than filling in the coarse bag house filter. The pictorial drawing of the downdraft gasifier system showed in Figure 2.

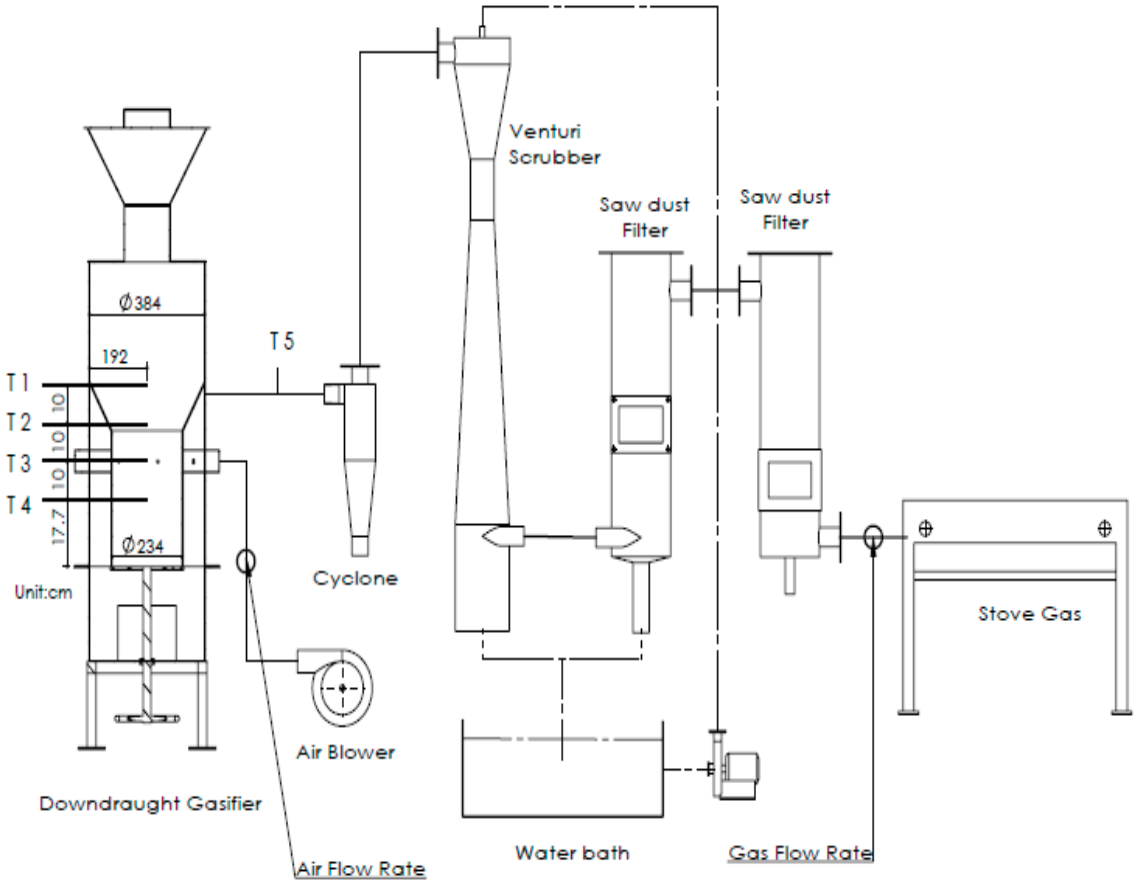

Figure 2. The pictorial drawing of the downdraft gasifier system

2. 2 Biomass

The woody biomass fuels used in this study comprise Eucalyptus wood chips, Mimosa wood twigs, and wood pellets. The photographs of the sample biomass used here are shown in Figure 3.

(a) Eucalyptus wood chip (b) Mimosa wood twig (c) wood pellet

Figure 3. Biomass fuels were used in this study.

2.3 Experimental setup

The preliminary experimental test was conducted to study the characteristic of temperature distribution during the gasification process within the gasifier. Based on the principle of downdraft gasifier, thus, to study the characteristic of the gasification process, we installed a thermocouple within the gasifier with four ports. Four thermocouples were fixed in the gasifier along the vertical reactor to measure the temperature at different positions. The thermocouples T_1, T_2, and T_3 were fixed in the gasifier with a 100-millimeter gap, while T_4 was fixed with a 117.7-millimeter hole from the grate. All thermocouples were connected to a data logger and computer to acquire data. Figure 4 shows the position installed thermocouple along the vertical reactor.

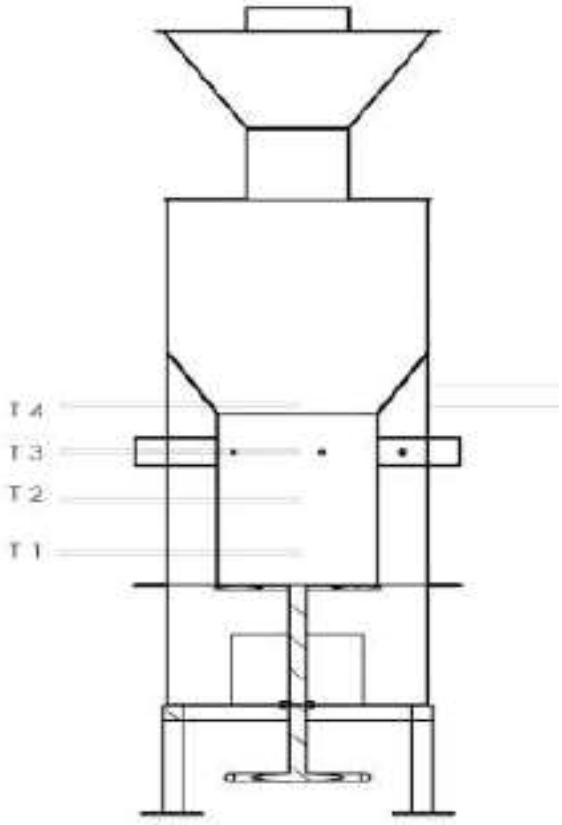

Figure 4. The temperature measurement within the gasifier.

3. Results and Discussion

3.1 Temperature distribution within the gasifier during gasified with Eucalyptus wood chip

The temperature distribution within the gasifier during the gasifying process of the Eucalyptus woodchip showed in Figure 1. The analysis results found that the temperature is highest at the thermocouple T3 port, as obvious according to the air supplied at this zone; thus, the combustion process has occurred. The temperature at the combustion zone is 789-983 °C, while the average temperature is 827 °C. At the zone underneath the combustion zone, the thermocouple T_2 was installed. The recorded temperature is 461-636 °C, while the average temperature in this zone is 514 °C. Based on the theoretical review, this implies that this zone is a reduction zone. At the zone adjoining the higher combustion zone, the thermocouple T_4 was installed. The temperature at this zone is 132-318 °C while the average temperature is 178 °C. This implies that this zone is the pyrolysis zone. At the zone underneath the reduction zone, the thermocouple T_1 was installed. The results showed that the temperature in this zone is 95-159 °C while the average temperature is 123 °C. The graphical temperature distribution within the gasifier during gasification with Eucalyptus wood chip showed in Figure 5.

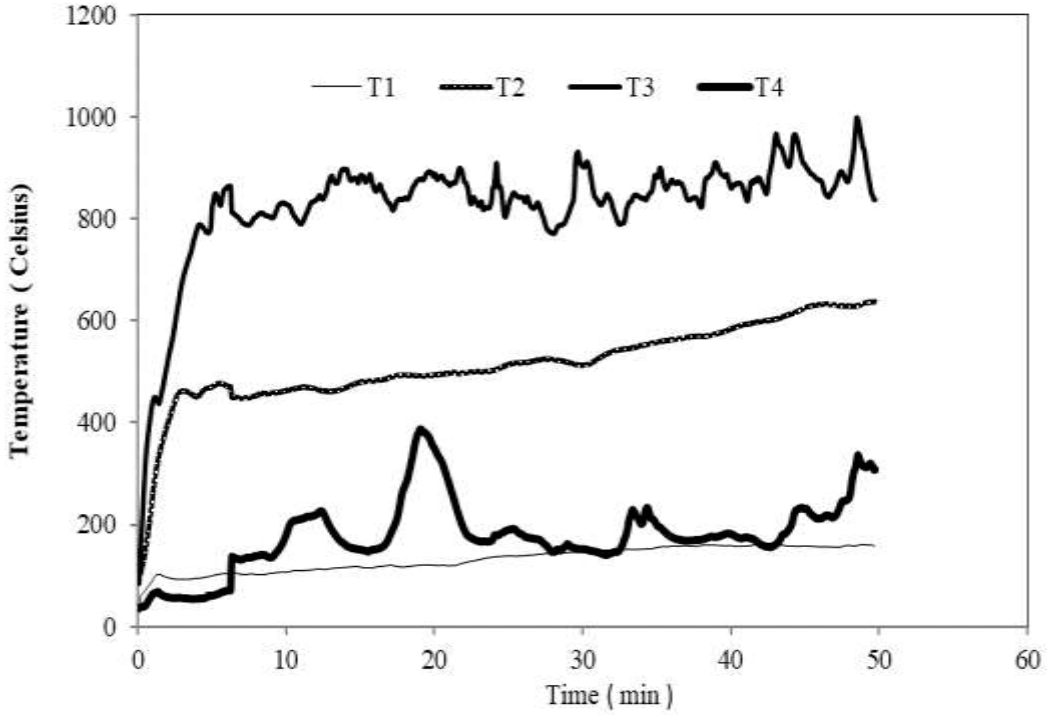

Figure 5. The graphical of temperature distribution within the gasifier during gasified with Eucalyptus wood chip

3.2 Temperature distribution within the gasifier during gasified with Mimosa wood twig

Figure 6 shows the downdraft gasifier's temperature distribution during Mimosa wood twig gasification. The analysis results of the temperature recorded and temperature distribution characteristics within the gasifier at each point showed the following results. The results showed that the temperature from every port would take around -3-5 minutes to reach a steady state. This means that the reaction within the gasifier has completely occurred. According to the basic principle of a downdraft gasifier, the combustion process will appear at the supply air zone. Heat and the combustion products from this zone will transfer to the biomass fuel, which lies next to each other in the combustion zone. Thus the author will start considering the temperature distribution from this zone. At the thermocouple T_3 port, The temperature is highest, as obvious. The results showed that the temperature was 772-1044 °C while the average was 783 °C. This implies that this zone is a combustion zone. At the zone underneath the combustion zone, the thermocouple T_2 was installed. The temperature at this zone is 450-590 °C while the average temperature is 501 °C. Based on the theoretical review, this implies that this zone is a reduction zone. At the zone adjoining higher with the combustion zone, the thermocouple T_4 was installed. The

temperature at this zone ranges from 125-492 °C while the average temperature is 174 °C. This implies that this zone is the pyrolysis zone. At the thermocouple T_1 port, this zone underneath the reduction zone, the producer gas will exit from the gasifier at this zone. The results showed that temperature is almost steady over time. The temperature ranges from 125-130 °C while the average temperature is 120 °C. The graphical temperature distribution within the gasifier during gasification with Mimosa wood twigs showed in Figure 6.

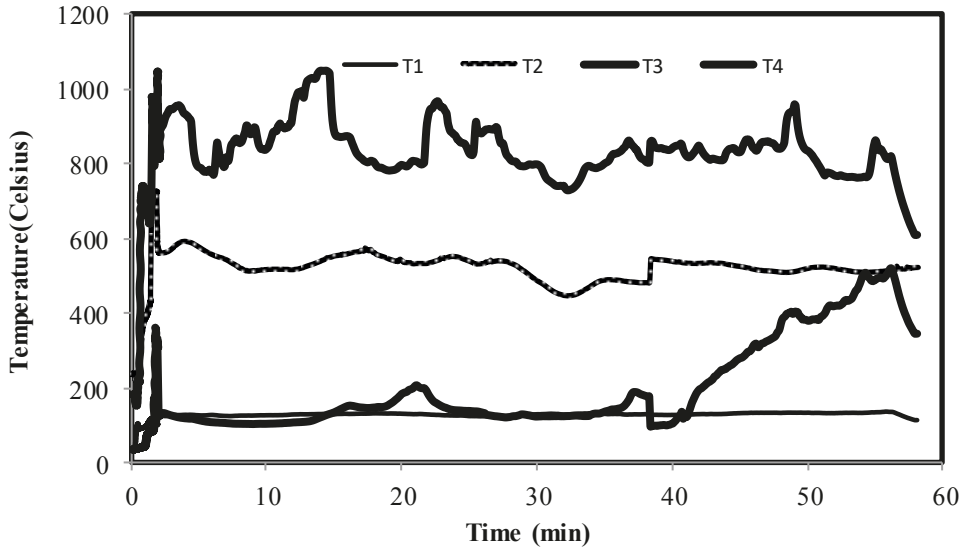

Figure 6. The graphical of temperature distribution within the gasifier during gasified with Mimosa wood twig

3.3 Temperature distribution within the gasifier operated with a wood pellet

Figure 7 shows the temperature distribution within the downdraft gasifier operated with a wood pellet. The analysis results of the temperature recorded and characteristics of temperature distribution within the gasifier at each point are as follows. The temperature from every port will take around 5 minutes to reach a steady state. At the thermocouple T_3 port, The temperature is highest, as obvious. The results showed that the temperature was 557-736 °C while the average was 619 °C. This implies that this zone is a combustion zone. At the zone underneath the combustion zone, the thermocouple T_2 was installed. The temperature in this zone is 507-547 °C, while the average temperature is 470 °C. Based on the theoretical review, this implies that this zone is a reduction zone. At the zone adjoining higher with the combustion zone, the thermocouple T_4 was installed. The temperature at this zone ranges from 125-492 °C while the average temperature is 168 degrees Celsius. This implies that this zone is the pyrolysis zone. At the thermocouple T_1 port, underneath the reaction zone, the producer will exit from the gasifier. At this zone, the temperature is steady at 133 °C.

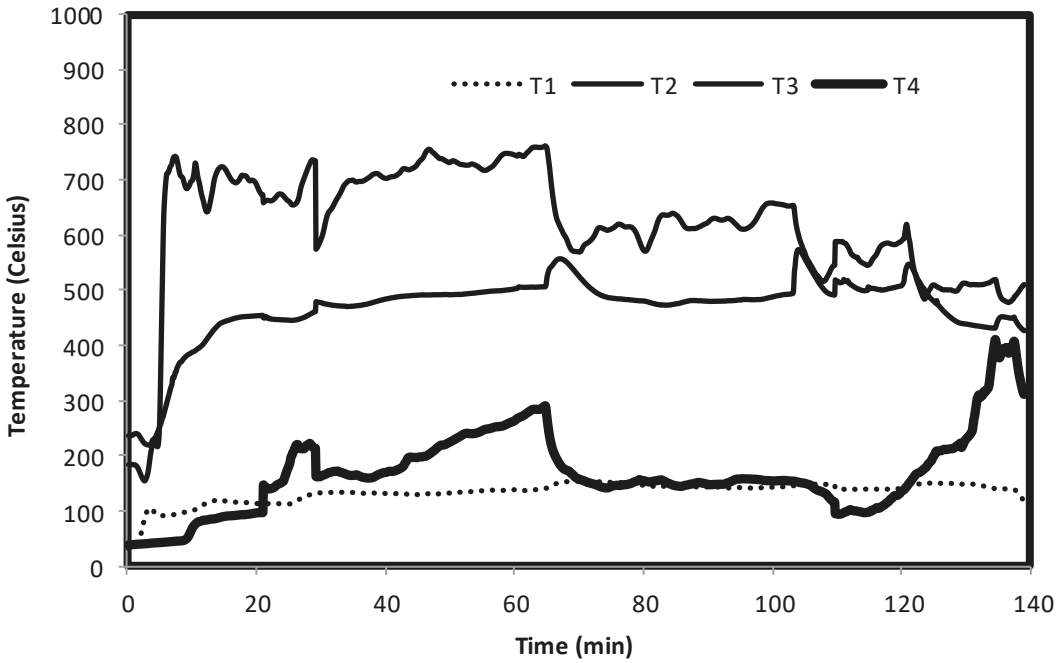

Figure 7. The graphical of temperature distribution within the gasifier during gasified with a wood pellet

3.4 The temperature profile from the gasification process of different biomass fuel

To investigate the temperature profile from the gasification process of three biomass fuels, the average temperature for each point within the gasifier was calculated and presented in graphical. The average temperature for each point within the gasifier during the gasification process of three biomass feeds along the gasifier's height was summarized as shown in Table 1.

Table 1. The average temperature for each point within the gasifier for three biomass feed

	Eucalyptus wood chip	Mimosa wood twig	wood pellet
T1	113	120	131
T2	514	501	470
T3	828	783	620
T4	179	175	168

From the average temperature at each point within the gasifier and plotted in the graph, The results showed that the temperature profile for each biomass feed is in the same pattern. The maximum temperature is in the combustion zone (T_3), and the temperature at the combustion zone results in the temperature at the reduction zone. The temperature at the pyrolysis zone and the gas exit are almost the same for all three biomass feeds.

Figure 8 shows the temperature profiles of the three biomass gasification processes over the operating time at different gasifier positions. The results showed that the temperature at the combustion zone is highest for all three biomass feeds. The maximum temperature at the Eucalyptus wood chip's combustion zone is the highest compared with that at the combustion zone of Mimosa wood twigs and wood pellets. The temperature at the combustion zone (T_3) of Eucalyptus wood chip, Mimosa wood twig, and wood pellet are 838, 783, and 620 °C, respectively. At the zone underneath the combustion zone(T_2), the combustion products will flow down through the product gas and are partly reduced chemically, and the temperature will also decrease. The reduction process will have occurred at this zone (T_2). The temperature at the reduction zone (T_2) of Eucalyptus wood chip, Mimosa wood twig, and wood pellet are 514, 501, and 470 °C, respectively. At the zone adjoining higher with the combustion zone, the thermocouple T_4 was installed, and at this zone, the pyrolysis process occurred. The temperature at the pyrolysis zone (T_4) of

Eucalyptus wood chip, Mimosa wood twig, and wood pellet are 179, 175, and 168 °C, respectively. The temperature at the gas exit (T_1) for all three biomass feeds is not a significant difference. The gas exit temperature is around 120 °C.

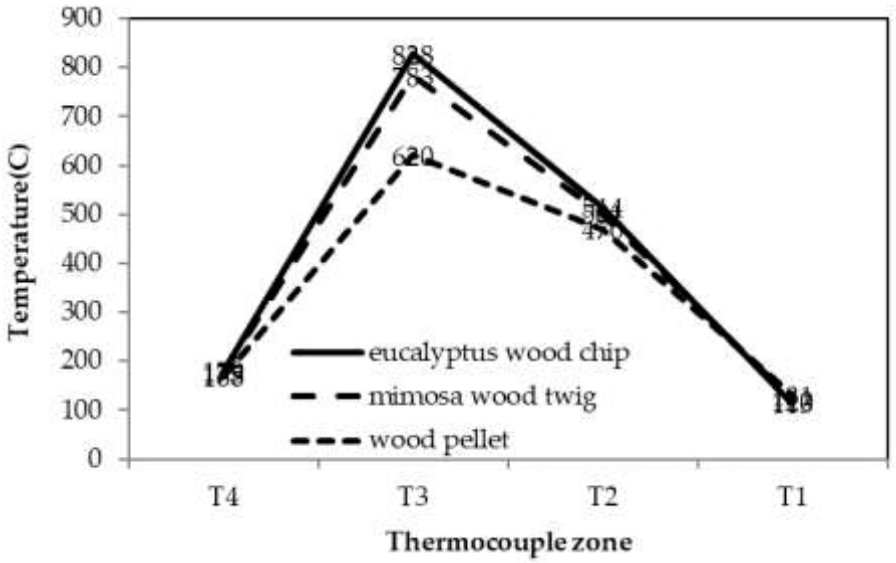

Figure 8. The temperature profiles of the three biomass gasification processes at the different positions inside the gasifier over the operating time.

4. Conclusions

The experimental study was conducted on an open core throat less downdraft gasifier. The study gives an insight into the behavior of the reaction within the gasifier. This paper aims to investigate the temperature distribution within the gasifier to confirm that the response within the gasifier can carry out continuously with a suitable temperature in each zone. The conclusions the results are as follows:

(1) The temperature distribution for each zone of all three biomass feeds is the same pattern.

(2) The temperature range for each zone corresponds with the characteristics of the gasifying process within the downdraft gasifier.

(3) At the combustion zone (T_3), the highest temperature is highest according to the air supplied at this zone. The product from the combustion zone, including heat, CO_2, and other substances, will pass through the zone underneath and adjoining higher with the combustion zone.

(4) Based on the downdraft gasifier design, the gas exit at the bottom; thus, the combustion products in the form of gas or particulates will pass through the zone underneath the combustion zone. The reduction reaction has occurred at this zone. Producer gas will be produced from the reaction in this zone. The thermocouple T_2 was installed at this zone. The results showed that the average temperature for gasifying all three biomass is 470-514 °C. This implies that this zone is a reduction zone.

(5) While the zone adjoining is higher than the combustion zone, only heat transfer through this zone, thus pyrolysis, will occur. The thermocouple T_4 was installed, and the results showed that the average temperature is 168-179 °C.

(6) At the gas exit, the average temperature of the three biomass feeds is not significant difference. The average temperature at the gas exit for all three biomass feeds is 120 °C.

5. Acknowledgements

The author would like to express her gratitude to the National Science and Technology Development Agency (NSTDA) for grant support for the research on this topic.

Author Contributions: W. J. contributes all parts of this paper, including conceptualization, methodology, formal analysis, experimental investigation, resources, data curation, writing—original draft preparation, writing—review, and editing.

Funding: This research received funding support from the National Science and Technology Development Agency (NSTDA)

Conflicts of Interest: The authors declare no conflict of interest.

References

[1] Govindjee, WJ.; The photosynthetic process. In Concepts in photobiology:photosynthesis and photomorphogenesis, Singhai, G.S.; Renger, G., Sopory, SK, Irrgang, K.D., Govindjee., editors. Boston: Kluwer Academic Publishers; 1999, 11-51.

[2] Piriou, B.; Vaitilingom, G.; Veyssiere, B.; Cuq, B.; Rouau, X.; Potential direct use of solid biomass in internal combustion engines. *Progr Energy Combust Sci* 2013, 39, 169-188.

[3] Wenbin, Zhang.; Hao, L,; Irfan, U.H.; York, N.; Philipp, S.; Holger, O.; Alexander, S.; and Axel, K.; Gas cleaning strategies for biomass gasification product gas. *International Journal of Low Carbon Technologies* 2012, 7, 69-74.

[4] Baldwin, R.M.; Magrini, K.A.; Nimlos, M.R.; Pepiot, P.; Donohoe, B.S.; Hensley, J.E.; Current reseach on thermochemical conversion of biomass at the National Renewable Energy Laboratory. *Appl Catal B: Environ* 2012, 115-116.

[5] Deshmukh, R.; Jacobson, A.; Chamberlin, C.; Kammen, D.; Thermal gasification or drect combustion. comparison of advanve cogeneration systems in the sugarcane industry. *Biomass Bioenergy* 2013, 55, 163-174.

[6] Mohammad, A.; Biomass gasification gas cleaning for downstream applications:A comparative critical Review. *Renewable and Sustainable Energy Reviews* 40 , 2014, 118-132.

[7] Mekendy, P.; Energy production from biomass (part 1) : oveview of biomass. *Bioresource Technology* 2002, 83, 37-46.

[8] Basu, P.; *Biomass gasification, Pyrolysis, and Torrefaction: Practical Design and Theory*.Secon edition, 2013, Academic Press is an imprint of Elsevier, London, UK.

[9] Mekendy, P.; Energy production from biomass (part 3) : oveview of biomass. *Bioresource Technology* 2002, 83, 55-63.

[10] Reed, T.B.; Das, A.; *Handbook of biomass downdraft gasifier engine system*.The Biomass Foundation Press, 1984, Colorado, USA.

[11] Groveneveld, M.J.; Japp, J.H.; Gasification of various eastes annular co current moving bed gasifier, Proceeding of 2 nd EL conference on energy from biomass. Applied Science Publisher, 1983, 406-407.

[12] Kaupp, A.; Gasification of rice husk:Theory and Praxis. Publication of Dt. Zentrum fur Entwickhings technologies; Wiesbaden; Vieweg, 1984.

[13] Kaupp, A.; Goss, J.R.; Small scale gas producer engine system. Published by GATE/GTZ. Germany, 1984. Brigwater, A,V.; Thermochemical processing of biomass. Butterworth, UK, 1984.

[14] Devi, L.; Ptasinski, K.J.; Janssen F.; A review of the primary measures for tar elimination in biomass gasification process. *Biomass Bioenergy* 2003, 24, 125-140.

[15] Corella, J.; Toledo, J.M.; Molina, G.; Calculation of the conditions to get less than 2 g tar /Nm3 in a fluidized bed biomass gasifier. *Fuel Process Technol* 2006, 87, 841-846.

[16] Jain, A.K.; Goss, J.R.; Determination of reactor sealing factors for throatless rice husk gasifier. *Biomass and Bioenergy* 2000,18, 249-256.

[17] Tiwari, G.; Sarkar, B.; Ghosh, L.; Design Parameters for a Rice husk throatless Gasifier reactor. Agricultural Engineering International: the CIGR Journal of Scientific Research and Development 2006, 8.

[18] Sims, R., Climate change solutions from biomass, bioenergy and biomaterials. Agricultural Engineering International: the CiCR Journal of Scientific Research and Development. 2003, 5.

JSTR
ASEAN Journal of Scientific and Technological Reports

Research article

Evaluation of Nutrient Digestibility and Metabolizable Energy of Yeast-Fermented *Acacia mangium* Leaf by Japanese Quails

Saichon Lerdsuwan[1*], Duangjai Pisuttharachai[2] ,Warrapong Nalinanon[3]

[1] Animal Science, Disciplines of Technology Agriculture, King Mongkut's Institute of Technology Ladkrabang, Prince of Chumphon Campus, Chumphon, 86160, Thailand; saichon.le@kmitl.ac.th
[2] Fishery Science and Aquatic Resources, Disciplines of Technology Agriculture, King Mongkut's Institute of Technology Ladkrabang, Prince of Chumphon Campus, Chumphon, 86160, Thailand; duangjai.pi@kmitl.ac.th
[3] Fishery Science and Aquatic Resources, Disciplines of Technology Agriculture, King Mongkut's Institute of Technology Ladkrabang, Prince of Chumphon Campus, Chumphon, 86160, Thailand; warrapong.na@kmitl.ac.th
[*] Correspondence: saichon.le@kmitl.ac.th

Citation:
Lerdsuwan, S.; Pisuttharachai, D.; Nalinanon, W. Evaluation of Nutrient Digestibility and Metabolizable Energy in Yeast-Fermented *Acacia mangium* Leaf by Japanese Quails.. *ASEAN J. Sci. Tech. Report.* **2023**, *26*(2), 11-19. https://doi.org/10.55164/ajstr.v26i1.247548

Article history:
Received: October 10, 2022
Revised: December 26, 2022
Accepted: January 20, 2023
Available online: March 21, 2023

Abstract: The nutrient digestibility and the metabolizable energy (AME) of *Acacia mangium* leaf (AM) and yeast-fermented AM (YFAM) by Japanese quails were investigated. Fifty-four of 4-weeks-old Japanese quails were divided into 3 groups with six replications of three quails. Each quail was randomly fed with an experimental diet composed of dextrose (protein-free diet for determining endogenous excretion) 40 % AM and 40% YFAM. The quails were raised individually in a metabolic cage, where feed and water were provided *ad-libitum*. Both feed intake and feces weight were recorded. Experimental diets and excreta were sampled and subjected to proximate analysis for gross energy. The results of nutrient composition indicated that the fermentation AM with yeast highly significantly increased ($P<0.01$) dry matter (DM), ash, and nitrogen-free extractives (NFE) content but decreased ($P<0.01$) crude protein (CP), crude fiber (CF), and gross energy (GE) content. In addition, the birds fed dietary YFAM compared with AM showed significantly increased ($P\leq0.01$) DM, organic matter (OM), CP, and GE digestibility but decreased ($P\leq0.01$) EE and CF digestibility. The protein utilization of birds fed dietary YFAM showed significantly greater ($P\leq0.01$) FI, protein retained, protein intake, net protein utilization (NPU), and AME than those fed dietary AM. In conclusion, the fermentation of AMLM with yeast improved nutrient composition and enhanced the digestibility of nutrients, protein utilization, and AME of AMLM in Japanese quail.

Keywords: *Acacia mangium* Leaf; Japanese Quail; Amino Acid; Digestibility; Metabolizable Energy

1. Introduction

Japanese quail also is the smallest avian species farmed for meat and egg production. Several aspects account for the utility of this bird. First, it has attained economic importance as an agricultural species producing eggs and meat that are enjoyed for their unique flavor. Second, the low maintenance cost associated with its small body size (80-300 g) coupled with its short generation interval (3-4 generations per year), disease resistance, and high egg production. Egg production is important in Japan and Southeast Asia, while meat is the main product in Europe, India, and Nigeria [1].

An accurate feed formulation is essential for optimizing feed efficiency and minimizing feed costs for poultry production. Because energy and amino

acid (AA) account for the major cost of poultry diets, determining the availability of energy and AA in feedstuffs is essential for accurate diet formulations [2]. In contrast, feed cost is approximately 65-70% of the total cost of poultry production [3]. High feed costs and competition between humans and poultry for food/feed resources [4,5] hinder the growth of the poultry production industry in most developing countries, Hence the necessity to explore the use of non-convention feed resources, especially those that do not attract competition between humans and monogastric animal [6]. Leaf meal from *the Acacia mangium* tree is one resource. An exotic and fast-growing tree can be used for furniture, sawn wood, pulp, and paper [7]. The waste, such as residual wood, branches/twigs, leaves, and bark, accounts for more than 60 % of the total biomass [8]. *Acacia mangium* leaves contain 14% CP, 2.15 % EE, 39.81 NFE, and 26.4 % CF [9], which can be used for ruminant animals [10,11]. It's possible to support broiler growth, optimum inclusion levels of *Acacia mangium* leaf meal (AMLM) in support growth without adverse effects on growth performance have been established at 5% in starter chicks and 10% in grower-finisher chicks [12]. The utilization of AMLM in poultry diets must be limited due to its high fiber content and anti-nutritional factors. For this reason, processes for upgrading the nutrient value of AMLM using microbial fermentation by-products may be a substitute to improve the nutrient availability of by-products [13].

Yeast is mainly used in single-cell protein (SCP) production [14], such as *Saccharomyces cerevisiae*, one of the most widely commercialized types of yeast. This is used in the diet of poultry because of its rapid growth rate and high efficiency in converting carbon sources into protein [15]. Fermentation of AMLM with Baker's yeast (Saccharomyces cerevisiae) could be one of the best solutions to enriching its nutritional value. During fermentation yeast requires some nutrients (carbon, nitrogen, trace mineral, and vitamins) to increase in the fermentation medium. The lack of these nutrients hinders their activity which hampers the beneficial effects of the fermentation technique [16]. Starch and molasses could serve as a carbon source in the fermentation system, while urea could supply nitrogen for yeast cell synthesis, which helps the yeast to perform a proper function in the fermentation system [17-18]. Yeast and yeast products produced from agro-industrial by-products are rich in protein contents [19]. Furthermore, live yeast addition to animal feed has been known to improve the nutritional quality of feed, nutrient digestibility [20], and performance of animals [21]. However, there is no information about the effects of AMLM and fermented AMLM on Japanese quails' digestive and metabolic processes. Thus, this study aimed to determine the chemical composition, amino acid profile, and metabolizable energy of *Acacia mangium* leaf meal (AM) and fermented *Acacia mangium* leaf meal (YFAM) in Japanese quail.

2. Materials and Methods

2.1 Sample preparation

Fresh *acacia mangium* leaves were harvested from one-year-old *acacia mangium* tree stands in the KMITL PCC forest in Chumphon province, Thailand. Whole fresh leaves were separated from a branch about 60 cm above. The Leaves (weight 10 kg) were cut and spread out on a clean concrete floor well-ventilated room for 7 days until they became crispy (weight 3.5 kg) [22]. Dried *Acacia mangium* leaves were ground through a 3-horse-power locally built Hammermill (NPT, Thailand) equipped with a 2 mm screen (weight 3.1 kg). Sample AM was taken and analyzed for proximate analysis [23], Tannin [24], amino acid [25], and Gross energy (GE) according to Analytical methods for oxygen bombs. Total carbohydrate content was determined by subtracting the percentage of moisture, crude ash fiber, protein, and fat from 100%.

The yeast used to be Pakmaya® baker's yeast, a commercial yeast culture (*Saccharomyces cerevisiae*) manufactured by the Pakmaya brand in Izmit, Turkey. That was purchased from a store at Pathiu market in Chumphon province, Thailand.

2.2 The preparation of solid-state AMLM yeast fermented

Dried *Acacia mangium* leave meal (1 kg) was weighed into a mixing bowl, and moisture content was adjusted to 60% by adding the calculated amount of distilled water. Adding nutrient solution with yeast (*Saccharomyces cerevisiae)* (50 g.), urea (10 g.), molasses (300 g), Tapioca starch (200 g), $MgSo_4.2H_2O$ (7 g) and KH_2PO_4 (13 g) mixed, collected in a plastic bag, and then allowed to incubate and fermentation in temperature room (27 ^{0}C) for 6 days. The sample was terminated by oven drying at 60 ^{o}C for 24 hours, cooled to a

temperature room, milled, and packaged in air-tight containers. The procedure described by Oboh and Akindahunsi [26] and Aruna et al. [27].

2.3 Digestibility and metabolizable energy

Fifty-four Japanese quail, 4 weeks of age, were used to test the metabolizable energy value of AMLM. The birds were assigned to 32 width x 41 length x 13 high cm individual metabolic cages and allotted to 3 groups with 6 replicates of 3 birds/ cage. A reference diet (protein-free diet for determining endogenous excretion) was used as a basal diet (control diet) to calculate the metabolizable energy, which was determined using the substitution method according to Scott *et al.* [28]. Dextrose in the basal diet was replaced by 40 % *Acacia mangium* leaf meal (AM) and 40 % Yeast fermented AM (YFAM) to make up test diets (Table 1).

Table 1. Ingredients composition of experimental diets.

Ingredients	Control diet	AM	YFAM
Dextrose	98.81	58.81	58.81
AMLM	-	40.00	-
Yeast fermented AMLM	-	-	40.00
Dicalcium phosphate (P17)	0.50	0.50	0.50
salt	0.19	0.19	0.19
Vitamins & trace mineral	0.50	0.50	0.50
total	100.00	100.00	100.00

1/ This premix provided the following microelements (μg/kg): vitamin A 4,500,000 IU; vitamin D 750,000 IU; vitamin E 10,000, vitamin K_3 750; vitamin B_1 1,100; vitamin B_2 3,000; vitamin B_3 10,000; vitamin B_6 2,000; vitamin B_{12} 12.5; pantothenic acid, 7,000; folic acid 425; biotin 100; Cu 5,000; Fe 4,800; I 500; Mn 30,000; Se 100; Zn 50,000.

The birds were fed a diet twice daily at 7.00 and 19.00, at a near maintenance level, and they were weight before and after each collection period. After 7 days adaptation period, a 7-day collection period was started with adding 0.5% chromium oxide in experimental diets as an initial and a marker. As a finishing marker, 0.5% chromium oxide was added to each experimental diet on the 6th day of the collection period. A collection of excreta (mixed feces and urine) was started when the chromium oxide appeared in the excreta and kept until the appearance of chromium oxide in the excreta. Total excreta were collected during the collection period. Every day, the excreta samples were dried in a drying oven at 60oC for 72 h and collected in plastic containers. At the end of each experimental period, total excreta were grounded to 1 mm in the blender mill grinder. Diet and excreta samples were taken for chemical analysis [23], consisting of dry matter (DM), ether extract (EE), crude protein (CP), crude fiber (CF), and gross energy GE). The apparent digestibility coefficients, protein utilization, and apparent metabolizable energy (AME) were computed.

The nutrient digestibility can be calculated according to kong and Adeola [29] as follows:

$$\text{Digestibility (\%)} = \left[\frac{Cinput - C\ output}{Cinput}\right] \times 100$$

Cinput and *Coutput* are the amounts of components ingested and voided via the feces, respectively.

The protein utilization can be calculated according to kong and Adeola [29] as follows:

Protein intake (g/bird) = the concentration of CP in diet (g/kg DM diet) X Feed intake

Net protein utilization (NPU; g/g) = Protein retained / Protein intake

The ME content of AM and YFAM were calculated according to the equation developed by Scott et al. [28] as follows:

ME per gm diet = Energy per gm diet – (excreta energy per gm diet + 8.22 x gm N retained per gm diet)

To compute the ME of material substituted for glucose, the following equation applies:

$$\text{ME per gm substitute} = 3.64 - [\frac{\text{ME per gm referent diet} - \text{ME per gm diet with substitute}}{\text{Proportion of substitute}}]$$

(3.64 = experimentally established ME per gm of glucose dry matter)

2.4 Statistical analysis

All data were analyzed through analysis t-test design with 6 replications in each treatment, using the GLM procedure of SAS [30] with the main effect of 2 experimental diets were AM and YFAM.

3. Results and Discussion

3.1. Results

3.1.1 Amino acid of AMLM

The amino acids of AM are evaluated and listed in Table 2. The sample contains 1) essential amino acids /100 g: Arginine 801 mg, Histidine 460 mg, Isoleucine 393 mg, Leucine 1,150 mg, Lysine 810 mg, Methionine 417 mg, Phenylalanine 742 mg, Threonine 680 mg, Tryptophan 31 mg and Valine 624 mg respectively. 2) non-essential amino acids/100 g: Alanine 642 mg, Aspartic acid 1,266 mg, Cystine 594 mg, Glutamic acid 1,672 mg, Glycine 879 mg, Proline 447 mg, Serine 771 mg and Tyrosine 540 mg respectively.

Table 2. Chemical analysis of amino acid content (% dry matter) of *AM*.

Amino acids	Concentration (mg/100g sample)	Amino acids	Concentration (mg/100g sample)
Essential amino acids		**Non-essential amino acids**	
Arginine	801	Alanine	642
Histidine	460	Aspartic Acid	1,266
Isoleucine	393	Cysteine	594
Leucine	1,150	Glutamic Acid	1,672
Lysine	810	Glycine*	879
Methionine	417	Proline	447
Phenylalanine	742	Serine*	771
Threonine	680	Tyrosine	540
Tryptophan	31		
Valine	624		

* Glycine and serine represent poultry diets' first-limiting non-essential amino acids [27].

3.1.2. Nutrient content of solid-state fermented AM by yeast (Saccharomyces cerevisiae)

The results from the nutrient content of AM and YFAM are presented in Table 3. Yeast fermentation highly significantly affected dry matter, crude protein, crude fiber, ash, nitrogen-free extract, and gross energy of AM ($P<0.01$). Dry matter, ash, and nitrogen-free extract content significantly increased ($P<0.01$) in YFAM compared to AM. YFAM tended to have a higher ($P=0.0513$) crude fat content than AM. Additionally, there were a significantly decreased crude protein, fiber, and gross energy content in YFAM compared to AM ($P<0.01$). However, yeast fermentation did not affect the ether extract, calcium, phosphorus, and tannin content of AM ($P>0.05$).

Table 3. The nutrient composition of AM and YFAM (% dry matter).

Nutrient composition (%)	AM	YFAM	P-value
Dry matter	91.44 ± 0.06 [b]	93.29 ± 0.05 [a]	0.0018
Crude protein	15.97 ± 0.14 [a]	14.47 ± 0.14 [b]	0.0088
Ether extract	2.25 ± 0.07	2.55 ± 0.07	0.0513
Crude fiber	25.00 ± 0.07 [a]	20.63 ± 0.03 [b]	0.0129
Ash	4.05 ± 0.08 [b]	5.97 ± 0.03 [a]	0.0011
Nitrogen free extract	44.17 ± 0.95 [b]	49.67 ± 0.28 [a]	0.0158
Calcium	0.54 ± 0.03	0.56 ± 0.01	0.4655
Phosphorus	0.27 ± 0.04	0.29 ± 0.01	0.5918
Tannin	3.45 ± 0.14	3.44 ± 0.01	0.9298
Gross energy (Kcal/kg)	4,963.14 ± 7.11 [a]	4,720.64 ± 28.45 [b]	0.0072

[a,b] Mean values ± SD in the same row with different superscripts were significantly different. (P<0.05)

3.1.3. Digestibility and Metabolizable energy

The effects of dietary treatment on the digestibility coefficients of the nutrients such as dry matter, organic matter, ether extract, crude protein, crude fiber, nitrogen-free extract, and gross energy are shown in Table 4. The data revealed significant differences between dietary treatments in the digestibility coefficients for all nutrients of the diets except nitrogen-free extract. It could be noticed that birds fed dietary YFAM showed significantly greater (P≤0.01) dry matter, Organic matter, crude protein, and gross energy digestibility than fed dietary AM. In contrast to ether extract and crude fiber digestibility, there was a decrease (P≤0.01) in birds fed dietary YFAM.

The protein utilization of birds fed dietary YFAM showed significantly greater (P≤0.01) feed intake, retained protein intake, and net protein utilization than those fed dietary AM. Additionally, the birds fed dietary YFAM had greater (P≤0.01) apparent metabolizable energy (AME) and apparent metabolizable energy corrected nitrogen balance (AME_n) compared with those fed dietary AM.

Table 4. Digestibility and metabolizable energy of AM and YFAM in Japanese quail.

Items	AM	YFAM	P-value
Apparent digestibility (%)			
Dry matter	66.36 ± 1.95 [b]	70.42 ± 1.81 [a]	0.0039
Organic matter	68.14 ± 2.07 [b]	72.00 ± 1.81 [a]	0.0064
Ether extract	23.34 ± 3.02 [a]	12.00 ± 2.34 [b]	0.0030
Crude protein	65.72 ± 2.09 [b]	74.93 ± 1.23 [a]	0.0001
Crude fiber	28.55 ± 4.34 [a]	19.08 ± 2.45 [b]	0.0109
Nitrogen free extract	86.48 ± 1.05	87.03 ± 0.94	0.3550
Gross energy	60.15 ± 2.47 [b]	65.31± 2.47 [a]	0.0048
Protein utilization			
Feed intake (g/bird)	69.09 ± 14.91 [b]	91.41 ± 8.68 [a]	0.0001
Protein intake (g/bird)	3.10 ± 0.67 [b]	4.47 ± 0.42 [a]	0.0018
Protein retained (g/bird)	2.04 ± 0.45 [b]	3.35 ± 0.36 [a]	0.0002
Net protein utilization (g/g)	0.66 ± 0.02 [b]	0.75 ± 0.01 [a]	0.0001
Metabolizable energy (Kcal/kg)[1/]			
- AME	1428.08 ± 228.60 [b]	1993.03 ± 232.23 [a]	0.0017
- AME_n	1424.95 ± 229.45 [b]	1992.96 ± 232.57 [a]	0.0017

[a,b] Mean values ± SD in the same row with different superscripts were significantly different. (P<0.01)

[1/] AME = Apparent metabolizable energy

AME_n = Apparent metabolizable energy corrected by nitrogen balance

3.2. Discussion

Studies using Acacia mangium leaf meal (AM) as a feed ingredient mainly were focused on ruminant nutrition., and showed that using AM as a protein source diet had a positive effect on production in dairy cows [10]and Sheep [11]. However, no information is available about using AM in poultry diets.

In Japanese quail, methionine, threonine, and lysine are the first, second, and third limiting amino acids [32]. In this experiment, AM contains significant qualities of methionine, threonine, and lysine, whose values were 417, 680, and 810 mg/100 g (0.42, 0.68, and 0.81 %), respectively. These amino acid values were near with NRC [33] recommendation. The NRC [33] recommended lysine levels of 1.3 and 1.0% and methionine levels of 0.5 and 0.45% for quails in the rearing and production periods, respectively. Furthermore, this methionine amount was higher than the values found in the Leucaena leaf meal, as reported by the Bureau of Animal Nutrition Development [34]. The amino acid profile of the studied sample suggests that its protein is of adequate nutritional value, which the feed industries can exploit for feed formulations.

Nutritional changes during the yeast fermentation in AM, dry matter, ash, and nitrogen-free extract content of YFAM were higher than in AM ($P<0.01$). This experimental result was in agreement with earlier reports. Kaewwongsa et al. [35] reported the dry matter content of the fermented cassava pulp by yeast (*Saccharomyces cerevisiae*) was higher than non-fermented ($P<0.05$). Azinnahar et al. [36] also reported that fermented De-oiled rice bran with yeast (*Saccharomyces cerevisiae*) induced increased dry matter and ash ($P<0.05$). The result shows that YFAM tended to have a higher ($P=0.0513$) crude fat content than AMLM. This was likely to Mu et al. [37] reported crude fat content of fermented rice bran was significantly higher ($P<0.05$) than those of untreated rice brans. In our experiment, crude protein, fiber, and gross energy content in YFAM were lower than in AM ($P<0.01$). Crude fiber content reduces the present experiment. Another experiment conducted by Azinnahar et al. [36] and Shi et al. [38] also reported the same result, which mentioned that microorganisms produce some fibrinolytic enzymes during fermentation, which are responsible for the reduction of fiber content.

In our study, the birds fed dietary YFAM improved dry matter, Organic matter, crude protein, and gross energy digestibility. In Addition, the protein utilization of birds fed YFAM showed significantly greater ($P\leq0.01$) feed intake, protein retained, protein intake, and net protein utilization than those fed dietary AM. These results are in congruence with early reports that supplementation with *Saccharomyces cerevisiae* improved ($P\leq0.05$) of dry matter, organic matter, crude fiber, ether extract [39,40], and crude protein [40] digestibility of Japanese quail. Afsharmanesh et al. [41] reported that the ileal digesta of broiler chickens fed with yeast in both wet and dry diets can also have enhanced absorption of nutrients, as acidification can reduce the emptying rate of the stomach and enhance the digestion process. The improvement of nutrient digestibility of the birds by fermentation of feedstuff with yeast. Kornegay et al. [42] and Abd El-Latif et al. [39] explained that live yeast, such as *Saccharomyces cerevisiae*, contains numerous enzymes that could be released into the intestine and aid existing enzymes in the digestive tract in the digestion of feed. Also, yeast contains vitamins and other nutrients that may produce beneficial production responses. The YFAM and AM have about 14.47 and 15.97% CP, showing net protein utilization results of 0.75 and 0.66, respectively. These results were agreeable with Omidiwura et al. [43], indicating that varying levels of protein in the diet (20-26% CP) of Japanese quails had a significant effect protein efficiency ratio (0.74-1.05) of the birds.

The AM's apparent metabolizable energy (AME) content for Japanese quail was analyzed to be 1,428.09 Kcal/kg. This value was lower than ME in broilers of *L. leucocephala* leaf meal (2,377 Kcal/kg) obtained by Hien et al. [44]. However, Fermentation AM with yeast significantly improved AME ($P<0.01$). The birds fed dietary YFAM was 1993.03 Kcal/kg AME. This result contradicts Nabila et al. [45] Supplementation of baker's yeast (at levels 0, 0.1, 0.2, 0.4, and 0.8 %) in broiler chicken's diet. Results showed no significant difference ($P>0.05$) was observed for metabolizable energy among all treatments. Our experiment using baker's yeast at level 5 % fermented AM was higher than Nabila et al. [45] Supplementation. Therefore, the bird-fed dietary yeast fermented caused an increase in the apparent metabolizable energy in this study.

4. Conclusions

The study shows that the fermentation AM with yeast (*Saccharomyces cerevisiae*) improved nutrient composition, enhanced nutrient digestibility, protein utilization, and apparent metabolizable energy of *Acacia mangium* leaf meal in Japanese quail. The apparent metabolizable energy of AM and YFAM was basic information for calculating feed formulation in Japanese quail.

5. Acknowledgements

The author would like to thank Asst. Prof. Dr. Seksom Attamangkune and Assoc. Prof. Dr. Neramit Sookmanee for help and support throughout this research. Moreover, I would like to thank The Agricultural Research Development Agency (ARDA) and King Mongkut's Institute of Technology Ladkrabang Prince of Chumphon Campus for funding and research equipment.

Author Contributions: Conceptualization, S.L. and W.N.; performed the experiments, S.L., D.P. and W.N.; formal analysis, S.L.; data collection, S. L., D. P. and W. N.; writing—original draft preparation, S.L.; writing—review and editing, S.L.; supervision, S.L.; project administration, S.L.; funding acquisition, S.L., and W.N.. All authors have read and agreed to the published version of the manuscript.

Funding: This research was funded by Agricultural Research Development Agency (ARDA), PRP6005011290.

Conflicts of Interest: The authors declare that there is no conflict of interest regarding the publication of this article.

References

[1] Vali, N. The Japanese Quail: A Review. *Int. J. Poult. Sci*. 2008. *7*(9), 925-931.

[2] Kong, C.; Adeola, O. Evaluation of amino acid and energy utilization in feedstuff for swine and poultry diets. *Asian Australas. J. Anim. Sci*. 2014, *27*(7), 917-925.

[3] Khan, M.K.A.; Akbar, M.A.; Khaleduzzaman, A.B.M.; Rahman, M.M. Utilization of *Leacaena* and *Sasbania* leaf meals as protein supplements in broiler ration. *Bangladesh. J. Anim. Sci*. 2009, *38*(1&2), 123-131.

[4] Bonsu, F.R.K.; Kagya-Agyemang, J.K.; Kwenin, W.K.J.; Zanu, H.K. Medicinal response of broiler chickens to diets containing Neem (Azadirachta indica) leaf meal, hematology and meat sensory analysis. *World Appl. Sci. J*. 2012, *19*(6), 800-805.

[5] Muktar, A.; Adzitey, F.; Teye, G. A.; Alhassan, M.; Dei. H. K. Effects of Albizia julibrissin leaf meal-based diet on carcass and sensory characteristics of broiler chickens. *Glob. J. Anim. Sci. Res*. 2015, *3*(2), 388-392.

[6] Ncube, S.; Halimani, T.E.; Chikosi, E.V.I.; Saidi, P.T. Effect of *Acacia angustissima* leaf meal on performance, yield of carcass components and meat quality of broilers. *S. Afr. J. Anim. Sci.* 2018, *48*(2), 271-283.

[7] Maelim, S.; Khlangsap, N.; Thaiutsa, B. Provenance trials of 1-year old *Acacia mangium* Willd. at wang nam khiew forestry research and training station, nakhon ratchasima province. *Thai J. Forest*. 2017, *36*(2), 35-45.

[8] Djarwanto; Tachibana, S. Decomposition of lignin and holocellulose on *Acacia mangium* leaves and twings by six fungal isolates from nature. *Pak. J. Biol. Sci*. 2010, *13*(12), 604-610.

[9] Lerdsuwan, S.; Nalinanon ,W. Reduction of fiber content in *Acacia mangium* leaves meal by commercial enzyme. *J. Sci. Technol. MSU*. 2016, (Suppl.1), 647-652.

[10] Sruamsiri, S. The use of acacia (*Acacia mangium*) as protein source in dairy ration. *J. Agri. Res. Ext*. 2001, 18, 82-91.

[11] Clavero, T.; Razz, R. Utilization of *Acacia mangium* as supplement for growing sheep. *Rev. Cient.* 1999, *9*(4), 311-313.

[12] Lerdsuwan, S.; Nalinanon, W. Effect of *Acacia mangium* leaf meal on production performance of broiler chickens. *J. Sci. Technol. MSU*. 2017, *36*(5), 614-620.

[13] Chen, K.L.; Kho, W.L.; You, S.H.; Yeh, R.H.; Tang, S.W.; Hsieh, C.W. Effects of Bacillus subtilis var. natto and Saccharomyces cerevisiae mixed fermented feed on the enhanced growth performance of broilers. *Poult. Sci.* 2009, *88*(2), 309–315.

[14] Sharif, M.; Shoaib, M.; Saif-ur-Rehman, M.; Fawwad, A.; Asif, J. Use of Distillery Yeast Sludge in Poultry: A Review. *Scholarly J. Agri. Sci.* 2016, *6*(8), 242-256.

[15] Glazer, A.G.; Nikaido, H. Microbial Biotechnology: Fundamentals of Applied Microbiology: 2nd Edition. Cambridge University Press, Cambridge. 2007.

[16] Azrinnahar, M.; Islam, N.; Shuvo, A.A.S., Ahsan Kabir, A.K.M.; Islam, K.M.S. Effect of feeding fermented (Saccharomyces cerevisiae) de-oiled rice bran in broiler growth and bone mineralization. *J. Saudi Soc. Agric. Sci.* 2021, 20, 476-481.

[17] Abramov, S.H.A.; Efendieva, D.A.; Kotecko, S.T. Effect of growth medium on protein content of yeast Saccharomyces cerevisiae. *Appl. Bioch. Biotech*. 1994, 30, 225–227.

[18] Fadel, M.; Keera, A.A.; Mouafi, F.E.; Kahil, T. High level ethanol from sugar cane molasses by a new thermotolerant Saccharomyces cerevisiae strain in industrial scale. *Biotechnol. Res. Int.* 2013. 1–6. https://doi.org/10.1155/2013/253286.

[19] Silva, V.K.; Silva, J.D.T.; Torres, K.A.A.; Filho, D.E.D.F.; Hada, F.H.; Moraes., V. Humoral immune response of broilers fed diets containing yeast extract and prebiotics in the prestarter phase and raised at different temperatures. *J. Appl. Poult. Res*. 2009, 18, 530-540.

[20] Abdel-Azeem, F. Digeston, neomycin and yeast supplementation in broiler diets under Egyptian summer conditions. *Egypt. Poult. Sci. J*. 2002**,** *22*(I), 235-257.

[21] Matin, S.A.; Nisbet, D.J.; Dean, R.G. Influence of commercial yeast supplement on the ruminal fermentation. *Nutr. Rep. int*. 1989, 40, 395-401.

[22] Zanu, H.K.; Mustapha, M.; Addo Nartey, M. Response of broiler chickens to diets containing varying levels of leucaena (*leucaena leucocephpla*) leaf meal. *Online J. Anim. Feed Res*. 2012, *2*(2), 108-112.

[23] A.O.A.C. Official Methods for Analysis. 5thed. Association of Official Analytical Chemists, Washington DC. 1980.

[24] Burns, R. E. Method for estimate of tannin in grain sorghum. *Agron. J.* 1971, 63, 511.

[25] Herbert, P.; Brrros, P.; Ratola, N.; Alves, A. HPLC determination of amino acids in musts and port wine using OPA/FMOC derivatives. *J. Food Sci.* 2000, *65*(7), 1130-1133.

[26] Oboh, G.; Akindahunsi, A.A. Biochemical changes in cassava products (flour & gari) subjected to *Saccharomyces cerevisiae* solid media fermentation. *Food Chem*. 2003, 82, 599-602.

[27] Aruna, T.E.; Aworh, O.C.; Raji, A.O.; olagnju, A.I. Protein enrichment of yam peels by fermentation with Saccharomyces cerevisiae (BY4743). *Ann. Agri. Sci*. 2017, 62, 33-37.

[28] Scott, M.L.; Nesheim, M.C.; Young, R.J. Nutrition of the Chicken. 3rded. M.L. Scott & Associates, Ithaca, New York. 1982.

[29] Kong, C.; Adeola, O. Protein utilization and amino acid digestibility of canola meal in response to phytase in broiler chickens. *Poult. Sci.* 2011, *90*(7), 1508–1515.

[30] SAS. SAS/SAT Guide for Personal Computers. Version 9.1.3 ed. SAS Inst., Inc., Cary, NC. 2003.

[31] Siegert, W; Rodehutscord, M. The relevance of glycine and serine in poultry nutrition: a review. *Br Poult Sci*. 2019, *60*(5), 579-588.

[32] Thomas, K.S.; Amutha, R.; Purushothaman, M.R.; Jagatheesan, P.N.R.; Ezhilvalavan, S.; Jayalalitha,V. Energy and protein requirements during various stages of production in Japanese quails. *Int. J. Sci. Environ. Technol.* 2019, *8*(4), 790 – 794.

[33] NRC. Nutrient Requirements of Poultry. National Research Council, National Academy Press, Washington, D. C., 9th Revised Edition. 1994, 234.

[34] Bureau of Animal Nutrition Development, 2018. Leucaena leaf meal. Available Source: http://nutrition.dld.go.th/exhibision/feed_stuff/ leucaena_leaf_meal.htm, March 15, 2021.

[35] Kaewwongsa, W.; Traiyakun, S.; Yuangklang, C.; Wachirapakorn, C.; Paengkoum, P. Protein enrichment of cassava pulp fermentation by *Saccharomyces cerevisiae. J. Anim. Vet. Adv*. 2011, *10*(18), 2434-2440.

[36] Azinnahar, M.; Islam, N.; Shuvo, A.A.S.; Kabir, A.K.M.A.; Islam, K.M.S. Effect of feeding fermented (*Saccharomyces cerevisiae*) de-oiled rice bran in broiler growth and bone mineralization. *J. Saudi Soc. Agric. Sci.* 2021, *20*(7), 476-481. https://doi.org/10.1016/j.jssas.2021.05.006

[37] Mu, K.S.; Kasim, A.B.; Ideris, A.; Saad, C.R. Effect of fermented rice bran, bioconverted byproduct on performance of broiler chickens. *J. Anim. Vet. Adv*. 2011, *10* (22), 2990–2995.

[38] Shi, C.; He, J.; Yu, J.; Yu, B.; Huang, Z.; Mao, X.; Zheng, P.; Chen, P. Solid state fermentation of rapeseed cake with Aspergillus niger for degrading glucosinolates and upgrading nutritional value. *J. Anim. Sci. Biotechnol*. 2015, *6*(13) 1–7.

[39] Abd El-Latif, S.A.; Ghally, K.A.; Shoulkamy, M.O. Effect of Fenugreek and yeast additions to Japanese quail diet on digestibility and economical responses. *Act. Sci. Nutr. Health*. 2019, *3*(6), 78-82.

[40] El-Kelawy, M. I.; ELnaggar, A.S. Inclusion of *Saccharomyces cerevisiae* in diet of Japanese quail. 1- effect on growth performance, some blood plasma constituents and carcass characteristics. *Egypt. Poult. Sci. J.* 2016, *35*(4), 1269-1282.

[41] Afsharmanesh, M.; Barani, M.; Silversided, F. Evaluation of wet feeding wheat-based diets containing *Saccharomyces cerevisiae* to broiler chickens. *Br. Poult. Sci*. 2010, 51, 776-783.

[42] Kornegay E.T.; Rhein-Welker, D.; Lindemamn, M.D.; Wood, C.M. Performance and nutrient digestibility in weanling pigs as influenced by yeast culture additions to starter diets containing dried whey or one of two fiber sources. *J. Anim. Sci.* 1995, *73*(5), 1381-1389.

[43] Omidiwura, B.R.O.; Odu, O.; Agboola, A.F.; Akinbola, A.A.; Iyayi, E.A. Crude Protein and Energy Requirements of Japanese Quail (*Coturnix coturnix japonica*) During Rearing Period. *J. World Poult. Res*. 2016, 6(2), 99-104.

[44] Hien, T.Q.; Trung, T.Q.; Ha, T.V. 2016. Determination of the metabolic energy value of leucaena leucocephala leaf meal on luong Phuong broiler chicken. *Vietnam J. sci. Technol*. 2016, *2*(9), 23-26.

[45] Nabila, M.; Yaakub, H.; Alimon, A.R.; Samsudin1, A.A. Effects of baker's yeast as a growth promoter supplemented at different levels on growth performance, gut morphology, and carcass characteristics of broiler chickens. *Mal. Soc. Anim. Prod*. 2017, *20*(2), 83-93.

JSTR
ASEAN Journal of Scientific and Technological Reports

Research article

Influence of Watering Regimes on Physiological Traits, Growth, Yield, and Capsaicin Content of Chilies

Pimvipa Arom[1] and Wanploy Jinagool[2*]

[1] School of Crop Production Technology, Institute of Agricultural Technology, Suranaree University of Technology, Nakhon Ratchasima, 30000, Thailand; pimvipaarom39@gmail.com
[2] School of Crop Production Technology, Institute of Agricultural Technology, Suranaree University of Technology, Nakhon Ratchasima, 30000, Thailand; wanploy.jinagool@sut.ac.th
* Correspondence: wanploy.jinagool@sut.ac.th

Citation:
Arom, P.; Jinagool, W. Influence of Watering Regimes on Physiological Traits, Growth, Yield, and Capsaicin Content of Chilies. *ASEAN J. Sci. Tech. Report.* **2023**, *26*(1), 20-31. https://doi.org/10.55164/ajstr.v26i1.247571.

Article history:
Received: October 10, 2022
Revised: December 26, 2022
Accepted: January 20, 2023
Available online: March 21, 2023

Abstract: Water stress is a major limiting factor affecting the physiological processes, growth, and productivity of crop plants, including chili. This study evaluated chili plants' responses regarding physiological traits, growth, yield, and capsaicin content under different irrigation levels. The experimental design was a 2x4 factorial in CBD. A pot experiment was conducted on two species of chilies: *Capsicum annuum* 'Super-Hot 2' and 'Huay-Siiton' and *C. frutescent* 'Prik-Kee-Nu-Suan.' The plants were irrigated at four watering regimes such as 100%, 80%, 60%, and 40% of maximum water holding capacity (MWHC) after the anthesis through fruit development. Midday leaf water potential (LWP_{md}) was ranked between -1.30 MPa in 100% MWHC to -2.11 MPa in 40% MWHC indicating the level of water stress. The 40% MWHC caused a drastic decrease in LWP_{md} and reduced the maximum quantum yield of PSII (F_v/F_m) and growth rate in canopy width. Observed leaf greenness was maximized at 60% MWHC. The irrigation regimes also affected the yield of chili, especially the 60% and 40% MWHC, with a reduced number of fruits/plant, fruit fresh and dry weights, and fruit sizes. In the case of 40% MWHC, the dry yield was too low, and it was impossible to analyze the capsaicin content. The reduced irrigation (80% and 60% MWHC) did not significantly induce the capsaicin content or pungency of the studied chili cultivars. Thus the capsaicin yield of studied chili cultivars was reduced considerably by severe reduction of dry fruit yield under restricted water.

Keywords: *Capsicum*; Water Deficit; Water Holding Capacity; Photosynthetic Efficiency, Capsaicinoid

1. Introduction

In Thailand, chili is an important spice used in various traditional dishes and an essential material in the industrial sector, particularly the capsaicinoids that can be extracted and used in the pharmaceutical and cosmetic industries [1-2]. Previous studies have demonstrated that water deficit can alter crop physiological processes, e.g., reducing the stomatal conductance, photosynthetic efficiency, chlorophyll content, and nutrient assimilation [3].

The mentioned changes may lead to a reduction in vegetative growth and a loss of reproductive parts, resulting in a declining yield and yield quality [4]. In chili, water deficit can also alter the pungency level of chili by modifying the capsaicinoid contents [5]. The capsaicinoids are secondary metabolites accumulated in chili fruits, comprising several compounds. The major

capsaicin and dihydrocapsaicin account for 90% of total capsaicinoids [6-7]. Studies have found that irrigation regimes below the field capacity (FC) contributed to an increase in secondary metabolites [8-11]. Therefore, irrigation management is of interest as a possible tool for optimizing chili growth and yield and increasing capsaicinoid content. This study aimed to investigate the effects of watering regimes on the physiological traits, growth, yield, and capsaicin content of *Capsicum annuum* and *C. frutescens* under nursery conditions.

2. Materials and Methods

The study was conducted in a nursery from October 2020 to March 2021 at Suranaree University of Technology's farm, Nakhon Ratchasima Province, Thailand. The 3x4 factorial in CRD with 5 replications was used as an experimental design. The studied factors were A) three chili cultivars (*C. annuum* cv. Super-Hot and Huay-Siiton and *C. frutescent* cv. Prik-Kee-Nu-Suan) and B) four watering regimes: 100 (control), 80, 60, and 40% of maximum water holding capacity (MWHC). The chosen chili cultivars are commonly grown in the Northeastern region of Thailand and have been reported to have a high capsaicinoid content and pungency level [12-14].

Seeds of the three cultivars were germinated in peat moss-filled trays under a plastic-covered nursery. The seedlings were regularly irrigated and 30 days after sowing, homogenous seedlings were selected and transplanted into a 5-liter-plastic pot filled with sandy loam soil from Suranaree University of Technology's Farm. Chili plants received the 21-0-0, 15-15-15, and 13-13-21 chemical fertilizers after transplanting, during the vegetative growth stage, and flowering to the fruiting stage, respectively [15]. After transplanting, plants were irrigated to the MWHC, and different irrigation regimes were applied from the flowering stage to the fruit ripening stage of each cultivar. Soil moisture content was regularly observed using the HH2 Moisture Meter (Delta-T Devices Ltd.), and the pots were rewatered when the moisture content dropped below the assigned regimes.

Data collection was started at the onset of anthesis (0 WAA, week after anthesis) for physiological, growth, and development traits. The measurement was retaken at 2, 4, 6, and 8 WAA.

2.1 Physiological traits

Three plants from each treatment were assigned to measure midday leaf water potential (LWP_{md}) to determine the effects of watering regimes on plant water status using a 3005-pressure chamber (Soilmoisture). A fully expanded leaf/plant was cut from the middle of the canopy height of each plant. On the same plants, three fully developed leaves at the middle of the canopy height were marked for the measurement of leaf greenness (SPAD) using the chlorophyll meter SPAD-502plus (Konica Minolta Inc.). A chlorophyll fluorescence meter measured the maximum quantum yield of PSII (Fv/Fm) (Handy PEA, Hansatech Instruments Ltd.). Before the F_v/F_m measurement, marked leaves were clamped with the Dark Leaf Cup (DLC-8) for 20 minutes. These physiological traits were performed before the irrigation, from 11:00 a.m. to 1.00 p.m.

2.2 Plant growth and development

The same plants used for measuring physiological traits were also assigned for measuring plant growth and development: canopy height and width. The values were later used to calculate the relative growth rate (RGR), and the calculation was done according to the following equations:

$$RGR_{height} = (ln\ H_2 - ln\ H_1)/(T_2 - T_1) \quad (1)$$

$$RGR_{width} = (ln\ W_2 - ln\ W_1)/(T_2 - T_1) \quad (2)$$

where H_1 and H_2 were canopy heights at times T_1 and T_2 and W_1 and W_2 were the canopy widths at times T_1 and T_2.

2.3 Yield and capsaicin content

The yield was collected during the 8-14 WAA. The fully ripened fruits were harvested, and the number of fruits harvested was counted. Thirty fruits were randomly sampled from each treatment to measure length and width. All fruits were weighed for fresh fruit weight and dried in a hot-air oven at 70 °C for 48 hours

before the dry fruit weight was measured. The dried chili fruits were grounded and stored in a freezer at -20 °C while waiting to measure capsaicin. The capsaicin content was measured using the high-performance liquid chromatography (HPLC) technique [16]. The capsaicin content, the pungency of the samples according to the Scoville organoleptic test, and the capsaicin yield were later calculated [17].

2.4 Statistical analysis

All the traits collected were statistically analyzed using the analysis of variance (ANOVA). The significant difference between treatments was determined using Duncan's New Multiple Range Test (DMRT) at a 95% confidence interval.

3. Results and Discussion

3.1 The physiological response

Chili cultivars had different LWP_{md} and SPAD characters. However, they were similar in the F_v/F_m. With decreasing watering regimes, the LWP_{md} was lowered compared to the control treatment except for the 80% MWHC. On the contrary, it appeared that lowering the water supply to a certain point (60% MWHC) can increase the SPAD of chili. At 100% MWHC, the F_v/F_m was the highest, and it was reduced with the decreased MWHC. The SPAD and F_v/F_m of each studied chili cultivar responded to different watering regimes in similar trends to those observed from the effects of the watering regime (Table 1).

When considering the changes in LWP_{md} between the studied weeks (Figure 1), it was clear that lower watering regimes can cause a reduction in the LWP_{md} of three chili cultivars. However, the degree of decrement has differed. The results indicated that a restricted water supply caused a decrease in LWP_{md} and chili cultivars responded differently to a similarly restricted water supply. Other studies also reported similar results that drought or restricted water supply can cause a reduction in LWP_{md} and differences dropped in LWP_{md} were also observed between studied chili cultivars which can be due to different adaptations to water deficit [18-19].

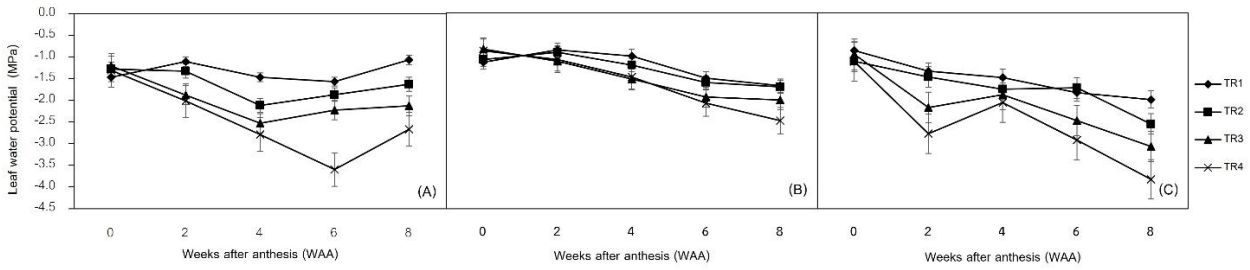

Figure 1. Leaf water potential of *C. annuum* cv. Super-Hot 2 (A) and Hueay-Sii-Ton (B) and *C. frutescens* cv. Kee-Nu-Suen (C) responded to different watering regimes at anthesis (0 WAA) to 8 weeks after anthesis. Means with different letters indicate significant differences by DMRT at a 95% confidence interval.

The SPAD of plant leaves is usually reduced by the effects of water stress [20], and to a certain degree, the result found in this study was contrasted with the previous findings. In this study, the SPAD of water-restricted plants was higher or remained close to the control (Table 2). However, a similar trend was also found in water-stressed Karen KPS chili [21]. Under the water restriction, delayed senescence (or stay-green) may reflect the maintenance of photosynthetic activity and capacity for light harvesting during the re-mobilization of carbon products to the harvested organs of the plant [22-23]. Maintenance of SPAD under drought stress can be considered a positive trait as it indicates the reduction of chlorophyll degradation [24].

Table 1. Effects of chili cultivars, watering regimes, and their interactions on physiological traits and growth rate of *C. annuum* (Super-Hot 2 and Hueay-Sii-Ton) and *C. frutescens* (Kee-Nu-Suen).

Studied factors		LWP_{md} (MPa)	SPAD	F_v/F_m	RGR_{height}	RGR_{width}
Chili cultivars (A)	Super-Hot 2	-1.86 ± 0.09^{b1}	56.96 ± 0.33^{a}	0.003 ± 0.001^{b1}	0.003 ± 0.001	0.759 ± 0.00
	Hueay-Sii-Ton	-1.40 ± 0.06^{a}	53.69 ± 0.28^{b}	0.00 7 ± 0.001^{a}	0.005 ± 0.001	0.759 ± 0.00
	Kee-Nu-Suan	-1.75 ± 0.09^{b}	56.91 ± 0.39^{a}	0.005 ± 0.001^{ab}	0.004 ± 0.001	0.754 ± 0.00
	F-test	**	**	*	ns	ns
Watering regimes (B)	100% MWHC	-1.30 ± 0.05^{a}	54.81 ± 0.37^{bc}	0.005 ± 0.001	0.006 ± 0.001^{a}	0.781 ± 0.00^{a}
	80% MWHC	-1.49 ± 0.07^{a}	55.85 ± 0.42^{b}	0.006 ± 0.001	0.006 ± 0.001^{a}	0.758 ± 0.00^{b}
	60% MWHC	-1.79 ± 0.10^{b}	58.13 ± 0.37^{a}	0.006 ± 0.001	0.003 ± 0.001^{b}	0.752 ± 0.00^{b}
	40% MWHC	-2.11 ± 0.14^{c}	54.62 ± 0.40^{c}	0.004 ± 0.001	0.001 ± 0.001^{b}	0.739 ± 0.00^{c}
	F-test	**	**	ns	**	**
AxB	Super-Hot 2 100% MWHC	-1.33 ± 0.08	55.55 ± 0.44^{cde}	0.004 ± 0.001	0.005 ± 0.002	0.778 ± 0.003^{a}
	Super-Hot 2 80% MWHC	-1.65 ± 0.11	58.79 ± 0.60^{ab}	0.004 ± 0.001	0.004 ± 0.002	0.762 ± 0.004^{b}
	Super-Hot 2 60% MWHC	-2.00 ± 0.13	60.11 ± 0.65^{a}	0.004 ± 0.001	0.002 ± 0.002	0.743 ± 0.006^{c}
	Super-Hot 2 40% MWHC	-2.47 ± 0.24	53.38 ± 0.74^{f}	0.002 ± 0.001	0.001 ± 0.001	0.754 ± 0.005^{bc}
	Hueay-Sii-Ton 100% MWHC	-1.24 ± 0.09	51.39 ± 0.53^{g}	0.007 ± 0.002	0.007 ± 0.002	0.787 ± 0.003^{a}
	Hueay-Sii-Ton 80% MWHC	-1.30 ± 0.09	54.06 ± 0.56^{ef}	0.007 ± 0.001	0.008 ± 0.001	0.752 ± 0.006^{bc}
	Hueay-Sii-Ton 60% MWHC	-1.49 ± 0.13	56.13 ± 0.54^{cd}	0.007 ± 0.002	0.004 ± 0.003	0.757 ± 0.005^{b}
	Hueay-Sii-Ton 40% MWHC	-1.58 ± 0.17	53.18 ± 0.50^{fg}	0.005 ± 0.001	0.001 ± 0.002	0.741 ± 0.005^{c}
	Kee-Nu-Suan 100% MWHC	-1.34 ± 0.11	57.50 ± 0.77^{bc}	0.003 ± 0.001	0.006 ± 0.001	0.778 ± 0.003^{a}
	Kee-Nu-Suan 80% MWHC	-1.53 ± 0.12	54.68 ± 0.89^{def}	0.007 ± 0.002	0.006 ± 0.002	0.758 ± 0.004^{b}
	Kee-Nu-Suan 60% MWHC	-1.88 ± 0.18	58.16 ± 0.69^{b}	0.006 ± 0.002	0.003 ± 0.002	0.757 ± 0.003^{b}
	Kee-Nu-Suan 40% MWHC	-2.26 ± 0.22	57.30 ± 0.76^{bc}	0.004 ± 0.001	0.001 ± 0.002	0.723 ± 0.007^{d}
	F-test	ns	**	ns	ns	**

[1] Values are means with SE. The letters indicate significant differences by DMRT at a 95% confidence interval.

Table 2. Leaf greenness of *C. annuum* (Super-Hot 2, Hueay-Sii-Ton) and *C. frutescens* (Kee-Nu-Suen) responded to different watering regimes at anthesis (0 WAA) to 8 weeks after anthesis (8 WAA).

Chili cultivars	Watering regimes (MWHC)	Leaf greenness (SPAD)				
		0 WAA	2 WAA	4 WAA	6 WAA	8 WAA
Super-Hot 2	100%	54.02 ± 0.61[1]	59.29 ± 0.68^{b}	56.86 ± 1.03^{b}	52.89 ± 1.12^{b}	54.69 ± 0.95
	80%	53.40 ± 0.55	66.05 ± 1.10^{a}	58.64 ± 1.08^{b}	58.29 ± 1.20^{a}	57.57 ± 1.43
	60%	52.43 ± 0.53	65.98 ± 1.07^{a}	65.15 ± 1.15^{a}	59.24 ± 0.85^{a}	57.73 ± 1.61
	40%	52.92 ± 0.52	58.57 ± 1.63^{b}	50.01 ± 1.62^{c}	51.89 ± 1.27^{b}	53.49 ± 2.31
F-test		ns	**	**	**	ns
Hueay-Sii-Ton	100%	52.86 ± 0.69^{bc}	52.99 ± 0.98^{b}	49.94 ± 1.04^{b}	50.43 ± 1.16^{b}	50.72 ± 1.77^{b}
	80%	54.78 ± 1.16^{ab}	51.02 ± 1.21^{b}	56.20 ± 0.85^{a}	57.15 ± 1.35^{a}	51.16 ± 1.22^{b}
	60%	56.32 ± 1.33^{a}	53.37 ± 0.95^{ab}	56.17 ± 0.99^{a}	58.69 ± 1.44^{a}	56.09 ± 1.07^{a}
	40%	50.56 ± 0.98^{c}	56.56 ± 1.37^{a}	49.77 ± 0.51^{b}	52.51 ± 0.78^{b}	56.50 ± 1.08^{a}
F-test		**	**	**	**	**
Kee-Nu-Suen	100%	58.44 ± 0.89	58.72 ± 1.68	58.79 ± 1.92	56.43 ± 2.00^{ab}	55.12 ± 1.90^{a}
	80%	55.40 ± 1.34	59.76 ± 2.11	57.45 ± 1.98	52.09 ± 1.97^{b}	48.72 ± 1.81^{b}
	60%	55.46 ± 1.53	56.13 ± 1.44	59.43 ± 1.55	58.96 ± 1.42^{a}	60.82 ± 1.62^{a}
	40%	56.48 ± 1.16	56.56 ± 1.47	57.09 ± 1.22	61.30 ± 1.74^{a}	55.10 ± 2.46^{a}
F-test		ns	ns	ns	**	**

[1] Values are means with SE. The letters indicate significant differences by DMRT at a 95% confidence interval.

When considering the changes in F_v/F_m between the studied weeks of the three chili cultivars, it was found that the F_v/F_m had already fluctuated even before the application of watering regimes (Table 3). After applying watering regimes, the F_v/F_m decreased under moderate to severe water deficit. Different watering regimes can cause drought stress on chili and alter the water status inside the plant. In this experiment, despite the apparent changes in LWP_{md}, the F_v/F_m was relatively stable. This contrast can be due to moderate drought's low impact on the F_v/F_m [25-28] and the small decreases can be interpreted as a photoprotection [29].

3.2 Growth and development

Both vegetative growth traits of studied chili plants were low during the experimental period. Chili cultivars differed in the RGR_{height}, in which, Super-Hot 2 had a significantly lower RGR_{height} than Hueay-Sii-Ton. The watering regimes affected the RGR_{width}, the 60 and 40% MWHC resulted in a considerably lower RGR_{width} when compared with the 100 and 80% MWHC. In contrast, the interaction effects were insignificant for the studied factors (Table 1).

It appeared that during the first two weeks after anthesis, chili plants still grew in height and canopy width, and they were affected by reduced water supply. After 2 weeks of anthesis, the growth of the chili plant mostly stopped or declined (Table 4). The mentioned growth pattern can be due to the vegetative growth after anthesis being minimum for chili, and it is not a drought-sensitive period for vegetative development [21]. In addition, the plants may enter the critical phase where the growth rate starts to decrease from abscission and senescence. It can also result from a water supply limitation, which causes a reduction in turgor pressure, wilting, and reduced vegetative growth [30].

Table 3. The maximum quantum yield of PSII (F_v/F_m) of *C. annuum* (Super-Hot 2, Hueay-Sii-Ton) and *C. frutescens* (Kee-Nu-Suen) responded to different watering regimes at anthesis (0 WAA) to 8 weeks after anthesis (8 WAA).

Chili cultivars	Watering regimes (MWHC)	Maximum quantum yield of PSII (F_v/F_m)				
		0 WAA	2 WAA	4 WAA	6 WAA	8 WAA
Super-Hot 2	100%	0.76 ± 0.01^{a1}	0.79 ± 0.00^{ab}	0.77 ± 0.01	0.80 ± 0.00^{a}	0.77 ± 0.01^{a}
	80%	0.73 ± 0.01^{b}	0.80 ± 0.00^{a}	0.77 ± 0.01	0.78 ± 0.01^{b}	0.74 ± 0.01^{a}
	60%	0.72 ± 0.01^{b}	0.78 ± 0.01^{b}	0.75 ± 0.01	0.77 ± 0.00^{b}	0.69 ± 0.02^{b}
	40%	0.78 ± 0.01^{a}	0.78 ± 0.00^{b}	0.75 ± 0.01	0.77 ± 0.01^{b}	0.70 ± 0.02^{b}
F-test		**	*	ns	**	**
Hueay-Sii-Ton	100%	0.80 ± 0.00^{a}	0.782 ± 0.01	0.790 ± 0.01^{a}	0.780 ± 0.00^{a}	0.780 ± 0.01^{a}
	80%	0.77 ± 0.00^{b}	0.769 ± 0.01	0.780 ± 0.01^{a}	0.754 ± 0.01^{b}	0.686 ± 0.02^{b}
	60%	0.77 ± 0.01^{b}	0.781 ± 0.01	0.767 ± 0.01^{ab}	0.764 ± 0.01^{b}	0.707 ± 0.02^{b}
	40%	0.72 ± 0.01^{c}	0.774 ± 0.01	0.751 ± 0.01^{b}	0.750 ± 0.01^{b}	0.707 ± 0.02^{b}
F-test		**	ns	*	**	**
Kee-Nu-Suen	100%	0.794 ± 0.00^{a}	0.771 ± 0.01	0.773 ± 0.01^{a}	0.790 ± 0.00^{a}	0.76 ± 0.01^{a}
	80%	0.770 ± 0.00^{b}	0.761 ± 0.01	0.782 ± 0.01^{a}	0.766 ± 0.01^{a}	0.713 ± 0.01^{b}
	60%	0.744 ± 0.01^{c}	0.779 ± 0.00	0.763 ± 0.00^{a}	0.763 ± 0.01^{a}	0.737 ± 0.01^{ab}
	40%	0.734 ± 0.01^{c}	0.766 ± 0.01	0.737 ± 0.01^{b}	0.716 ± 0.02^{b}	0.664 ± 0.03^{c}
F-test		**	ns	**	**	**

[1] Values are means with SE. The letters indicate significant differences by DMRT at a 95% confidence interval.

3.3 Yield and capsaicin content

The analysis found the effects of cultivars and watering regimes on all studied traits (Table 5). Watering regimes caused a significant reduction in all fruit characteristics and yield. At the same time, the interaction effects indicated that all cultivars had smaller fruit sizes and lower yields when growing under liming water supply. These findings affirm the impact of water supply on crop production [31-32]. The lower watering regimes affected leaf water potential and caused decreases in the number of fruit, fruit weight, and size. If focusing on yield, reducing water supply is not recommended for chili production since it can reduce yield and yield quality by restricting irrigation to 80% of MWHC. The results differed from a previous study suggesting that 80% MWHC can be used to produce *C. frutescens* cv. Karen KPS because it did not affect the yield of studied chili [21]. The contrasted result may be due to the sensitivity of chili cultivars to water stress.

The 40% MWHC yielded a very small yield from the three studied chili cultivars. It was impossible to prepare the dry chili powder to analyze capsaicin content. Thus, Table 6 only showed the capsaicin content, pungency level, and capsaicin yield results from 100, 80, and 60% MWHC treatments. The results show that the capsaicin content and pungency of the three cultivars that grew under different watering regimes were similar. Only capsaicin yield was affected by the combined effects of the chili cultivar and watering regime. Super-Hot 2 was a cultivar with the highest capsaicin yield, followed by Kee-Nu-Suan and Hueay-Sii-Ton. This resulted from different fruit dry weights obtained from chili cultivars, as shown in Table 6. A similar reason can be applied to the effect of watering regimes on capsaicin yield.

The findings were not inconsistent with a previous study which found that restricting water supply to 40% of field capacity resulted in the highest capsaicin yield [7]. In contrast, another study showed no benefit of restricted water supply on the capsaicin content of *C. annuum* [33]. Thus, the restricted watering regime can affect capsaicinoid production in chili cultivars differently. A study suggested that it may depend on the pungency level of the chili cultivars. Those cultivars with low to moderate pungency were more affected by restricted water supply than those with higher pungency [19] in a previous study on *C. frutescens* cv. Karen KPS, the watering regimes at 40% MWHC resulted in the highest capsaicin content and pungency level, while capsaicin yield did not significantly differ [34]. Similarly, a study found that lower water availability can increase capsaicin levels of *C. frutescens* cayenne pepper plants [35].

Table 4. The relative growth rate of *C. annuum* (Super-Hot 2, Hueay-Sii-Ton) and *C. frutescens* (Kee-Nu-Suen) responded to different watering regimes at anthesis (0 WAA) to 8 weeks after anthesis (8 WAA).

Chili cultivars	Watering regimes	RGR_{height} (cm/day)				RGR_{width} (cm/day)			
		Duration (WAA)				Duration (WAA)			
		0-2	2-4	4-6	6-8	0-2	2-4	4-6	6-8
Super-Hot 2	100%	0.016 ± 0.002[a1]	-0.001 ± 0.002	0.002 ± 0.001	-0.001 ± 0.002	0.016 ± 0.002	-0.006 ± 0.001	0.011 ± 0.001[a]	-0.001 ± 0.002
Super-Hot 2	80%	0.015 ± 0.002[a]	0.001 ± 0.001	-0.002 ± 0.001	0.000 ± 0.002	0.015 ± 0.001	-0.006 ± 0.002	0.007 ± 0.002[a]	0.001 ± 0.004
	60%	0.015 ± 0.003[a]	-0.002 ± 0.001	0.000 ± 0.001	0.000 ± 0.001	0.014 ± 0.001	-0.007 ± 0.002	0.006 ± 0.001[a]	-0.004 ± 0.001
	40%	0.008 ± 0.001[b]	0.000 ± 0.001	0.001 ± 0.001	-0.001 ± 0.001	0.012 ± 0.001	-0.008 ± 0.001	-0.002 ± 0.002[b]	0.001 ± 0.001
F-test		*	ns	ns	ns	ns	ns	**	ns
Hueay-Sii-Ton	100%	0.025 ± 0.006	0.003 ± 0.001	0.002 ± 0.000	-0.001 ± 0.000	0.017 ± 0.002[a]	0.010 ± 0.002	0.000 ± 0.001	-0.000 ± 0.001[a]
	80%	0.020 ± 0.002	0.007 ± 0.001	0.002 ± 0.001	0.001 ± 0.000	0.016 ± 0.002[a]	0.010 ± 0.002	0.002 ± 0.002	0.002 ± 0.001[a]
	60%	0.021 ± 0.002	0.008 ± 0.006	0.000 ± 0.005	0.000 ± 0.001	0.010 ± 0.004[ab]	0.007 ± 0.007	-0.005 ± 0.008	0.003 ± 0.002[a]
	40%	0.016 ± 0.002	0.004 ± 0.001	0.000 ± 0.001	-0.001 ± 0.001	0.006 ± 0.002[b]	0.010 ± 0.003	-0.005 ± 0.001	-0.006 ± 0.001[b]
F-test		ns	ns	ns	ns	*	ns	ns	**
Kee-Nu-Suen	100%	0.012 ± 0.003[b]	0.001 ± 0.002	0.000 ± 0.001	0.000 ± 0.001	0.016 ± 0.002	0.004 ± 0.002[ab]	0.004 ± 0.002[a]	-0.001 ± 0.002
	80%	0.022 ± 0.002[a]	0.006 ± 0.002	-0.001 ± 0.002	0.000 ± 0.001	0.017 ± 0.003	0.008 ± 0.002[a]	0.001 ± 0.002[a]	-0.001 ± 0.002
	60%	0.021 ± 0.003[a]	0.002 ± 0.002	-0.002 ± 0.001	0.001 ± 0.001	0.019 ± 0.003	0.002 ± 0.001[ab]	-0.005 ± 0.001[b]	-0.004 ± 0.002
	40%	0.017 ± 0.002[ab]	0.001 ± 0.001	-0.002 ± 0.001	0.000 ± 0.001	0.016 ± 0.001	-0.000 ± 0.002[b]	-0.009 ± 0.002[b]	-0.001 ± 0.003
F-test		*	ns	ns	ns	ns	*	**	ns

[1] Values are means with SE. The letters indicate significant differences by DMRT at a 95% confidence interval.

Table 5. Changes in fruit characteristics of *C. annuum* (Super-Hot 2 and Hueay-Sii-Ton) and *C. frutescens* (Kee-Nu-Suen) responded to different watering regimes and the interaction effects.

	Studied factors	Number of fruits/plant	Fruit fresh weight (g/plant)	Fruit dry weight (g/plant)	Yield (kg/ha)	Fruit length (cm)	Fruit width (mm)
Chili cultivars (A)	Super-Hot 2	17.00 ± 3.06^{a1}	5.84 ± 3.09^{a}	4.68 ± 0.90^{a}	633.65 ± 123.66^{a}	4.45 ± 0.07^{a}	6.02 ± 0.07^{b}
	Hueay-Sii-Ton	5.07 ± 1.68^{b}	4.05 ± 1.54^{c}	1.45 ± 0.53^{c}	325.61 ± 61.51^{b}	3.52 ± 0.09^{c}	6.49 ± 0.10^{a}
	Kee-Nu-Suan	8.52 ± 2.61^{b}	8.14 ± 2.43^{b}	2.77 ± 0.81^{b}	161.71 ± 97.29^{b}	4.14 ± 0.09^{b}	5.97 ± 0.08^{b}
	F-test	**	**	**	**	**	**
Watering regimes (B)	100% MWHC	22.27 ± 3.38^{a}	20.92 ± 3.54^{a}	6.61 ± 1.00^{a}	836.54 ± 141.49^{a}	4.72 ± 0.08^{a}	6.84 ± 0.06^{a}
	80% MWHC	9.60 ± 2.55^{b}	8.93 ± 2.28^{b}	2.85 ± 0.69^{b}	357.65 ± 91.10^{b}	4.16 ± 0.09^{b}	6.19 ± 0.08^{b}
	60% MWHC	5.80 ± 1.31^{bc}	4.58 ± 1.23^{c}	1.46 ± 0.34^{c}	183.22 ± 49.10^{b}	3.68 ± 0.09^{c}	5.63 ± 0.08^{c}
	40% MWHC	3.11 ± 1.02^{c}	2.93 ± 0.85^{c}	0.94 ± 0.23^{c}	117.22 ± 34.10^{b}	3.54 ± 0.10^{c}	5.72 ± 0.10^{c}
	F-test	**	**	**	**	**	**
AxB	Super-Hot 2 100% MWHC	32.00 ± 3.14	31.53 ± 2.50	9.16 ± 0.68	1,261.01 ± 100.12^{a}	4.94 ± 0.09^{ab}	6.71 ± 0.10^{b}
	Super-Hot 2 80% MWHC	19.33 ± 1.68	17.26 ± 1.14	5.31 ± 0.38	690.48 ± 45.50^{b}	4.66 ± 0.12^{bc}	6.18 ± 0.13^{c}
	Super-Hot 2 60% MWHC	10.33 ± 0.37	9.18 ± 0.36	2.68 ± 0.13	367.31 ± 14.58^{cd}	4.00 ± 0.12^{de}	5.45 ± 0.08^{d}
AxB	Super-Hot 2 40% MWHC	6.33 ± 1.99	5.39 ± 1.36	1.57 ± 0.35	215.81 ± 54.32^{cde}	4.12 ± 0.12^{df}	5.66 ± 0.14^{d}
	Hueay-Sii-Ton 100% MWHC	14.40 ± 1.22	12.60 ± 1.50	4.40 ± 0.50	502.94 ± 59.89^{bc}	4.11 ± 0.12^{de}	7.12 ± 0.13^{a}
	Hueay-Sii-Ton 80% MWHC	3.40 ± 0.76	2.27 ± 0.49	0.80 ± 0.17	91.95 ± 19.47^{e}	3.38 ± 0.14^{f}	6.18 ± 0.16^{c}
	Hueay-Sii-Ton 60% MWHC	1.47 ± 0.35	0.87 ± 0.14	0.37 ± 0.07	34.08 ± 5.70^{e}	3.05 ± 0.18^{f}	6.05 ± 0.21^{c}
	Hueay-Sii-Ton 40% MWHC	1.00 ± 0.50	0.47 ± 0.24	0.23 ± 0.13	17.87 ± 9.47^{e}	3.23 ± 0.20^{f}	6.40 ± 0.20^{bc}
	Kee-Nu-Suan 100% MWHC	20.40 ± 6.97	18.64 ± 6.93	6.27 ± 2.33	745.68 ± 277.07^{b}	5.12 ± 0.22^{a}	6.71 ± 0.23^{b}
	Kee-Nu-Suan 80% MWHC	6.07 ± 1.44	7.26 ± 1.62	2.45 ± 0.55	290.53 ± 64.90^{cde}	4.39 ± 0.12^{cd}	6.20 ± 0.14^{c}
	Kee-Nu-Suan 60% MWHC	5.60 ± 0.42	3.71 ± 0.07	1.34 ± 0.14	148.26 ± 2.79^{de}	3.78 ± 0.14^{e}	5.54 ± 0.10^{d}
	Kee-Nu-Suan 40% MWHC	2.00 ± 0.40	2.95 ± 0.84	1.02 ± 0.18	117.97 ± 33.43^{de}	3.28 ± 0.13^{f}	5.42 ± 0.14^{d}
	F-test	ns	ns	ns	**	**	*

[1] Values are means with SE. The letters indicate significant differences by DMRT at a 95% confidence interval.

Table 6. Changes in capsaicin content, pungency level, and capsaicin yield of *C. annuum* (Super-Hot 2 and Hueay-Sii-Ton) and *C. frutescens* (Kee-Nu-Suen) responded to different watering regimes and the effects of the interaction.

	Studied factors	Capsaicin content (ug/g)	Pungency level (SHU)	Capsaicin yield (ug/plant)
Chili cultivar (A)	Super-Hot 2	462.52 ± 13.69[1]	7,588.27 ± 219.00	2,683.70 ± 445.48[a]
	Hueay-Sii-Ton	464.88 ± 0.40	7,312.84 ± 6.41	848.94 ± 299.78[c]
	Kee-Nu-Suan	469.23 ± 0.74	7,545.11 ± 11.78	1,575.49 ± 473.00[b]
	F-test	ns	ns	**
Watering regimes (B)	100%	471.85 ± 4.45	7,423.11 ± 71.21	3,072.83 ± 470.08[a]
	80%	454.63 ± 7.56	7,476.76 ± 120.96	1,341.13 ± 317.79[b]
	60%	469.15 ± 11.35	7,546.36 ± 181.57	694.17 ± 164.82[b]
	F-test	ns	ns	**
AxB	Super-Hot 2 100%	463.03 ± 14.14	7,447.20 ± 226.19	4,268.72 ± 393.65
	Super-Hot 2 80%	470.28 ± 24.58	7,563.20 ± 393.26	2,492.31 ± 58.72
	Super-Hot 2 60%	482.23 ± 36.74	7,754.40 ± 587.89	1,290.06 ± 32.10
	Hueay-Sii-Ton 100%	454.91 ± 0.65	7,317.20 ± 10.39	2,014.07 ± 228.95
	Hueay-Sii-Ton 80%	454.46 ± 0.41	7,310.00 ± 6.58	374.55 ± 76.50
	Hueay-Sii-Ton 60%	454.54 ± 1.13	7,311.33 ± 18.08	158.20 ± 34.10
	Kee-Nu-Suan 100%	466.63 ± 1.17	7,504.93 ± 18.74	2,935.69 ± 1,082.83
	Kee-Nu-Suan 80%	469.90 ± 0.28	7,557.07 ± 4.43	1,156.53 ± 259.90
	Kee-Nu-Suan 60%	470.92 ± 0.22	7,573.33 ± 3.45	634.24 ± 63.50
	F-test	ns	ns	ns

[1] Values are means with SE. The letters indicate significant differences by DMRT at a 95% confidence interval.

4. Conclusions

Restricted water supply affects the physiological traits of the chili plant. It can reduce midday leaf water potential and maximum quantum yield of PSII. The leaf greenness can be enhanced under irrigation of 60% MWHC. The restricted water supply during anthesis to fruit ripening did not affect the relative growth rate in plant height, but the 60% and 40% MWHC can reduce the growth rate of canopy width. The reduction of water supply (80%, 60%, and 40% MWHC) also decreased the yield and fruit size of the three chili cultivars. It cannot significantly induce the capsaicin content or pungency of the studied chili cultivars. Thus, a severe reduction of dry fruit yield significantly reduced the capsaicin yield. Therefore, a reduced water supply during the anthesis through fruit development should be avoided for the three chili cultivars. In addition, the restricted water supply may not be a suitable management for the high capsaicinoid production in chili. However, further study is required since the effects found in pot-grown plants may differ from field-grown plants.

5. Acknowledgements

The authors sincerely thank the Center for Scientific and Technological Equipment and University Farm, the Suranaree University of Technology, for supporting their facilities in this research.

Author Contributions: Experimental design, P.A.; W.J.; experiment works and data analysis, P.A.; writing - original draft preparation, P.A.; writing - review and editing, W.J.; supervision, W.J. All authors have read and agreed to the published version of the manuscript.

Funding: This research was partially funded by the Suranaree University of Technology.

Conflicts of Interest: The authors declare no conflict of interest.

References

[1] Gurung, T.; Techawongstien, S.; Suriharn, B.; Techawongstien, S. Impact of environments on the accumulation of capsaicinoids in *Capsicum* spp. *HortScience*. 2011, *46*(12), 1,576–1,581.

[2] Hernández-Pérez, T.; Gómez-García, M.R.; Valverde, M.E.; Paredes-López, O. *Capsicum annuum* (hot pepper): An ancient Latin-American crop with outstanding bioactive compounds and nutraceutical potential. A review. *Comprehensive reviews in food science and food safety* 2020, *19*(6), 2,972–2,993.

[3] Sun, Y.; Wang, C.; Chen, H.Y.; Ruan H. Response of plants to water stress: a meta-analysis. *Frontiers in plant science*, 2020, 11, 978.

[4] Farooq, M.; Hussain, M.; Wahid, A.; Siddique, K. Drought stress in plants: an overview. In *Plant responses to drought stress*, Aroca, R., Ed., Springer: Heidelberg, Germany, 2012, 1–33.

[5] Naves, E.R.; de Ávila Silva, L.; Sulpice, R.; Araújo, W.L.; Nunes-Nesi, A.; Peres, L.E.P.; Zsögön, A. Capsaicinoids: Pungency beyond *Capsicum*. *Trends Plant Sci.* 2019, *24*(2), 109-120.

[6] Tewksbury, J.J.; Reagan, K.M.; Machnicki, N.J.; Carlo, T.A.; Haak, D.C.; Peñaloza, A.L.; Levey, D.J. Evolutionary ecology of pungency in wild chilies. *PNAS* 2008, *105*(33), 11,808–11,811. https://doi.org/10.1073/pnas.0802691105

[7] Othman, Z.A.A.; Ahmed, Y.B.H.; Habila, M.A.; Ghafar, A.A. Determination of capsaicin and dihydrocapsaicin in *Capsicum* fruit samples using high performance liquid chromatography. *Molecules* 2011, *16*(10), 8,919–8,929.

[8] Szabó, B.; Tyihák, E.; Szabó, G.; Botz, L. Mycotoxin and drought stress induced change of alkaloid content of *Papaver somniferum* plantlets. *Acta. Bot. Hung.* 2003, *45*(3), 409–417.

[9] Selmar, D.; Kleinwächter, M. Influencing the product quality by applying drought stress during the cultivation of medicinal plants. *Ind. Crops Prod.* 2013, *42*(1), 558–566.

[10] Bloema, E.; Haneklausa, S.; Kleinwächterb, M.; Paulsenb, J.; Schnuga, E.; Selma, D. Stress-induced changes of bioactive compounds in *Tropaeolum majus* L. *Ind. Crops. Prod.* 2014, *60*, 349–359.

[11] Arum, P.; Seto-Sugianto, P.R. The effect of water stress on growth and capsaicin content of cayenne pepper (*Capcisum frutences* L.). *J. Appl. Environ. Biol. Sci.* 2017, *7*(6), 76–80.

[12] Kraikruan, W.; Sukprakarn, S.; Mongkilporn, O.; Wasee, S. Capsaicon and dihydrocapsaicin contents of Thai chili cultivars. *Kasetsart J. (Nat. Sci.)*. 2008, *42*, 611–616.
[13] Panyanil, P.; Spreer, W.; Max, J.; Naphrom, D. Effects of ultraviolet-B on capsaicin and dihydrocapsaicin contents of hot chili cvs. Red-devil and Superhot F1. *Journal of Agriculture*. 2008, *33*(1), 61–70.
[14] Inprasit, K.; Chookaew, L.; Suksawad, J.; Chuenwatthana, S. Physicochemical properties and capsicinoids content of Thai chili cultivars used in southern sour curry paste (Kaeng Som). *Bulletin of Applied Sciences*. 2022, *11*(11), 121–132.
[15] Sitathani, K. *Chilli growing guide*. Tropical Vegetable Research and Development Center, Kasetsart University Kamphaeng Saen Campus, Nakhon Pathom, Thailand, 2013, 1–19.
[16] Collins, M.D.; Wasmund, L.M.; Bosland, P.W. (1995). Improved method for quantifying capsaicinoids in *Capsicum* using high-performance liquid chromatography. *HortScience* 1995, *30*(1), 137–139.
[17] Sanatombi, K.; Sharma, G.J. Capsaicin content and pungency of different *Capsicum* spp. cultivars. *Not. Bot. Hort. Agrobot. Cluj.* 2008, *36*, 89–90.
[18] Sato, S.; Moreshet, S.; Takagaki, M.; Shinohara, Y.; Ito, T. Effects of drought stress on sap flow, stomatal conductance, and leaf water potential of pepper cultivars (*Capsicum annuum* L.). *Japanese Journal of Tropical Agriculture* 2003, *47*(2), 61–69.
[19] Phimchan, P.; Techawongstien, S.; Chanthai, S.; Bosland, P.W. Impact of drought stress on the accumulation of capsaicinoids in *Capsicum* cultivars with different initial capsaicinoid levels. *HortScience* 2012, *47*(9), 1,204–1,209.
[20] Sae-Tang, W.; Nawata, E. Effect of water stress on the growth, physiological response and antioxidative gene expression of grafted sweet pepper plants. *Agr. Nat. Resour*. 2019, *53*, 581–589.
[21] Arom, P.; Jinagool, W. Water deficit and its impacts on physiological traits, growth, and yield of chili (*Capsicum frutescens* L.). Proceeding of the 2nd international conference on science and technology (SUT-IVCST 2021), Suranaree University of Technology: Nakhon Ratchasima, 2021, 477–483.
[22] Borrell, A.K., Hammer, G.L., and Henzell, R. G. Does maintaining green leaf area in sorghum improve yield under drought? II. Dry matter production and yield. *Crop science* 2000, *40*(4), 1,037–1,048.
[23] Yan, J.; He, C.; Wang, J.; Mao, Z.; Holaday, S. A.; Allen, R. D.; Zhang, H. Overexpression of the Arabidopsis 14-3-3 protein GF14*λ* in cotton leads to a "stay-green" phenotype and improves stress tolerance under moderate drought conditions. *Plant and Cell Physiology* 2004, *45*(8), 1,007–1,014.
[24] Sikuku, P.A.; Netondo, G.W.; Onyango, J.C.; Musyimi, D.M. Chlorophyll fluorescence, protein and chlorophyll content of three Nerica rainfed rice varieties under varying irrigation regimes. *ARPN Journal of Agricultural and Biological Science* 2010, *5*(2), 19–25.
[25] Genty, B.; Briantais, J. M., Viera da Silva, J.B. Effects of drought on primary photosynthetic processes of cotton leaves. *Plant Physiol.* 1987, *83*, 360–364.
[26] Tezara, W.; Mitchell, V.; Driscoll, S.; Lawlor, D. Water stress inhibits plant photosynthesis by decreasing coupling factor and ATP. *Nature* 1999, *401*, 914–917.
[27] Christen, D.; Schönmann, S.; Jermini, M.; Strasser, R. J.; Défago, G. Characterization and early detection of grapevine (*Vitis vinifera*) stress responses to esca disease by in situ chlorophyll fluorescence and comparison with drought stress. *Environ. Exp. Bot.* 2007, *60*, 504–514.
[28] Oukarroum, A.; Madidi, S.Ø.E.; Schansker, G.; Strasser, R.J. Probing the responses of barley cultivars (*Hordeum vulgare* L.) by chlorophyll a fluorescence OLKJIP under drought stress and rewatering. *Environ. Exp. Bot*. 2007, *60*, 438–446.
[29] Adams, W.W.III.; Zarter, C.R.; Mueh, K.E.; Amiard, V.; Demmig-Adams, B. Energy dissipation and photoinhibition: a continuum of photoprotection. In *Photoprotection, Photoinhibition, Gene Regulation, and Environment*, Demmig-Adams, B., Adamsa, W.W.III., and Mattoo, A.K., Eds.; Springer: Dordrecht, The Netherlands, 2006, 49–64.
[30] Ahmed, A.F.; Yu, H.; Yang, X.; Jiang, W. Deficit irrigation affects growth, yield, vitamin C content, and irrigation water use efficiency of hot pepper grown in soilless culture. *HortScience* 2014, *49*(6), 722–728.

[31] Jeeatid, N.; Techawongstien, S.; Suriharn, B.; Chanthai, S.; Bosland, P.W. Influence of water stresses on capsaicinoid production in hot pepper (*Capsicum chinense* Jacq.) cultivars with different pungency levels. *Food Chemistry* 2014, *245*, 792–797.

[32] Yang, H.; Liu, H.; Zheng, J.; Huang, Q. Effects of regulated deficit irrigation on yield and water productivity of chili pepper (*Capsicum annuum* L.) in the arid environment of Northwest China. *Irrigation Science* 2018, *36*(1), 61–74.

[33] Khan, A.L.; Shin, J.H.; Jung, H.Y.; Lee, I.J. Regulations of capsaicin synthesis in *Capsicum annuum* L. by *Penicillium resedanum* LK6 during drought conditions. *Scientia Horticulturae* 2014, *175*, 167–173.

[34] Arom, P.; Jinagool, W. Influence of irrigation regimes on physiological traits, growth, yield, and capsaicin in chili. SUT 7th International Colloquium, Institute of Agricultural Technology, Suranaree University of Technology, Nakhon Ratchasima, Thailand, 21-22 August 2022.

[35] Lathifah, F.; Siswanti, D.U. Effects of Water Availability on Physiological Factors of Cayenne Pepper Plant *Capsicum frutescens* L. Proceedings of the 7th International Conference on Biological Science (ICBS 2021): Gadjah Mada University, Indonesia, 2021, 344–349.

JSTR
ASEAN Journal of Scientific and Technological Reports

Research article

Frequency Analysis of High Amplitude δ Scuti Star V593 Lyr by American Association of Variable Stars Observers International Database

Nareemas Chehlaeh[1]*, Tatphicha Promfu[2], and Nusreen Masae[3]

[1] Department of Science, Faculty of Science and Technology, Prince of Songkla University, Pattani, 94000, Thailand; nareemas.c@psu.ac.th
[2] Department of Physics and Materials Science, Faculty of Science, Chiang Mai University, Chiang Mai, 50200, Thailand; tatphicha_p@cmu.ac.th
[3] Independent researcher, 86/2 Juab, Cho I Rong, Narathiwat, 96130, Thailand; nasreen.masae@gmail.com
* Correspondence: nareemas.c@psu.ac.th

Citation:
Chehlaeh, N.; Promfu, T.; Masae, N. Frequency Analysis Analysis of High Amplitude δ Scuti Star V593 Lyr by American Association of Variable Stars Observers International Database. *ASEAN J. Sci. Tech. Report.* **2023**, 26(1), 32-39. https://doi.org/10.55164/ajstr.v26i1.247847.

Article history:
Received: December 12, 2022
Revised: January 20, 2023
Accepted: January 25, 2023
Available online: March 21, 2023

Abstract: The new results of light variability and frequency analysis of a high amplitude δ Scuti star (HADS) V593 Lyr were reported. δ Scuti-type variable stars are fascinating short-period stars with luminosity classes from III to V and spectral types from A0 to F6. Their location on the Hertzsprung-Russell (H-R) diagram is in the classical cepheid instability strip. The photometric data in the *V* filter and clear filter of V593 Lyr were collected from the American Association of Variable Stars Observers (AAVSO) international database. Discrete Fourier transformation and pre-whitening methods were used in the Period04 package to examine time-series light curve data. During 15 observational nights, we obtained 28 times of new light maxima magnitude variability and significant pulsation frequencies for the star. The study found that the fundamental frequency of V593 Lyr is 9.7894180 ± 0.0000002 d^{-1}, corresponding to the main pulsation period of about 0.1021511 d and detected its second to fifth harmonics with a signal-to-noise ratio (S/N) of more than four. A study of the pulsation frequencies and period change of HADS stars can estimate their pulsation modes and evolution. Moreover, HADS stars are suitable targets for understanding asteroseismology, which is the subject that applies a star's pulsations to investigate its internal structure, and the high amplitude stars provide reference points for calculating cosmic distances in the Universe.

Keywords: V593 Lyr; Hight-amplitude δ Scuti; Frequency Analysis; AAVSO

1. Introduction

δ Scuti variable stars are intermediate-mass pulsators located on the Hertzsprung-Russell (H-R) diagram close to the main sequence (MS) and within the classical instability strip. This location corresponds to luminosity classes from III to V and spectral types from A0 to F6. This type of variable star consists of several stages of stellar evolution, including main sequence stars, pre-main sequence (PMS), and post-main sequence stars [1], and within the effective temperature range of $6300 \leq T_{eff} \leq 8600$ K [2]. Pulsation periods of δ Scuti stars range from about haft an hour to 5 hours. The known δ Scuti variables are either a part of the main sequence or are up to three magnitudes above it [3]. From ground-based observations, most of δ Scuti stars are discovered to oscillate in radial and nonradial modes, and their frequencies are within the limits of 5–50 d^{-1}.

The partial ionization of He II causes the κ mechanism, which forces the stellar oscillations [4]. The high amplitude δ Scuti star (HADS) is a subclass of δ Scuti stars and pulsates with amplitude in the *V*-filter of $\Delta V \geq$ 0.3 magnitudes [5]. According to statistics from the catalog of Rodriguez et al. in 2000, the study found 155 HADS stars out of 636 δ Scuti stars in the study, equal to a quarter of all targets [6]. HADS stars are suitable targets for understanding asteroseismology, which is the subject that applies a star's pulsations to investigate its internal structure. The photometric and spectroscopic studies of the pulsation frequency and mode of HADS stars reveal information about the internal structure of the stars. The convective core and surface convection zones of these stars are shallow. Therefore, chemical elements from the convective core have the potential to pierce the surrounding radiative zones, both increasing the amount of hydrogen available for nuclear fusion and the main-sequence stars' lifetimes. Asteroseismology can provide a measurement of this convective overshooting [7]. From a pulsational point of view, HADS stars are the simplest case of stellar oscillators because most pulsate in radial mode. They are good examples of understanding asteroseismology. The physics of stellar oscillations is given in the accepted book Asteroseismology [8].

The object in our study is V593 Lyr, one of δ Scuti stars in the HADS list of Wils et al. [9]. Table 1 presents the list of δ Scuti stars, coordinates, the magnitude in *B* and *V*, the possibility for observation, and the approximate value of the highest altitude of the stars from the horizon at the Thai National Observatory (TNO, 98.4853°E, 18.5725°N).

Table 1. The noticeable δ Scuti targets in the HADS list of Wils et al. [9]. The coordinates and magnitude in the stars' B and V filters were extracted from the SIMBAD database.

No.	δ Scuti star	R.A. J2000 (hh:mm:ss)	Dec. J2000 (dd:mm:ss)	*B* (mag)	*V* (mag)	Possibility for observation at TNO[1]	Approximate highest altitude of the star (deg)
1	V367 Cam	04:40:55.19	+53:38:06.46	11.53	10.80	Yes	55
2	DY Her	16:31:17.95	+11:59:52.46	10.80	10.50	Yes	83
3	EH Lib	14:58:55.92	-00:56:53.01	10.09	9.83	Yes	72
4	SZ Lyn	08:09:35.75	+44:28:17.60	9.73	9.08	Yes	64
5	V593 Lyr	18:32:06.43	+40:35:56.52	12.39	11.66	Yes	68
6	V337 Ori	05:59:20.58	+20:02:07.53	11.79	11.43	Yes	88
7	GSC 1442-1358	12:13:40.78	+17:14:37.81	12.26	11.76	Yes	89
8	GSC 3428-1497	09:21:02.52	+49:05:53.93	9.55	9.29	Yes	59
9	GSC 3832-0152	11:48:42.07	+54:43:07.52	11.72	11.63	Yes	54
10	NSVS 11672463	21:51:52.32	+17:44:43.46	14.00	13.62	Yes	89

[1] TNO is the Thai National Observatory (98.4853°E, 18.5725°N) at Doi Inthanon, Chiang Mai, Thailand.

V593 Lyr (V593 Lyra, GSC 3109-00162, TIC 289325437; R.A. = $18^h\,32^m\,06.435^s$; Dec = +40° 35′ 56.517″) is a HADS star, which was first discovered by Wils et al. [10]. They reported that V593 Lyr has a pulsation period of 0.102145 d in the approximate magnitude range of 12.4-12.9 in the *B* filter. Recently, Gaia Early Data Release 3 (Gaia EDR3) reported the proper motion of μ_α= 0.806 ± 0.018 mas·year^{-1}, μ_δ= -6.808 ± 0.016 mas·year^{-1}, and parallax of 0.6855 ± 0.0141 mas. In 2012, Wils et al. published a list of 64 HADS and presented four values of maximum time of V593 Lyr [9]. Furthermore, there is not much scientific publication on this target compared to other HADS stars in the list.

In the present paper, we reported the new values of 28 times of maxima from 15 observational nights and the light curve and frequency analyses of the HADS V593 Lyr. The paper is organized as follows. Section 2 describes the materials and method. Section 3 presents the results and discussion, including the new light maximum time, the light curve behavior, and frequency analyses. Finally, section 4 reports the conclusions of the recent results of the study.

2. Materials and Methods

2.1 Data and Observations

The photometric data of V593 Lyr in the *V* filter (*V*) and clear filter (*CV*) were collected from the American Association of Variable Stars Observers international database (AAVSO), which is the world's largest and most extensive digital database of variable stars. The primary goal of the database is to organize observations and data of variable stars, made mainly by amateur astronomers from around the world, to assess their accuracy, process them, and make them accessible to students, teachers, educators, and researchers worldwide. The AAVSO is a non-profit international scientific and educational organization where professional, and amateur astronomers collaborate for variable star searching [11].

The scientific quality frames in the study consist of 2,968 frames collected from 15 observational nights in 2010–2021. The data were observed and published by professional and amateur astronomers from several institutes worldwide. The photometric data can be downloaded from the website of the AAVSO database: https://www.aavso.org/data-download. In addition, the HADS V593 Lyr can be observed in Thailand using telescopes at the Thai National Observatory (TNO), Doi Inthanon, Chiang Mai, Thailand. The observatory has been organized by the National Astronomical Research Institute of Thailand (NARIT). The best period for full-night observation at TNO is between the 12th of June and the 3rd of July, with the star's altitude of more than 30 degrees and considering the good sky conditions. The information on CCD observations in the study is presented in Table 2. The last column shows the times maximum light was collected in each observational night.

Table 2. The journal of CCD observations, the light maximum times of V593 Lyr were collected in 2010-2021.

No.	Date of Observation	Filter	Frames	Time Span (hours)	Duration time (HJD+2450000)	Observer code[1]	No. of Maxima
1	08/06/2010	*V*	257	6.8989	5356.60424 - 5356.89045	DKS	2
2	09/06/2010	*V*	295	6.9817	5357.60616 - 5357.89707	DKS	3
3	08/08/2010	*V*	129	3.6803	5782.40865 - 5782.56200	PXR	1
4	25/05/2012	*V*	247	2.8208	6073.39030 - 6073.50783	VMAE	2
5	14/06/2014	*V*	162	4.6494	6823.39120 - 6823.58493	VMAE	1
6	15/04/2015	*V*	221	5.9837	7128.40032 - 7128.64964	VMAE	3
7	12/10/2015	*V*	159	2.2189	7308.25315 - 7308.34561	DUBF	1
8	13/03/2016	*V*	130	5.2058	7461.49786 - 7461.71477	VMAE	2
9	09/08/2018	*V*	68	1.9879	8340.42803 - 8340.51086	VMT	1
10	09/10/2018	*V*	252	3.8326	8401.30103 - 8401.46072	SDWA	2
11	28/05/2020	*CV*	185	3.1950	8998.48036 - 8998.61349	PXR	2
12	03/08/2020	*V*	217	3.5236	9065.49594 - 9065.64275	DFS	2
13	28/05/2021	*CV*	113	4.8821	9363.36094 - 9363.56435	HMB	2
14	24/07/2021	*V*	324	7.1954	9420.31456 - 9420.61436	PMAK, DFS	2
15	30/07/2021	*V*	209	3.8680	9426.29290 - 9426.45407	PMAK	2
-	-	-	2968	66.8941	-	-	28

[1] The AAVSO observer codes: DKS = Shawn Dvorak, PXR = Roger Pickard, VMAE = Maarten Vanleenhove, DUBF = Franky Dubois, VMT = Tonny Vanmunster, SDWA = David Smith, PXR = Roger Pickard, DFS = Sjoerd Dufoer, HMB = Franz-Josef Hambsch, PMAK = Maksym Pyatnytskyy.

2.2 Analyses

During 15 observational nights of V593 Lyr from the AAVSO database, we measured 28 times of maximum light by Kwee and van Woerden fitting [12] on each time of light maximum using the Maxima astronomical program version 27. These 28 maxima and their errors are provided in Table 3. The new times of light maximum are crucial preliminary results to study period variation rate. The first and previous ephemeris for V593 Lyr [10] is:

$$HJD_{Max} = 2452084.4974\ (\pm 0.0003) + 0.1021497\ (\pm 0.0000002)E. \quad (1)$$

Table 3. The light maximum times of V593 Lyr and their accuracies.

No.	HJD (+2450000)	Error (days)	No.	HJD (+2450000)	Error (days)
1	5356.70600	0.00023	15	7461.63274	0.00021
2	5356.80834	0.00027	16	8349.43852	0.00021
3	5357.62547	0.00017	17	8401.32068	0.00020
4	5357.72749	0.00028	18	8401.42233	0.00011
5	5357.82995	0.00031	19	8998.49603	0.00022
6	5782.47251	0.00039	20	8998.59902	0.00024
7	6073.39804	0.00026	21	9065.50765	0.00013
8	6073.50031	0.00012	22	9065.61025	0.00031
9	6823.49497	0.00039	23	9363.38032	0.00042
10	7128.41547	0.00040	24	9363.48287	0.00040
11	7128.51770	0.00018	25	9420.38054	0.00011
12	7128.61984	0.00031	26	9420.58472	0.00013
13	7308.30322	0.00010	27	9426.30509	0.00012
14	7461.53114	0.00028	28	9426.40784	0.00031

We performed a frequency analysis for the light curves of V593 Lyr using the excellent and popular tool Period04 package software [13], based on the discrete Fourier analysis and the pre-whitening techniques. In this procedure, we selected large data strings with well-defined zero points and covered more than one complete cycle. Amplitudes of the light curves are presented as half of the peak-to-peak value. Assuming $mag(t)$ is the magnitude observed at a time t or a measurement of light variation from a star. The fitting formula used for the HADS light curves is in the form [5]:

$$mag(t) = Z + \sum_{i=1}^{n} A_i \sin\left[2\pi(\omega_i t + \emptyset_i)\right], \quad (2)$$

Where Z is zero-point, A_i is amplitude, ω_i is frequency, and $\emptyset_i$ is a phase of the i-th harmonic. Only frequencies that reach the criteria $A_i/\sigma_i > 4$ were used in the fitting [14-15]. Firstly, the dominant frequency was measured using terminal fitting in the Period04 software package. As a criterion for detecting a pulsation frequency, only the peak with S/N larger than four was selected in this procedure and a frequency in the range of 0-100 c/d. Then the residuals were examined for farther signals after removing the main frequency and its additional frequencies. If its S/N is higher than four, the process continues to detect a new frequency. On the other hand, if the value of the S/N is lower than four, the process is terminated [1], then significant frequencies and their analytical errors of the star are reported.

3. Results and Discussion

3.1 Light Curve Behavior

Figure 1 presents the differential magnitude light curve in the *V* and *CV* filters of 15 observational nights in 2010-2021. It shows that the synthetic light curves fit the observational data well. It suggests that the fundamental frequency and its harmonics can explain the pulsation behavior of V593 Lyr. The light variation of V593 Lyr in the *V*-filter is more than 0.3 magnitudes corresponding to the specific characteristics of HADS stars, which have high amplitudes of their light curves of more than 0.3 magnitudes in the *V*-band ($\Delta V \geq 0.3$ mag) [5, 16].

3.2 New Light Maximum Time

The study used adequate quality data from the Johnson *V* and *CV* filters. Based on a visual examination of the light curves, the data has no obvious bad points. The data set used for the Fourier analysis consists of 2,968 data points, covering a time base of 15 observational nights. The light maximum times of V593 Lyr and their errors are presented in Table 3. They are preliminary results for the period change rate (dP/dt) study in the future.

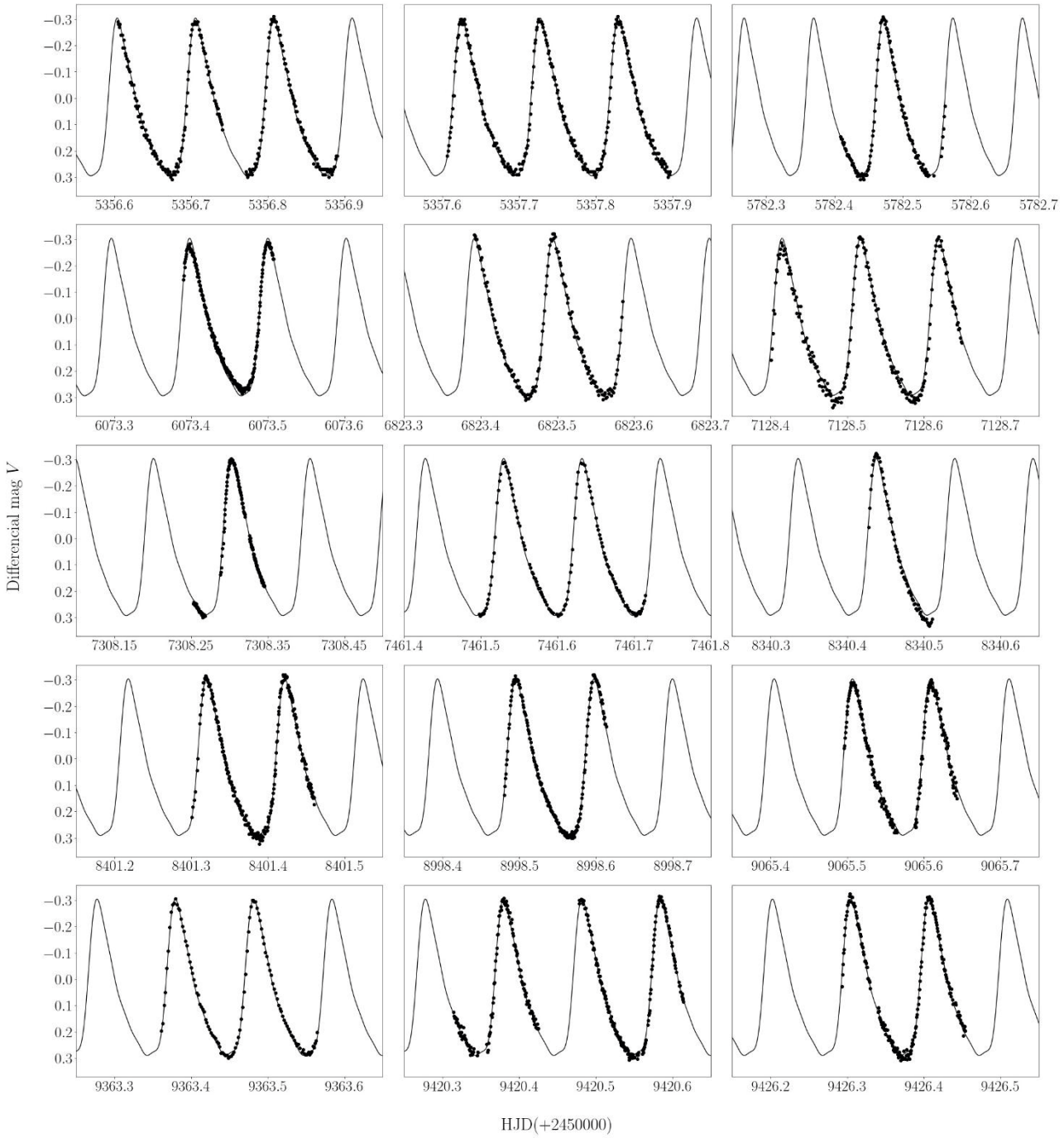

Figure 1. The observed and synthetic light curves in the *V* and *CV* bands of the high amplitude δ Scuti V593 Lyr. These sub-figures present the light curves from the total 15 observational nights. The points represent the observed light curve, and the solid curves show the synthetic light curves fitted with the five significant frequency solutions.

3.3 Frequency Analysis

From the frequency analysis of V593 Lyr, we found a fundamental frequency (f_0) and its four harmonic frequencies ($2f_0, 3f_0, 4f_0, 5f_0$) with the criterion of an S/N ratio larger than four. It was found that the fundamental frequency (f_0) of about 9.7894180 ± 0.0000002 d^{-1} corresponds to the main pulsation period of about 0.1021511 d or 2.4516268 hr, and the second to fifth harmonics of the fundamental frequency were also determined. Frequencies, amplitudes, and phases of the best-fitting sinusoids with their analytical errors are given in Table 4. The uncertainty values of frequency, amplitude, and phase were performed by the Monte

Carlo simulation contained in the Period04 software. After the fundamental frequency (f_0) was detected as the value of 9.7894180 ± 0.0000002 d^{-1}, and the pulsation period was calculated by dividing one over the frequency. Finally, we obtain the star fold's orbital phase diagram by the pulsation period value 0.1021511 d, as presented in Figure 2. The power spectrum of the high amplitude δ Scuti V593 Lyr is presented in Figure 3. The last column of Table 4 shows the frequency ratios between i-th harmonic relative to the fundamental frequency to confirm the relationship between the corresponding frequencies and the fundamental frequency.

Table 4. The results of frequency fitting to the light curves of V593 Lyr includes frequencies, amplitudes, phase, their errors, S/N value, and the ratio between harmonic and fundamental frequencies.

No.	ID	Frequency (d^{-1})	Amplitudes (mmag)	Phase (rad)	S/N	f_n/f_1
1	f_0	9.7894180 ± 0.0000002	259.5 ± 0.4	0.6383 ± 0.0002	121.43	1.0
2	$2f_0$	19.5788338 ± 0.0000005	95.0 ± 0.4	0.6794 ± 0.0006	88.88	2.0
3	$3f_0$	29.368248 ± 0.000001	38.0 ± 0.4	0.762 ± 0.002	57.19	3.0
4	$4f_0$	39.157671 ± 0.000002	19.2 ± 0.4	0.764 ± 0.003	27.80	4.0
5	$5f_0$	48.947098 ± 0.000005	9.5 ± 0.4	0.756 ± 0.006	15.82	5.0

In this study, only one dominant frequency and its four harmonics were detected with the criteria of an S/N of more than four. On the other hand, independent frequencies were not detected from the frequency analysis. It can be concluded that the HADS V593 Lyr pulsates in a multiple-frequency radial mode, which means it symmetrically increases and decreases in stellar radius during each pulsation period. This type of pulsation was also found in other HADS stars, for instance, GP And [5], V460 And [17], and YZ Boo [18]. In HADS stars, slow rotation is typically required for high-amplitude radial pulsation [19].

HADS stars are the H-R diagram's transitional objects between high-amplitude Cepheids and low-amplitude pulsating MS stars. They pulsate in one or several radial modes with high amplitudes [1], and about 0.24% of all δ Scuti stars are in our Milky Way Galaxy [20]. In addition to radial pulsations, several investigations indicate that low-amplitude nonradial modes may also be present in HADS stars.

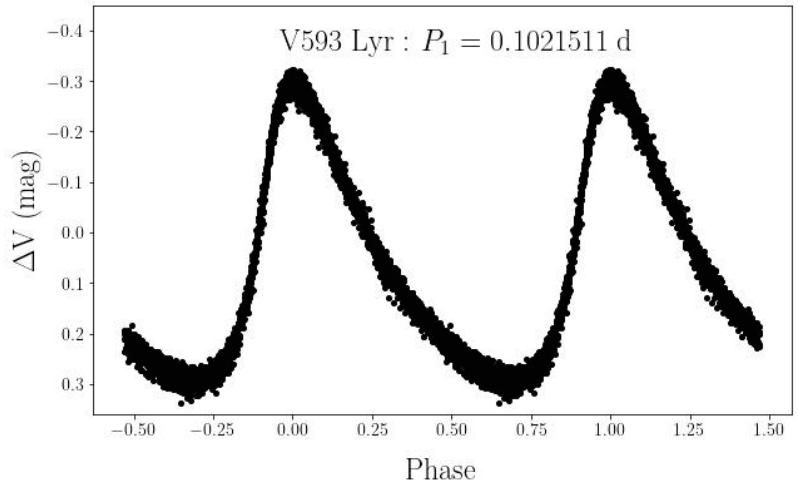

Figure 2. The orbital phase of V593 Lyr folded with the main period of 0.1021511 d.

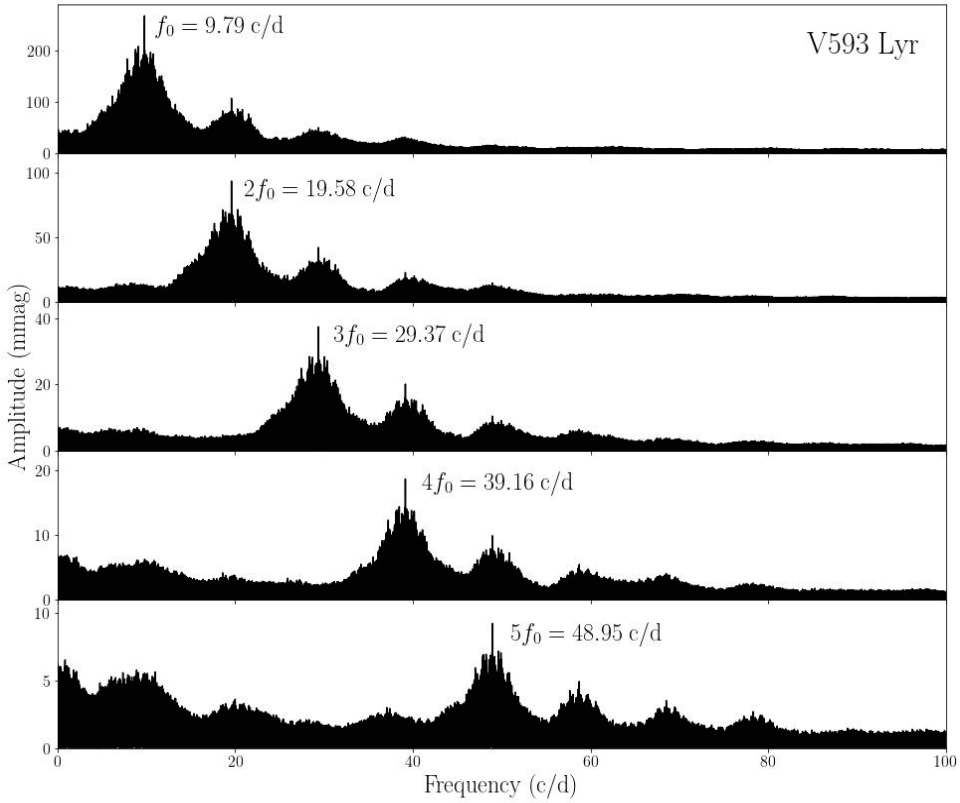

Figure 3. Power spectrum of the high amplitude δ Scuti V593 Lyr. The first top panel is a spectrum of the fundamental frequency. The lower four panels are spectrums of the second to fifth harmonics of the dominant frequency, respectively.

This step detects the second to fifth harmonics of the dominant frequency. From the value of the significant frequencies of the star, we can confirm that V593 Lyr is a HADS star with multiple frequency radial pulsation. It is limited research publications about V593 Lyr after the first discovery as GSC 3109-00162 in 2002 [10] and after the work of Wils et al. in 2012 [9]. Additional data from photometric and spectroscopic observations are requisite for more complete and accurate results regarding HADS stars. We intend to use the Thai National Telescope (TNT) and the Thai Regional Telescope (TRT) to observe HADS stars. With these facilities in Thailand, we can observe many HADS targets (see Table 1), collect a large amount of data to obtain highly accurate ground-based observations, and gather photometric and spectroscopic data for further research.

4. Conclusions

The new time-series CCD observations of V593 Lyr were collected using AAVSO international database covering 15 nights from June 2010 until July 2021. We measured 28 new light maximum times for V593 Lyr as preliminary results for the period change rate study in the future. In frequency analysis, it was found that the dominant frequency of V593 Lyr of about 9.7894180 ± 0.000002 d^{-1} corresponds to the pulsation period of 0.1021511 d.

5. Acknowledgements

We gratefully acknowledge the contributions made by observers worldwide to the American Association of Variable Stars Observers (AAVSO) international database used in this research to study δ Scuti variable stars. We thank the observers of the Working Group on Variable Stars of the Belgian Vereniging Voor Sterrenkunde (VVS, Society for Astronomy). This research used information from the SIMBAD database, operated by CDS in Strasbourg, France, and the NASA Astrophysics Data System. Period04 was used in our frequency analysis.

Author Contributions: Conceptualization, C.N.; methodology, C.N. and P.T.; software, P.T.; formal analysis, C.N., P.T. and M.N.; investigation, C.N., P.T. and M.N.; writing—original draft preparation, C.N., M.N.; writing—review and editing, C.N., P.T. and M.N.

Funding: This research received no external funding.

Conflicts of Interest: The authors declare no conflict of interest.

References

[1] Netzel, H.; Pietrukowicz, P.; Soszynski, I.; Wrona, M. Frequency analysis of δ Scuti stars towards the Galactic bulge. *Mon. Not. R. Astron*. 2021, *510(2)*, 1748–1764.

[2] Uytterhoeven, K.; Moya, A.; Grigahcène, A.; Guzik, J.A.; Gutiérrez-Soto, J.; Smalley, B.; Handler, G.; Balona, L.A.; Niemczura, E.; Fox Machado, L.; Benatti, S.; Chapellier, E.; Tkachenko, A.; Szabó, R.; Suárez, J.C.; Ripepi, V.; Pascual, J.; Mathias, P.; Martín-Ruíz, S.; Lehmann, H.; Jackiewicz, J.; Hekker, S.; Gruberbauer, M.; García, R.A.; Dumusque, X.; Díaz-Fraile, D.; Bradley, P.; Antoci, V.; Roth, M.; Leroy, B.; Murphy, S.J.; De Cat, P.; Cuypers, J.; Kjeldsen, H.; Christensen-Dalsgaard, J.; Breger, M.; Pigulski, A.; Kiss, L. L.; Still, M.; Thompson, S.E.; Van Cleve, J. The Kepler characterization of the variability among A- and F-type stars I. General overview. *Astron. Astrophys.* 2011, *534*, A125.

[3] Baglin, A.; Breger, M.; Chevalier, C.; Hauck, B.; Le Contel, J.M.; Sareyan, J.P.; Valtier, J.C. Delta Scuti stars. *Astron. Astrophys*. 1973, *23*, 221–240.

[4] Chang, S.W.; Protopapas, P.; Kim, D.W.; Byun, Y.I. Statistical properties of Galactic δ Scuti stars: revised. *Astron. J.* 2013, *145*, 132.

[5] Zhou, A.Y.; Jiang, S.Y. Period and amplitude variability of the high-amplitude δ Scuti star GP Andromedae. *Astron. J.* 2011, *142*, 100.

[6] Rodriguez, E.; Lopez-Gonzalez, M.J. SX Phe stars in globular clusters. *Astron. Astrophys.* 2000, *359*, 597–600.

[7] Dziembowski, W. A.; Pamyatnykh, A. A. *Astron. Astrophys.* 1991, *248*, L11–L14

[8] Aerts, C.; Christensen-Dalsgaard, J.; Kurtz, D.W. A*steroseismology*, 1st ed.; Springer Dordrecht, 2010; 1–866.

[9] Wils, P.; Panagiotopoulos, K.; Van Wassenhove, J.; Ayimamitis, A.; Nieuwenhout, F.; Robertson, C.W.; Vanleenhove, M.; Hambsch, F.J.; Hautecler, H.; Pickard, R.; Baillien, A.; Staels, B.; Kleidis, S.; Lampens, P.; Van Cauteren, P. Photometry of high-amplitude Delta Scuti stars. *Inf. Bull. Var. Stars.* 2012, *6015*, 1–8.

[10] Wils, P.; Van Cauteren, P.; Groenendaels, R. The high amplitude Scuti variable star GSC 3109-00162. *Inf. Bull. Var. Stars.* 2002, 142, 54–56.

[11] Percy, J.R.; Mattei, J.A. The AAVSO database of variable star observations. *Astrophys. Space Sci*. 1993, *210*, 137–138.

[12] Kwee, K.K.; van Woerden, H. A method for computing accurately the epoch of minimum of an eclipsing variable. *Bull. Astron. Inst. Netherlands* 1956, 12, 327–330.

[13] Lenz, P.; Breger, M. Period04 user guide. *Comm. in Asteroseismology* 2005, *146*, 53-136.

[14] Breger, M.; Stich, J.; Garrido, R.; Martin, B.; Jiang, S.Y.; Li, Z.P.; Hube, D.P.; Ostermann, W.; Paparo, M.; Scheck, M. Nonradial pulsation of the Delta-Scuti Star Bu-Cancri in the Praesepe cluster. *Astron. Astrophys* 1993, *271*, 482–486.

[15] Kuschnig, R.; Weiss, W.W.; Gruber, R.; Bely, P.Y.; Jenkner, H. Microvariability survey with the Hubble space telescope fine guidance sensors: exploring the instrumental properties. *Astron. Astrophys* 1997, *328*, 544–550.

[16] Rodriguez, E.; Breger, M. δ Scuti and related stars: Analysis of the R00 Catalogue. *Astron. Astrophys* 2001, 366, 178-196.

[17] Alton, K. B.; Stępień, K. CCD Photometry, light curve deconvolution, period analysis, kinematics, and evolutionary status of the HADS variable V460 Andromedae. *JAAVSO* 2019, *47*, 53–65.

[18] Abdel-Sabour, M.; Nouh, M.I.; Ata, S.; Darwish, M. Frequency and photometric analysis of the short period pulsating star YZ Boo. *NRIAG J. Astron. Geophys.* 2021, *10*, 416–422.

[19] Breger, M. Nonradial and radial period changes in the δ Scuti star 4 CVn I. 700+ nights of photometry. *Astron. Astrophys* 2016, *592*, A97.

[20] Lee, Y.H.; Kim, S.S.; Shin, J.; Lee, J. Incidence of high-amplitude δ Scuti-type variable stars. *Publ. Astron. Soc. Japan* 2008, 60, 551–555.

JSTR
ASEAN Journal of Scientific and Technological Reports

Research article

Experimental Study on Convective Heat Transfer and Pressure Drop Characteristics of an Alternating Cross-Section Flattened Tube with Different Twist Angle

Kunlakarn Warnropru[1], Jatuporn Kaew-On[2] and Nares Chimres[3*]

[1] Energy Engineering Program, Faculty of Engineering, Thaksin University, Phatthalung, 93210, Thailand; kunlakarn.fah@gmail.com
[2] Mechanical Engineering Program, Faculty of Engineering, Thaksin University, Phatthalung, 93210, Thailand; kaew_on@yahoo.com
[3] Mechanical Engineering Program, Faculty of Engineering, Thaksin University, Phatthalung, 93210, Thailand; nares_ch@yahoo.com
* Correspondence: nares_ch@yahoo.com

Citation:
Warnropru, K.; Kaew-On, J.; Chimres, N. Experimental Study on Convective Heat Transfer and Pressure Drop Characteristics of an Alternating Cross-Section Flattened Tube with Different Twist Angle. *ASEAN J. Sci. Tech. Report.* **2023**, *26*(1), 40-51. https://. 10.55164/ajstr.v26i1.248061

Article history:
Received: December 31, 2022
Revised: February 7, 2023
Accepted: February 10, 2023
Available online: March 21, 2023

Abstract: In this research, the heat transfer coefficient (HTC) and pressure drop of alternating cross-section flattened (ACF) tubes were investigated experimentally and compared with the same parameters of a circular tube. Three different ACF tubes were fabricated from circular copper tubing with an internal diameter of 4.5 mm, a thickness of 1 mm, and a length of 400 mm. The twist angles were 30, 45, and 90°. The experimental ranges covered a mass flux of 729–1,434 kg/m^{2}s and a heat flux of 12–30 kW/m^2. The results showed that the HTC and pressure drop increased with mass flux. The HTC decreased with increments of heat flux, but the pressure drop did not change. The HTC and pressure drop of the ACF tubes were higher than those of the circular tube. The ACF tube with 90° twist angles produced the highest HTC, and the thermal performance of that tube was about 27% better than the thermal performance of the circular tube.

Keywords: Alternating Cross-section Flattened (ACF) Tube; Heat Transfer Coefficient (HTC); Pressure Drop; Single-phase Heat Transfer

1. Introduction

Heat exchangers are widely used in industrial and household applications. They can be found in refrigerating systems, air-conditioning systems in power plants, electronic cooling systems, air-conditioners, and water heaters. Therefore, improvements in the thermal performances of heat exchangers can provide widespread benefits. Methods of increasing heat transfer can be divided into three categories: active, passive, and compound techniques [1]. The passive technique is generally preferred because this method does not need any external energy to enhance heat transfer. The objective can be achieved by inserting twinned coil/twisted tape into the tube [2-6], adding nanoparticles to the base fluid [7-11], and modifying the tube structure of the heat exchanger, such as with a corrugated tube [12-14], a micro-fin tube [15-16], a flattened tube [17-18], a twisted flattened tube [19], or a twisted oval tube [20-21]. These reports concluded that modifying the tube shape to enhance the heat transfer of the internal flow was an attractive approach.

In 2020, Sajadi and Talebi [22] investigated the convective heat transfer, pressure drop, and efficiency of ZnO/water nanofluid flowing in alternating elliptical axis (AEA) tubes in a Reynolds number (Re) range of 400 to 1,900. The rotation angle of the AEA was 90° along the tube length. They found that

increasing the tube flattening increased the heat transfer rate. The heat transfer and pressure drop of the AEA tube were greater than that of a circular tube. In addition, a tube with medium flattening was the most efficient among the tested tubes. In 2022, they investigated the heat transfer and pressure drop of alternating flattened (AF) tubes filled with a TiO_2/oil nanofluid. Experiments were conducted on three different AF tubes with oil as the base fluid carrying TiO_2 nanoparticles at 1% and 2% volumetric concentrations between 400 and 1,800 Re. They reported that the heat transfer and pressure drop of the AF tubes were higher than those of a circular tube. Flattening the tube affected heat transfer and pressure drop, which were enhanced by increasing the concentration of TiO_2 nanoparticles [23].

Luo and Song [24] investigated the thermal performance enhancement of a double-tube heat exchanger with twisted annulus formed by counter-twisted oval tubes. The studied twisted oval tubes were configured with aspect ratios of 0.4, 0.5, and 0.6, and thermal performances were compared with the performances of conventional oval tubes. They found that the Nusselt number (Nu) and friction factor (f) increased by up to 157% and 118%, respectively.

Farsi et al. [25] examined the heat transfer and flow characteristics of an AF tube with a 90° twist angle. The factors of interest were straight pitch (a), transient length (b), and minimum axis (c). The numerical study focused on the laminar flow conditions within a Re range from 500 to 1,500. They found that the minimum axis produced the largest effects, followed by the transient length and straight pitch. The model tube with a = 10, b = 5, and c = 5.5 mm produced the best thermal performance factor of 2.27. Furthermore, Babaei et al. [26] conducted an experiment that simulated solar pond conditions. They evaluated the performance of serpentine AF coils with the same geometric factors (a), (b), and (c) as [25]. The results found that the deeply flattened (c) had the most effect, followed by (b) and (a), respectively.

Rukruang et al. [27] studied the heat transfer coefficient (HTC) and pressure drop of water flowing through a 90° alternating cross-section flattened (ACF) tube compared with a circular tube. The result showed that the HTC and flow resistance of the ACF tube were higher, and the thermal performance was 3.4 times better. Moreover, vortices were produced at the curved wall of the ACF tube and intensified in the flow direction. They reported that an alternating cross-section tube produced secondary flow and turbulence intensity through the tube curvature. Multi-longitudinal vortices formed along the length of the tube, which produced a significant enhancement in the heat transfer performance of the tube [28]. Furthermore, their study investigated the air-side performance of ACF tube heat exchangers with three hydraulic diameters of 4.16, 4.75, and 5.20 mm. All the ACF tube heat exchangers produced better heat transfer than circular tube heat exchangers. The 5.20 mm ACF tube provided the best heat transfer rate and pressure drop [29].

These previous studies have shown that flattening the tube increases the convective heat transfer potential of fluid near the tube wall by creating secondary flows and by increasing the turbulence of the flow. The characteristics of an ACF tube's cross-section area generate vortices and improve the mixing of fluids inside the tube. However, the pressure drop is also increased. Therefore, the heat transfer and the pressure drop of ACF tubes must be studied to improve thermal performance. Moreover, the effect of the twist angle of the ACF tube on heat transfer is very interesting, but little has been published about it.

2. Methodology

2.1 Experimental apparatus

The experimental study determined the HTC and pressure drop of single-phase water flowing inside ACF tubes with twist angles of 30° (ACF-30), 45° (ACF-45), and 90° (ACF-90). The ACF tubes were formed by pressing a circular copper tube with an internal diameter of 4.5 mm, a thickness of 1 mm, and a length of 400 mm (Fig. 1). The main components of the experimental apparatus consisted of a test section, a hot-water loop, a cold-water loop, a control panel, and a data acquisition system (Fig. 2). The detailed configurations of the ACF tubes are presented in Fig. 3(a-c).

Figure 1. The circular and alternating cross-section flattened (ACF) tubes

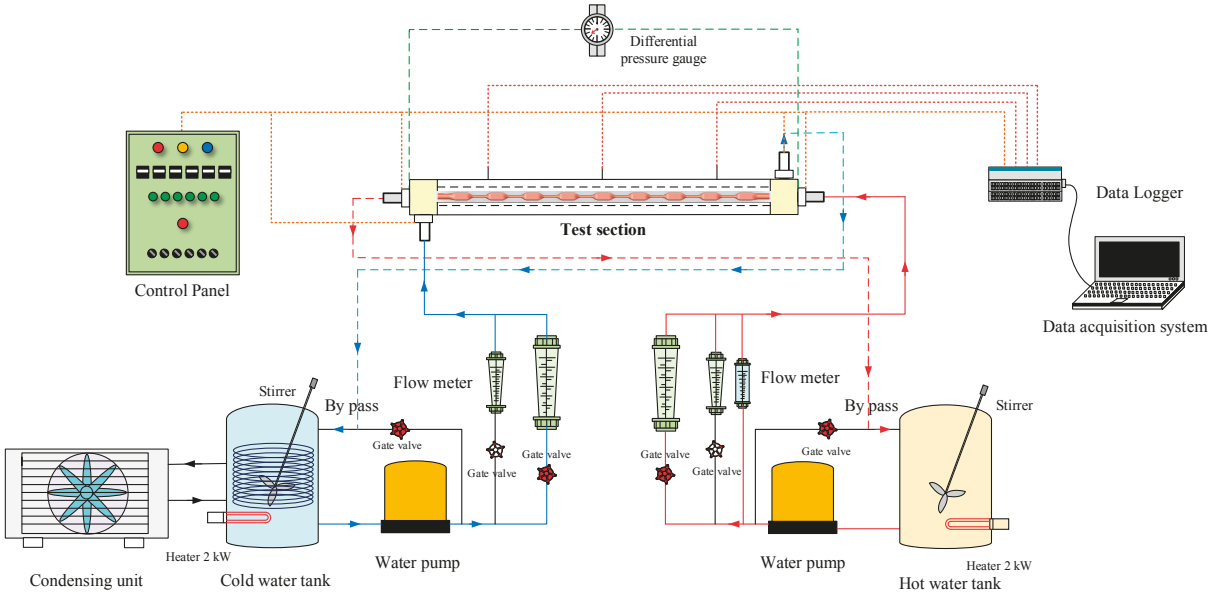

Figure 2. Schematic diagram of the experimental apparatus

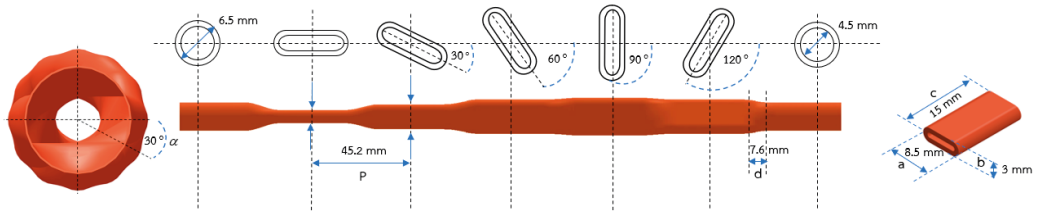

(a)

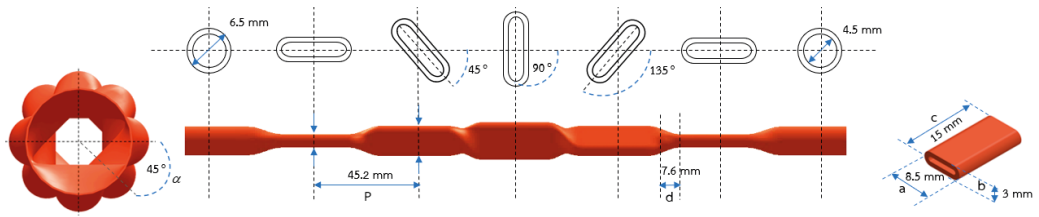

(b)

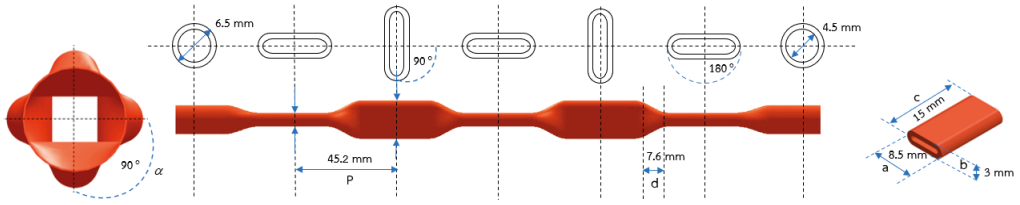

(c)

Figure 3. Configurations of alternating cross-section flattened tubes with twist angles of 30 ° (ACF-30) (a), 45° (ACF-45) (b), and 90° (ACF-90) (c)

The water in the hot-water loop was heated by an electrical heater and driven by a water pump through a flow meter to the inner tube of the test section. The hot water exchanged heat with the cold water flowing outside the ACF tube in the cold-water loop. A water pump drove the water in the cold-water loop through the shell in the test section. Seven thermocouples were installed: four at the headers and three along the wall of the ACF tube. A data logger collected all temperature measurements. The test section was a counterflow double-tube heat exchanger (Fig. 4). The outside of the test section was insulated with rubber insulation. The length between the two pressure taps was 400 mm, and a differential pressure gauge detected the pressure drop across the test section. The geometric configurations of the tested tubes and the test conditions are shown in Tables 1 and 2, respectively. Moreover, the direct measurement uncertainties and maximum experiment uncertainty are demonstrated in Table 3.

Table 1. Geometric configurations of the experimental tubes.

Tube Name	L (mm)	$D_{h,i}$ (mm)	a (mm)	b (mm)	c (mm)	d (mm)	P (mm)	α (degree)
Circular	400	4.50	-	-	-	-	-	-
ACF-30	400	1.96	8.50	3.00	15.00	7.60	45.20	30
ACF-45	400	2.05	8.50	3.00	15.00	7.60	45.20	45
ACF-90	400	2.18	8.50	3.00	15.00	7.60	45.20	90

Table 2. Test conditions.

Parameter	Operating conditions
Inlet water temperature $(^{\circ}C)$	30-40
Mass flux (kg/m²s)	729-1,434
Heat flux (kW/m²)	12-30

Table 3. Uncertainties of measurement devices and calculated parameters.

Parameter	Uncertainty
T-type thermocouple	$0.1\,^{\circ}C$
Flow meter of water	3% of full scale
Differential pressure gauge	1.6% of full scale
Heat transfer rate at test section $(\dot{Q}_{TS})$	14.87%
Heat transfer rate at preheater $(\dot{Q}_{PH})$	10.51%
Reynolds number (Re)	3.00%
Heat transfer coefficient (h_i)	9.82%
Nusselt number (Nu)	4.72%
Friction factor (f)	6.21%

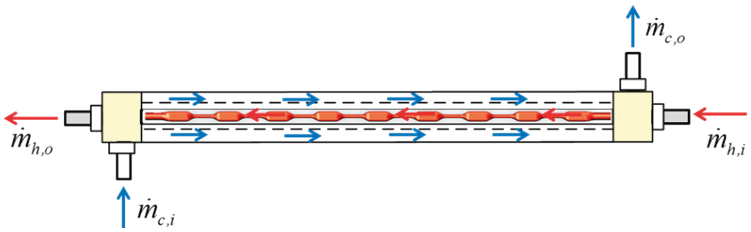

Figure 4. Diagram of the counterflow in the test section

2.2 Data Reduction

The data reduction of this experiment was classified into the following three categories.

2.2.1 Heat transfer

The heat transfer between the hot fluid and the cold fluid was calculated from

$$\dot{Q} = \dot{m}C_p(T_i - T_o) \tag{1}$$

where $\dot{Q}$ is the heat transfer rate, $\dot{m}$ is the mass flow rate of the fluid, T is the temperature of the fluid, and i and o are defined as the inlet and outlet of the test section, respectively.

The overall heat transfer coefficient was calculated as

$$U = \frac{\dot{Q}}{A \cdot LMTD} \tag{2}$$

where U is the overall heat transfer coefficient, A is the heat transfer area, and $LMTD$ is the log mean temperature difference.

The total thermal resistance of the ACF tube was determined from

$$\frac{1}{UA} = \frac{1}{h_o A_o} + \frac{1}{2\pi kL}\ln\left[\frac{D_{h,o}}{D_{h,i}}\right] + \frac{1}{h_i A_i} \tag{3}$$

where h_o is the heat transfer coefficient at the outside tube; A_i and A_o are the inner and outer surface area of the tube, respectively; k is the thermal conductivity of the tube; L is the total tube length, $D_{h,i}$ and $D_{h,o}$ are the inner and outer hydraulic diameter of the tube; h_i is inside heat transfer coefficient.

Since the ACF tube is a non-circular tube, the hydraulic diameter must be calculated. The hydraulic diameter was determined by

$$D_h = \frac{4A_{c,avg}}{p} \tag{4}$$

where $A_{c,avg}$ is the average cross-section area of the tube and p is the wetted perimeter of the tube.

2.2.2 Pressure drop

The total pressure drop (ΔP_{total}) is obtained from the sum of four pressure drop components as follows:

$$\Delta P_{total} = \Delta P_f + \Delta P_a + \Delta P_{cont} + \Delta P_{\exp} \tag{5}$$

Where ΔP_f is the frictional pressure drop, ΔP_a is the acceleration pressure drop, ΔP_{cont} is the sudden contraction pressure drop, and $\Delta P_{\exp}$ is the sudden enlargement pressure drop.

However, in the case of a single-phase horizontal flow such as the tested system, the acceleration pressure drop can be ignored. Moreover, the sudden contraction and sudden enlargement pressure drop are

very small compared to the frictional pressure and thus were not considered in this study. Therefore, the total pressure drop was represented as

$$\Delta P_{total} = \Delta P_f \tag{6}$$

The pressure drop of flow in the tube was determined by using the Darcy-Weisbach equation,

$$\Delta P = f \frac{L}{D_h} \rho \frac{v^2}{2} \tag{7}$$

where ΔP is the pressure drop, f is the Darcy friction factor, L is the tube length, D_h is the hydraulic diameter of the tube, ρ is the density of the fluid, and v is the average velocity.

The friction factors (f) were expressed as the calculated frictional pressure drop (ΔP_f) as

$$f = \frac{2D_{h,i}\Delta P}{L\rho v^2} \tag{8}$$

2.2.3 Thermal enhancement factor

Thermal enhancement factors (TEF) were calculated as the ratio between the Nusselt number and the friction factor of each ACF tube and the circular tube [30-31], using the following equation:

$$TEF = \frac{Nu_{ACF} / Nu_{cir}}{(f_{ACF} / f_{cir})^{1/3}} \tag{9}$$

Where Nu_{cir} and f_{cir} are respectively the Nusselt number and friction factor of the circular tube, and Nu_{ACF} and f_{ACF} are respectively the Nusselt number and friction factor of the ACF tube.

3. Results and Discussion

3.1 Validation of the experimental apparatus

The experimental apparatus was validated by comparing the experimental results with existing correlations. The selected parameters were the HTC and the frictional pressure drop of water flowing through the circular tube. The HTCs obtained in this experiment were compared with the correlations of Dittus-Boelter (1930), Colburn (1933), Petukhov (1970), and Gnielinski (1976). The frictional pressure drops obtained compared with the correlations of Moody (1947), Altshul (1952), Petukhov (1970), Churchil (1973), and Haaland (1983).

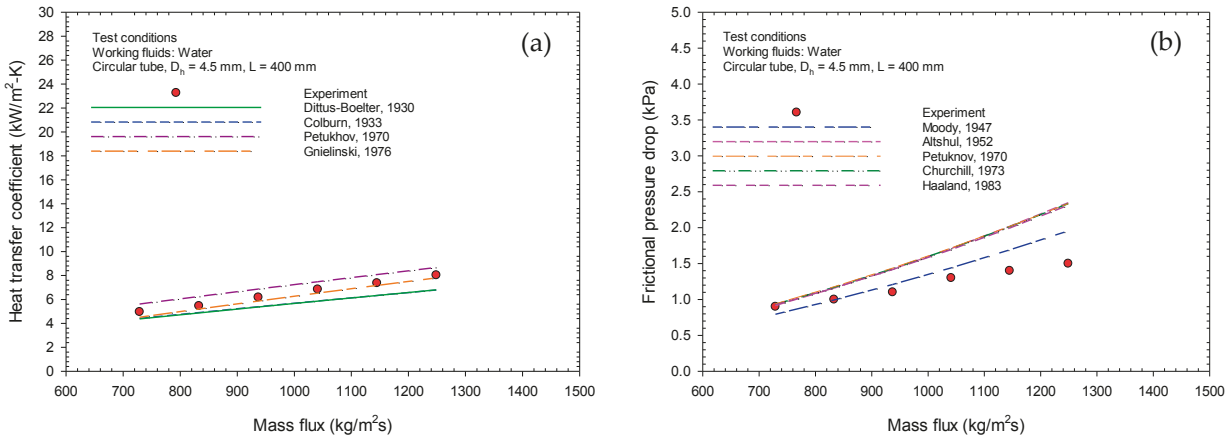

Figure 5. Comparison with existing correlations of the effect of mass flux on (a) the heat transfer coefficient and (b) the frictional pressure drop in the present study

It was found that when the mass flux was increased, the HTC and the pressure drop from friction increased. The experimental HTCs were similar to the HTCs obtained by Gnielinski (1976), with an average error of 4.77% (Fig. 5). The experimental frictional pressure drops were lower than those obtained in the previous works, but the trend of change was similar. The experimental results were closest to those of Moody (1947), with an average error of 14.02%.

3.2 Effect of heat flux on the HTC and pressure drop

The effects of heat flux on HTC and pressure drop were investigated for the ACF and circular tubes. The inlet water temperature (IWT) was fixed at 35 °C . The mass flux range was 800-900 kg/m²s. The four different heat fluxes in this investigation were 13, 17, 21, and 25 kW/m².

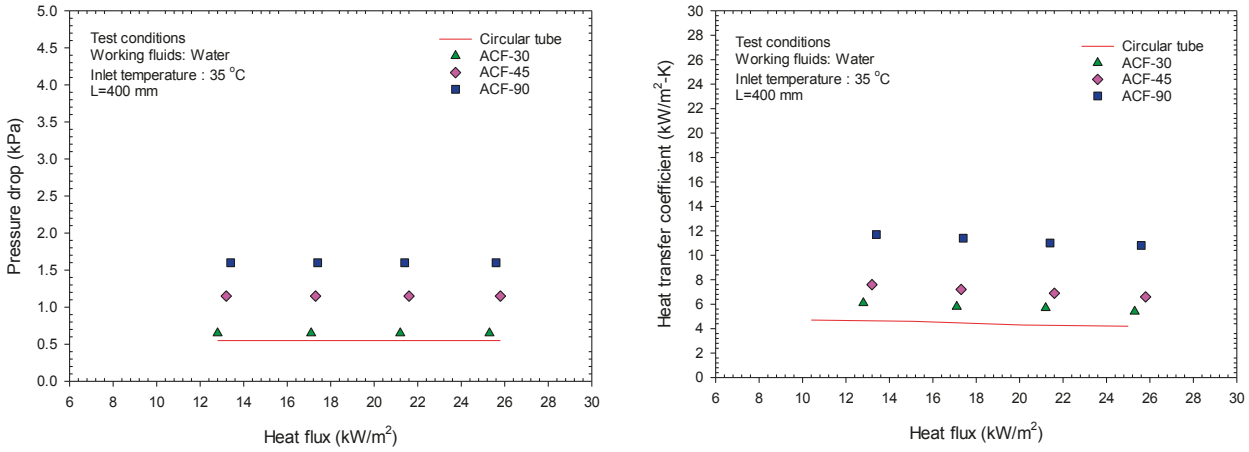

(a) (b)

Figure 6. Effect of heat flux on (a) the pressure drop and (b) the heat transfer coefficient in a circular tube and alternating cross-section flattened tubes with twist angles of 30° (ACF-30), 45° (ACF-45) and 90° (ACF-90)

Increases in heat flux did not affect the pressure drop. The pressure drop was larger in all the ACF tubes than in the circular tube (Fig. 6(a)). The largest pressure drop was observed in the ACF-90, followed by the ACF-45 and ACF-30. The mean pressure drop of the ACF-90 was about 190.91% higher than that of the circular tube. The mean pressure drops of the ACF-45 and ACF-30 were 109.09% and 18.18% higher than the mean pressure drop of the circular tube. Regarding the twist angle, the ACF-90 provided the best HTC because the change in the internal cross-section area of the ACF-90 was more sudden. The change in the cross-section area of the ACF-45 was less than the change in the ACF-90 but greater than the ACF-30 (Fig. 7). The different tube structures caused different pressure drops. The change in pressure drop is greater when the change in the cross-sectional area of the tube is greater. Therefore, the ACF-90 gave the largest pressure drop, followed by the ACF-45 and ACF-30, respectively. The pressure drop in the circular tube was the lowest because the cross-sectional area of a circular tube is constant.

Increases in heat flux resulted in slight decreases in the HTC. All three ACF tubes gave a higher HTC than the circular tube (Fig. 6(b)). The ACF-90 provided the highest HTC, followed by the ACF-45 and ACF-30. The average HTC of the ACF-90 was about 152.43% higher than that of the circular tube. The average HTCs of the ACF-45 and ACF-30 was 58.72% and 28.91% higher than the average HTC of the circular tube, respectively. The fluid flowing in the outer tube could not absorb the heat so efficiently from the surface of the circular inner tube because the hottest fluid, in the mainstream at the center of the inner tube, was far from the tube surface. In the ACF tubes, the flow of fluid was different. The flattened shape of the inner tube brought the hottest fluid closer to the inner tube surface, so the colder fluid in the outer tube could absorb the heat of the fluid in the ACF tubes better than the heat of the fluid flowing in the circular tube.

Since the variation in the change of the cross-section area of the ACF-90 is very high, the turbulence of the heated fluid is increased more. The turbulence of the heated fluid in the inner tube directly affects the HTC; therefore, the HTC produced by the ACF-90 was highest, followed by the HTC produced by the ACF-45, the ACF-30, and finally, the circular tube.

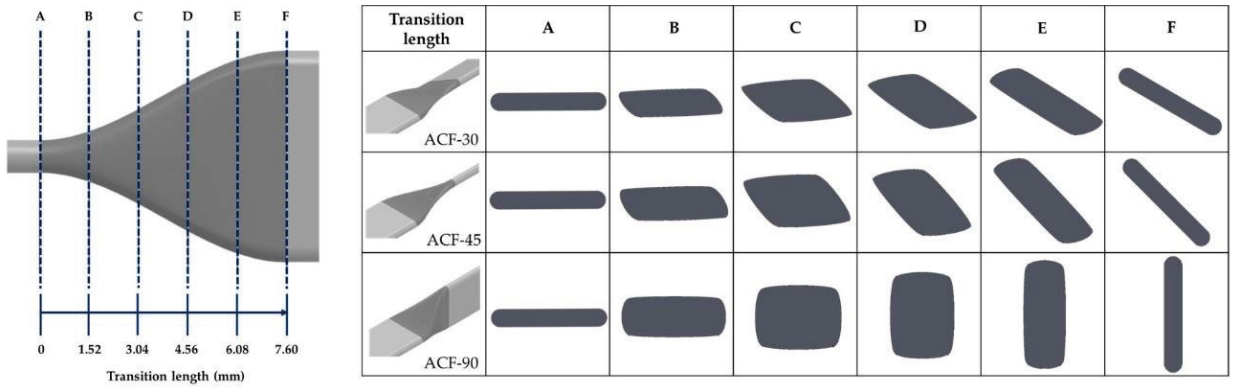

Figure 7. The cross-section area variation in the transition region of the alternating cross-section flattened (ACF) tubes

3.3 Effect of mass flux on the HTC and pressure drop

The effects of mass flux were investigated on the HTC and pressure drop. The mass flux affected both the HTC and pressure drop. The HTC and pressure drop increased when the mass flux increased (Fig. 8). The effects of the ACF tube twist angle on the HTC and pressure drop at different mass fluxes showed the same tendency as the effect of twist angles at different heat fluxes. The mass flux range in this investigation was 729-1,434 kg/m^{2}s at an inlet temperature of 35 $^\circ$C , while the heat flux range was 12.7-15.2 kW/m^2.

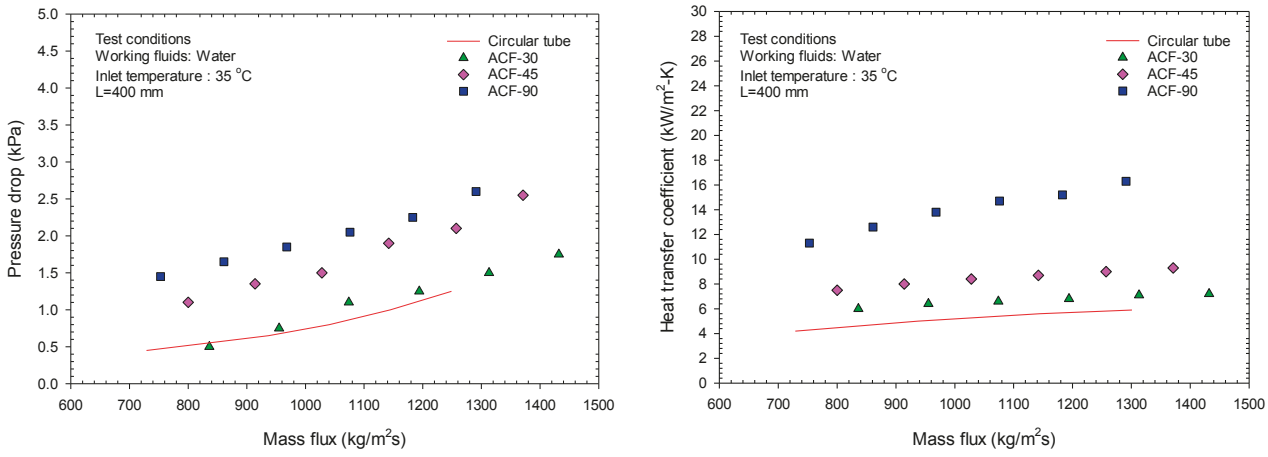

(a) (b)

Figure 8. Effect of mass flux on (a) the pressure drop and (b) the heat transfer coefficient of a circular tube and alternating cross-section flattened tubes with twist angles of 30° (ACF-30), 45° (ACF-45), and 90° (ACF-90)

3.4 Effect of the inlet water temperature on the HTC and pressure drop

The inlet water temperature (IWT) effects on the HTC and pressure drop were investigated (Fig. 9). The IWTs in this study were 30, 35, and 40 $^\circ$C under 17 kW/m^2 of heat flux and 800 kg/m^{2}s of mass flux.

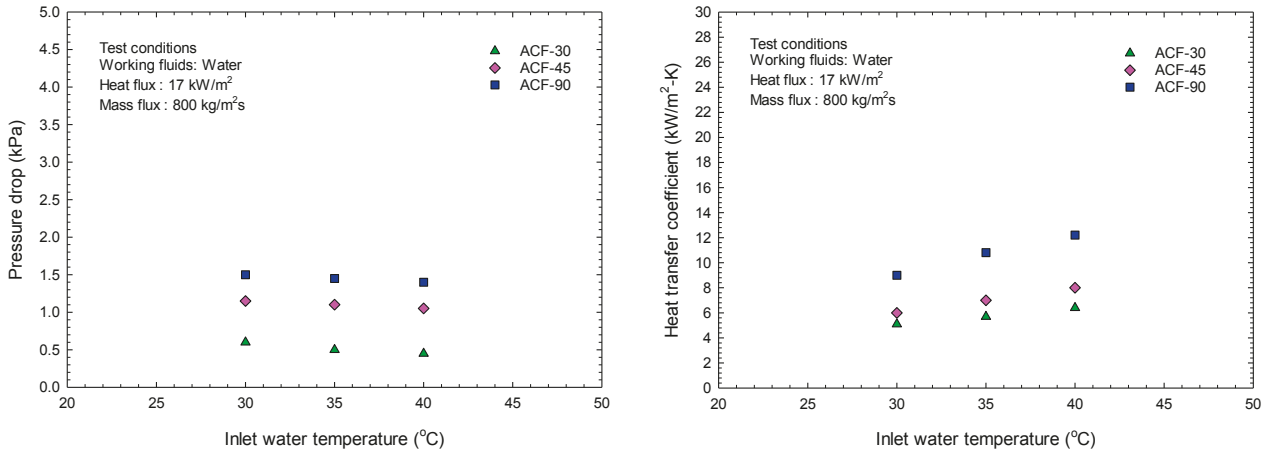

Figure 9. Effect of the inlet water temperature on (a) the pressure drop and (b) the HTC of a alternating cross-section flattened tubes with twist angles of 30° (ACF-30), 45° (ACF-45), and 90° (ACF-90)

The IWT affected the HTC and pressure drop, but the change trends differed. The HTC increased when the IWT increased, but the pressure drop decreased when the IWT increased (Fig. 9). Some thermal properties of water vary with the water temperature. The thermal conductivity of water increases when the temperature increases, which mainly affects the HTC. On the other hand, as the temperature of water increases, its viscosity decreases, which causes the pressure drop to decrease as the IWT increases.

3.5 Performance index comparison

The performance index (PI) was determined by the TEF. The TEF as a function of the Re is shown for each tube in Fig. 10.

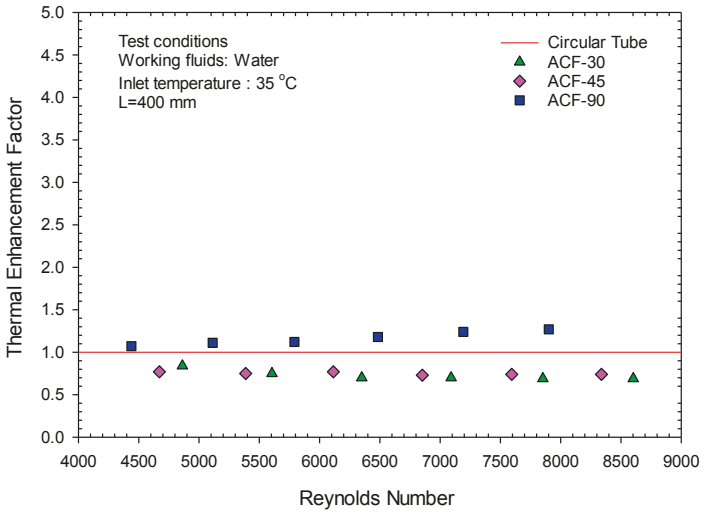

Figure 10. The TEF with Reynolds numbers of each tube

The results show that only the ACF-90 gave a higher TEF than the circular tube. The other ACF tubes produced lower TEFs than the circular tube. Although the HTCs of the ACF-45 and ACF-30 were higher than the HTC of the circular tube, the increases in friction factors were greater. As a result, the TEFs of these ACF tubes were lower than the TEF of the circular tube. The ACF-90 produced a TEF of 1.27, which was 27% larger than the TEF of the circular tube.

4. Conclusions

The flow and heat transfer characteristics of water flowing through alternating cross-section flattened (ACF) tubes were studied. The effects of the twist angle of ACF on heat transfer and pressure drop were also investigated. The thermal performances of three different ACF tubes were compared with the thermal performance of a circular tube. The following conclusions are presented.

- The HTC and pressure drop produced by the most effective ACF exceeded the HTC and pressure drop of the circular tube by approximately 28.91%-152.43% and 18.18%-190.91%, respectively.

- The ACF tube with a twist angle of 90 degrees produced the highest HTC and pressure drop. Compared with the circular tube, the HTC and pressure drop increased by 152.43% and 190.91%.

- The thermal enhancement factor (TEF) of the ACF tube was about 27% higher than the TEF of the circular tube. Therefore, alternating cross-section flattened tubes are suitable replacements for circular tubes in heat exchangers.

5. Acknowledgements

This work was supported by the Research and Development Intitute, Thaksin University (RDITSU)'s Research Fund, grant number 10-01/2563.

Author Contributions: Kunlakarn Warnropru carried out the experimental results, interpreted the results, and aided in drafting the manuscript. Nares Chimres and Jatuporn Kaew-On participated in designing the study and analysis and gave final proof of the manuscript.

Funding: The Research and Development Intitute, Thaksin University (RDITSU)'s Research Fund, grant number 10-01/2563.

Conflicts of Interest: The authors declare that there is no conflict of interest regarding the publication of this article.

References

[1] Webb, R.L.; Kim, N.H. *Principles Enhanced Heat Trans*, 2nd ed.; Taylor & Francis Group: 270 Madison Avenue, New York, 2005, 3-10. https://doi.org/10.1201/b12413

[2] Dang, W.; Wang, L.B. Convective heat transfer enhancement mechanisms in circular tube inserted with a type of twined coil. *Int. J. Heat Mass Transf.* 2021, *169*, 120960. https://doi.org/10.1016/j.ijheatmasstransfer.2021.120960

[3] Cong, T.; Wang, B.; Gu, H. Numerical analysis on heat transfer enhancement of sCO_2 in the tube with twisted tape. *Nucl. Eng. Des.* 2022, *397*, 111940. https://doi.org/10.1016/j.nucengdes.2022.111940

[4] Harish, H.V.; M-Tech.; Manjunath, K. Heat and fluid flow behaviors in a laminar tube flow with circular protruded twisted tape inserts. *Case Stud. Therm. Eng.* 2022, *32*, 101880. https://doi.org/10.1016/j.csite.2022.101880

[5] Kaood, A.; Fadodun, O.G. Numerical investigation of turbulent entropy production rate in conical tubes fitted with a twisted-tape insert. *Int. Commun. Heat Mass Transf.* 2022, *139*, 106520. https://doi.org/10.1016/j.icheatmasstransfer.2022.106520

[6] Zhang, H.; Nunayon, S.S.; Jin, X.; Lai, A.C.K. Pressure drop and nanoparticle deposition characteristics for multiple twisted tape inserts with partitions in turbulent duct flows. *Int. J. Heat Mass Transf.* 2022, *193*, 121474. https://doi.org/10.1016/j.ijheatmasstransfer.2021.121474

[7] Pourpasha, H.; Heris, S.Z.; Mahian, O.; Wongwises, S. The effect of multi-wall carbon nanotubes/turbine meter oil nanofluid concentration on the thermophysical properties of lubricants. *Powder Technology.* 2020, *367*, 133-142. https://doi.org/10.1016/j.powtec.2020.03.037

[8] Ho, C.J.; Huang, S.H.; Lai, C.M. Enhancing laminar forced convection heat transfer by using Al_2O_3/PCM nanofluids in a concentric double-tube duct. *Case Stud. Therm. Eng.* 2022, *35*, 102147. https://doi.org/10.1016/j.csite.2022.102147

[9] Ozenbiner, O.; Yurddas, A. Numerical analysis of heat transfer of a nanofluid counterflow heat exchanger. *Int. Commun. Heat Mass Transf.* 2022, *137*, 106306. https://doi.org/10.1016/j.icheatmasstransfer.2022.106306

[10] Zhang, C.; Han, S.; Wu, Y.; Zhang, C.; Guo, H. Investigation on convection heat transfer performance of quaternary mixed molten salt based nanofluids in smooth tube. *Int. J. Therm. Sci.* 2022, *177*, 107534. https://doi.org/10.1016/j.ijthermalsci.2022.107534

[11] Ma, H.; He, B.; Su, L.; He, D. Heat transfer enhancement of nanofluid flow at the entry region of microtubes. *Int. J. Therm. Sci*. 2023, *184*, 107944. https://doi.org/10.1016/j.ijthermalsci.2022.107944

[12] Cruz, G.G.; Mendes, M.A.A.; Pereira, J.M.C.; Santos, H.; Nikulin, A.; Moita, A.S. Experimental and numerical characterization of single-phase pressure drop and heat transfer enhancement in helical corrugated tubes. *Int. J. Heat Mass Transf.* 2021, *179*, 121632. https://doi.org/10.1016/j.ijheatmasstransfer.2021.121632

[13] Cheng, X.; Li, Z-R.; Wan, H-N.; Bi, Q.; Ji, W-T. Experimental investigation on convective heat transfer of hydrocarbon fuel in transverse corrugated tubes. *Int. J. Heat Mass Transf*. 2023, *201*, 123586. https://doi.org/10.1016/j.ijheatmasstransfer.2022.123586

[14] Liao, W.; Lian, S. Effect of compound corrugation on heat transfer performance of corrugated tube. *Int. J. Therm. Sci.* 2023, *185*, 108036. https://doi.org/10.1016/j.ijthermalsci.2022.108036

[15] Holagh, S.G.; Abdous, M.A.; Rastan, H.; Shafiee, M.; Hashemian, M. Performance analysis of micro-fin tubes compared to smooth tubes as a heat transfer enhancement technique for flow condensation. *Energy Nexus*. 2022, *8*, 100154. https://doi.org/10.1016/j.nexus.2022.100154

[16] Moon, S.H.; Lee, D.; Kim, M.; Kim, Y. Evaporation heat transfer coefficient and frictional pressure drop of R600a in a micro-fin tube at low mass fluxes and temperatures. *Int. J. Heat Mass Transf*. 2022, *190*, 122769. https://doi.org/10.1016/j.ijheatmasstransfer.2022.122769

[17] Kaew-On, J.; Naphattharanun, N.; Binmud, R.; Wongwises, S. Condensation heat transfer characteristics of R134a flowing inside mini circular and flattened tubes. *Int. J. Heat Mass Transf*. 2016, *102*, 86-97. http://dx.doi.org/10.1016/j.ijheatmasstransfer.2016.05.095

[18] Azarhazin, S.; Sajadi, B.; Fazelnia, H.; Behabadi, M.A.A.; Zakeralhoseini, S. Boiling heat transfer coefficient and pressure drop of R1234yf flow inside smooth flattened tubes: An experimental study. *Appl. Therm. Eng*. 2020, *165*, 114595. https://doi.org/10.1016/j.applthermaleng.2019.114595

[19] Razzaghi, M.J.P; Ghassabian, M.; Daemiashkezari, M.; Abdulfattah, A.N.; Afrouzi, H.H.; Ahmad, H. Thermo-hydraulic performance evaluation of turbulent flow and heat transfer in a twisted flat tube: A CFD approach. *Case Stud. Therm. Eng.* 2022, *35*, 102107. https://doi.org/10.1016/j.csite.2022.102107

[20] Liu, S.; Yin, Y.; Tu, A.; Zhu, D. Experimental investigation on shell-side performance of a novel shell and tube oil cooler with twisted oval tubes. *Int. J. Therm. Sci.* 2020, *152*, 106290. https://doi.org/10.1016/j.ijthermalsci.2020.106290

[21] Li, X.; Wang, L.; Feng, R.; Wang, Z.; Liu, S.; Zhu, D. Study on shell side heat transport enhancement of double tube heat exchangers by twisted oval tubes. *Int. Commun. Heat Mass Transf.* 2021, *124*, 105273. https://doi.org/10.1016/j.icheatmasstransfer.2021.105273

[22] Sajadi, A.; Talebi, S. Investigation of convective heat transfer, pressure drop and efficiency of ZnO/water nanofluid in alternating elliptical axis tubes. *Energy Equip. Sys.* 2020, *8*, 203-215. 10.22059/EES.2020.44634

[23] Sajadi, A.; Talebi, S. Experimental investigation of heat transfer, pressure drop, and efficiency of TiO_2/Oil nanofluid in alternating flattened tubes. *Energy Equip. Sys*. 2022, *10*, 123-136. https://doi.org/10.22059/EES.2022.253058

[24] Luo, C.; Song, K. Thermal performance enhancement of a double-tube heat exchanger with novel twisted annulus formed by counter-twisted oval tubes. *Int. J. Therm. Sci*. 2021, *164*, 106892. https://doi.org/10.1016/j.ijthermalsci.2021.106892

[25] Farsi, M.; Khoshvaght-Aliabadi, M.; Alimoradi, A. A parametric study on heat transfer and pressure drop characteristics of circular tube with alternating flattened flow path. *Int. J. Therm. Sci*. 2021, *160*, 106671. https://doi.org/10.1016/j.ijthermalsci.2020.106671

[26] Babaei, H.R.; Khoshvaght-Aliabadi, M.; Mazloumi, S.H. Analysis of serpentine coil with alternating flattened axis: An insight into performance enhancement of solar ponds. *Solar Energy*. 2021, *217*, 292-307. https://doi.org/10.1016/j.solener.2021.02.017

[27] Rukruang, A.; Chimres, N.; Kaew-On, J.; Wongwises, S. Experimental and numerical study on heat transfer and flow characteristics in an alternating cross-section flattened tube. *Heat Transf. Res*. 2019, *48*, 817-834. https://doi.org/10.1002/htj.21407

[28] Rukruang, A.; Chimres, N.; Kaew-On, J.; Mesgarpour, M.; Mahian, O.; Wongwises, S. A critical review on the thermal performance of alternating cross-section tubes. *Alexandria Eng. J.* 2022, *61*, 7315-7337. https://doi.org/10.1016/j.aej.2021.12.070

[29] Rukruang, A.; Chittiphalungsri, T.; Chimres, N.; Kaew-On, J.; Mesgarpour, M.; Mahian, O.; Wongwises, S. Experimental Investigation of Thermal Performance of a Novel Alternating Cross-Section Flattened Tube Heat Exchanger. *Int. J. Heat Mass Transf*. 2022, *195*, 123159. https://doi.org/10.1016/j.ijheatmasstransfer.2022.123159

[30] WEBB, R.L. Performance evaluation criteria for use of enhanced heat transfer surfaces in heat exchanger design. *Int. J. Heat Mass Transf*. 1981, *24*, 715-726. https://doi.org/10.1016/0017-9310(81)90015-6

[31] Skullong, S.; Promvonge, P.; Thianpong, C.; Jayranaiwachira, N. Thermal behaviors in a round tube equipped with quadruple perforated-delta-winglet pairs. *Appl. Therm. Eng*. 2017, *115*, 229-243. https://doi.org/10.1016/j.applthermaleng.2016.12.082

JSTR
ASEAN Journal of Scientific and Technological Reports

Research article

Properties of Biochar from Coconut Waste and Application in Agriculture

Parichat Dittakit[1*], Junya Singkham[1], Wanalai Viriyasuthee[1] and Katsirin Sangmanee[2]

[1] School of Agriculture and Cooperatives, Sukhothai Thammathirat Open University, 11120, Thailand; puy_1980@hotmail.com
[2] Faculty of Science and Technology, Phranakhon Rajabhat University, 10220, Thailand; katsirinsangmanee@gmail.com
* Correspondence: puy_1980@hotmail.com

Citation:
Dittakit, P.; Singkham, J.; Viriyasuthee, W.; Sangmanee, K. Properties of biochar from Coconut Waste and Application in Agriculture. *ASEAN J. Sci. Tech. Report.* **2023**, *26*(1), 52-58. https://doi.org/10.55164/ajstr.v26i1.247574.

Article history:
Received: October 19, 2022
Revised: February 14, 2023
Accepted: February 17, 2023
Available online: March 21, 2023

Abstract: Coconut plantation waste was in massive quantities affecting the environment in the community. Hence, the coconut plantation was charcoal full of carbon. The objective of this research was to study the properties of biochar from coconut plantation waste and the consequences of adopting biochar to mix with organic fertilizer on the growth and lettuce productivity by analyzing the physical and chemical properties of biochar from coconut plantation waste. The organic fertilizer mixed with the biochar on lettuce growth and productivity was investigated by three treatments no application of organic fertilizer (control), the application of organic fertilizer, and the application of organic fertilizer added with potassium humate. The result showed that the highest level of biochar from coconut shells had the total density, total porosity, water holding capacity, C/N ratio, and humidity at the highest level, equaling 0.58 gram/cubic centimeter, 56.50%, 54.25%, 67%, and 2.41%, respectively. The biochar from the coconut leaves had the highest air gap, pH, conductivity, organic carbon, phosphorus, calcium, and magnesium quantity, respectively (13.50%, 9.90, 2.34 dS/m, 58.94%, 0.12%, 1.25%, and 2.26%, respectively). The biochar from the fallen young coconut fruits had organic matter, cation exchange, nitrogen, and phosphorus quantity at the highest level: 72.37%, 36.19 cmol/kg, 0.57%, and 2.11%, respectively. The results of the organic fertilizer mixed with biochar and Potassium Humate added formula led to the growth and productivity in all 3 types of lettuce more than not applying organic fertilizers ($p<0.05$).

Keywords: Biochar; Agricultural Waste; Coconut Charcoal

1. Introduction

Thailand is an agricultural country that created agricultural waste or biomass at approximately 43 million tons [1]. The value and policy of the New Sustainable Growth Engine (Bio-Circular-Green Economy) partly create zero-waste agriculture. Most agricultural wastes can be beneficial as valuable economic waste. They can reuse by adopting efficient technology. Adopting biomass through the pyrolysis process will cause the dissolution of raw material full of carbon. The charcoal created has high porosity and the highest nutrient level, especially phosphorus, potassium, calcium, and magnesium. In addition, it also has alkaline properties and a high positive cation exchange capacity which causes the ability to modify the acidic soil to highly acidic soil. Once biochar was adopted into the soil, it was revealed that it would reduce the use of fertilizer application and reduce the release of Carbon Dioxide from the soil, which affected the work of beneficial microbes in the soil. The biochar used for the soil's physical and chemical properties depends on the conditions in the pyrolysis process and the raw materials deployed [2,3,4]. In Samut Songkram province,

there are many coconut plantation wastes, such as coconut shells, fallen young coconut fruit, and coconut leaves which impact the environment. Hence, these wastes need to be demolished. Adopting the coconut plantation waste into raw materials for biochar making to help with soil improvement in coconut plantations would reduce the expenses on fertilizers, create fertile soil, and strengthen the coconut trees with good growth. Furthermore, it helps with soil improvement for other plants as well. Using biochar as organic fertilizer at the ratio produced from agricultural waste at 100 kilogram/rai results in that durian has grown in both growth and productivity. It can also prevent phytophthora in the soil [5]. In this research, the objectives were to study the properties of biochar from coconut plantation waste and the results of adopting biochar from coconut plantation waste as a mixing ingredient of organic fertilizer for lettuce growth and productivity.

2. Materials and Methods

Properties of biochar from coconut plantation waste and application in agriculture can be classified into 2 parts: the analysis of physical and chemical properties of the biochar from coconut plantation waste and the results of the application of organic fertilizer mixed with biochar towards lettuce growth and productivity by using coconut plantation waste at Samut Songkram province such as parts of coconut shells, fallen young coconut fruits, and coconut leaves. After that, the raw material would be brought to dry and passed through the pyrolysis process at 600 – 700 Celsius for 2-3 hours until the biochar turns shiny. Then, it would get crushed for property analysis.

2.1 The analysis of physical and chemical properties of biochar from coconut plantation waste

Physical properties of biochar from coconut plantation waste: the study of biochar structure with the Scanning electron microscope (SEM), the density, total porosity, air gap, and the water holding ability. Chemical properties of biochar from coconut plantation waste: electric conductivity, pH, organic material, organic carbon, C/N ratio, cation exchange capacity, moisture, nitrogen, phosphorus, potassium, calcium, magnesium, and brimstone sent for analysis at the department of land development.

2.2 The effects of the organic fertilizer mixed with biochar on the growth and productivity of lettuce

The test planning was done by using Latin Square Design (LSD) divided into 3 treatments with 4 replications: 1) no application of organic fertilizer (control), 2) the application of organic fertilizer, and 3) the application of organic fertilizer mixed with potassium humate treatments. The organic fertilizer was compost fertilizer derived from mixed with the biochar the ingredient of banana peels: biochar: phosphate stone: rice bran with a ratio of 70:10:10:10. The treatment of the fertilizer application, which added potassium humate of 1 gram/raw material in the making of the compost of 100 kilograms. Later on, fermented add oxygen for 45 days. Data on chemical properties were pH, electric conductivity, organic matter quantity, nitrogen, phosphorus, and potassium, and the growth and productivity of 3 types of lettuces: green cos, baby cos, and red Batavia. Data were analyzed using the analysis of variance (ANOVA) and different comparisons of statistical averages at the significant level of 0.05.

3. Results and Discussion

3.1 Biochar from coconut plantation waste properties

3.1.1 Physical properties of biochar from coconut plantation wastes

Each biochar was burnt using a Pyrolysis process at 400-500 degrees Celsius for 2 hours until the materials turned black to form the biochar from coconut plantation waste. They had different structures when looking through the SEM with the magnifying power of 30 LM showed that crushed biochar with a size of no larger than 0.5 centimeters received from the coconut shells was strengthened with a lot of porous and small size. Regarding biochar from fallen young coconut fruit and coconut leaves, it was found that the structure was fragile, had a smaller quantity of porous, and was larger than biochar from coconut shells. Once using magnifying power, it showed a clearer image of the space. Biochar from coconut shells had a high amount of porous and smaller in comparison with biochar from the fallen young coconut fruit and coconut leaves to bring each of the biochar for crushing into power and dent to the SEM at the magnifying value of 400 LM and

1.00 K showed that biochar from coconut shells had empty area, the small size of the space with the clearer structure than biochar from fallen young coconut fruit and leaves; figure 1:

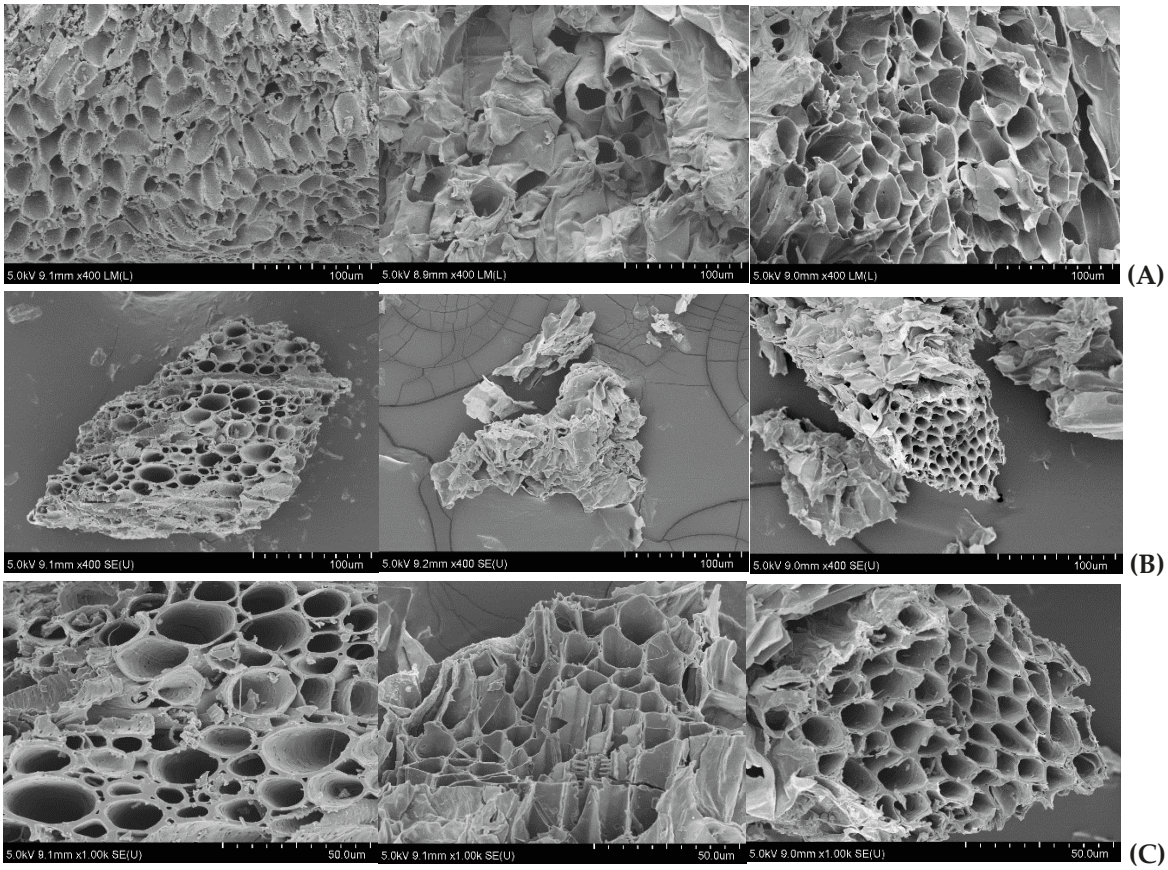

Biochar from coconut shell Biochar from fallen young coconut fruit Biochar from coconut leaf

Figure 1. The SEM of (A) 400 LM of < 0.5 cm biochar, (B) 400 LM for biochar that crushed into powder, and (C) 1K for biochar that crushed into powder.

Biochar from coconut shells had the highest density, total porosity, and water-holding ability at the highest level, equaling 0.58 gram/ m^3, 56.50%, and 54.25%, respectively. Biochar from coconut leaves had the highest air gap at 13.50% (Table 1). Biochar with the highest amount of air gaps or porous and small size would help with storing water for plant benefits while also absorbing nutrients along with the fact that these air gaps were the living area of microbe that was beneficial to the plants. Moreover, biochar has a strong structure with carbon at a high composition. The degradation will be slow once fertilizers or soil improvement materials are adopted, impacting fertilizer application reduction and better soil structure. [2, 4]

Table 1. Physical properties biochar from coconut shell, fallen young coconut fruit, and coconut leaf

Property	Coconut shell	Fallen young coconut fruit	Coconut leaf
Total density (gram/m^3)	0.58	0.43	0.29
Total porosity (%)	56.50	48.23	50.00
Air gap (%)	3.61	3.50	13.50
Water holding ability (%)	54.25	53.00	36.50

3.1.2 Chemical properties of biochar from the highest coconut plantation waste

The biochar from coconut shells had the C/N ratio and moisture content at 67 and 2.41%, respectively. The biochar from coconut leaves had the pH, electric conductivity, organic carbon, amount of phosphorus, calcium, and magnesium at the highest value of 9.90, 2.34 dS/m, 58.94%, 0.12%, 1.25%, and 2.26%, respectively. The biomass from fallen young coconut fruit had the organic matter, cation exchange capacity, and amount of Nitrogen and Phosphorus at the highest value of equal to 72.37%, 36.19 cmol/kg, 0.57%, and 2.11%, respectively (Table 2).

The pH value of biochar from coconut leaves was equaled to 9.90, which were alkaline found results similar to biochar from coconut husks and shells in Florida, the United States, Indonesia, and Malaysia [6,7]. However, the biochar from coconut shells and fallen young coconut fruits was equal to 6.38 and 7.42, respectively. It was mild acid appropriate with the difference in the adoption of soil improvement. The C/N ratio of the biochar in all 3 types was at a high value; hence, the degradation was slow and, once placed in the soil, can last for a long time. The number of nutrients in biochar from coconut shell and coconut leaf differed depending on the structure and the composition. The dry materials that passed the pyrolysis process showed much nitrogen loss but not for phosphorus, potassium, calcium, magnesium, or Sulfur. In comparison with the study of nutrients in coconut leaf and bearing a dwarf variety of coconut [8], they had no different nutrients from biochar from coconut leaf

Table 2. Chemical properties of biochar from coconut shell, fallen coconut fruit, and coconut leaf

Chemical properties	Coconut shell	Fallen young coconut fruit	Coconut leaf
pH	6.38	7.42	9.90
Electric Conductivity (dS/m)	0.88	1.78	2.34
Organic Matter (%)	43.67	72.37	58.94
Organic carbon (%)	25.33	41.98	58.94
C/N ration	67	74	78
Cation Exchange Capacity (cmol/kg)	21.84	36.19	29.47
Moisture content (%)	2.41	4.86	11.13
Nitrogen (%)	0.38	0.57	0.44
Phosphorus (%)	0.09	0.11	0.12
Potassium (%)	1.39	2.11	0.84
Calcium (%)	0.27	0.44	1.25
Magnesium (%)	0.15	0.48	2.26
Sulfur (%)	1.48	1.63	1.39

3.1.3 Effects of the organic fertilizer with the addition of biochar on the growth and productivity of lettuce

The properties of organic fertilizer mixed with biochar through the process of fermentation for 45 days revealed that the pH value, EC value, OM value, and amount of nitrogen, phosphorus, and potassium of all organic fertilizer treatments were higher than the standardized criteria of high-quality organic fertilizer determined by the Department of Land Development [9] (Table 3).

The results of organic fertilizer mixed with biochar on the growth and productivity of 3 types of lettuce such as green cos, baby cos, and red Batavia, found that the number of leaves per green cos lettuce had no statistical difference ($p \geq 0.05$). Still, the fresh weight of lettuce had a statistical difference ($p<0.05$), for green cos lettuce fresh weight, which received organic fertilizer with potassium humate added, had the highest level of weight in the fresh plant at 61.17 grams. For the lettuce, the fresh weight that did not receive the fertilizer had the lowest level of weight at 34.66 grams (Table 4). Baby cos lettuce had the amount of leaves at the statistical difference ($p<0.05$) at 7, 14, and 28 days. Baby cos lettuce had the highest number of leaves once applying organic fertilizer but had no difference with applying organic fertilizer added with potassium humate. The fresh weight of baby cos lettuce differed statistically ($p<0.05$). Baby cos lettuce with organic fertilizer mixed

with potassium humate had the highest level of fresh weight at 60.16 grams. The fresh weight was the lowest at 33.66 grams for the lettuce with no fertilizer applied (Table 5). The red Batavia lettuce had the number of leaves at a statistical difference ($p<0.05$) at 28 days. Red Batavia had the highest number of leaves when applying organic fertilizer mixed with potassium humate at 18.33 grams. The fresh weight of red Batavia lettuce was a statistical difference ($p<0.05$). Red Batavia, which applied organic fertilizer mixed with potassium humate, had the highest level of fresh weight at 42.83 grams. The lettuce with no organic fertilizer had the lowest weight at 28.83 grams (Table 6). The biochar added to high-quality fertilizer helped with the modification of air and soil transfer, modified water holding ability, reduced the hardening of the soil, and affected the operation of beneficial microbe in the soil [2,3,4]. Hence when mixing it with other materials until they become high-quality fertilizer, it will have sufficient nutrients for the growth of lettuces.

Table 3. Chemical properties of high-quality organic fertilizer from banana and coconut waste

Chemical properties	Organic Fertilizer	Organic fertilizer with added Potassium Humate
pH	8.41	8.62
EC (dS/m)	1.73	1.80
OM (%)	21.73	22.02
N (%)	1.53	1.57
P (%)	2.84	2.88
K (%)	1.60	1.77

Table 4. Results of fertilizer on the growth and productivity of Green cos lettuce

Treatment	Number of Green Cos leaf				Fresh Weight plant (gram)
	7 Days	14 Days	21 Days	28 Days	
-No fertilizer applied	5.50	9.00	12.33	17.50	34.66 b[1/]
-Organic fertilizer	6.00	9.16	11.83	18.16	37.83 b
-Organic fertilizer with added Potassium Humate	5.16	7.66	11.00	18.33	61.17 a
T-test	ns	ns	ns	ns	*
C.V. (%)	13.42	15.91	15.91	14.03	21.13

Note: [1/] the different alphabets represent statistical differences at the level of confidence of 95% by using the LSD method

Table 5. Results of fertilizer on the growth and productivity of Baby cos lettuce

Treatment	Number of Green Cos leaf				Fresh Weight plant (gram)
	7 Days	14 Days	21 Days	28 Days	
-No fertilizer applied	5.00 b[1/]	7.16 b	10.50	14.16 b	33.66 b
-Organic fertilizer	5.83 ab	8.83 a	10.83	15.83 a	34.33 b
-Organic fertilizer with added Potassium Humate	6.33 a	8.16 ab	10.83	15.67 ab	60.16 a
T-test	*	*	Ns	*	*
C.V. (%)	12.89	13.02	8.74	8.48	24.25i

Note: [1/] the different alphabets represent statistical differences at the level of confidence of 95% by using the LSD method

Table 6. Results of fertilizer on the growth and productivity of red Batavia lettuce

Treatment	Number of Green Cos leaf				Fresh Weight plant (gram)
	7 วัน	14 Days	21 Days	28 Days	
-No fertilizer applied	5.66	7.66	10.83	15.66 b[1/]	28.83 b
-Organic fertilizer	5.50	8.00	10.66	14.83 b	30.50 b
-Organic fertilizer with added Potassium Humate	5.33	7.83	10.16	18.33 a	42.83 a
T-test	ns	ns	ns	*	*
C.V. (%)	11.66	11.05	16.04	12.84	20.75

Note: [1/] the difference in alphabet represents the difference in confidence level statistically at 95% by using the LSD method

4. Conclusions

Biochar from the coconut shells, fallen young coconuts, and coconut leaves had a lot of porous and small air gaps. The biochar from coconut shells had the total density, porosity, and water-holding capability at the highest level. However, the biochar from the coconut leaves had the most air gaps. The chemical properties of all 3 types of biochar were different in pH, EC, OM, OC, C/N ratio, CEC, humidity, and other quantity of nutrients. All of them can be used to mix with organic fertilizer. The organic fertilizers that had the mixing of biochar in both formulas could be high-quality organic fertilizers according to the standard specified by the Department of Land Development. They all had high nutrient quantities. The results of organic fertilizers mixed with biochar on the growth and productivity of both 2 formulas and the new formula with added potassium humate led to the growth and productivity of all 3 types of lettuces such as green cos, baby cos, and red Batavia more than not applying high-quality organic fertilizer ($p<0.05$). The newly developed formula, which added potassium humate, led to the growth and productivity of all 3 types of lettuce at the highest level ($p<0.05$).

5. Acknowledgements

This research was funded by the National Research Council of Thailand (NRCT), Thailand.

Author Contributions:

1. Variety Characteristic Assessment and Genetic Relationship Analysis of Okra Using ISSR Markers. funding: Sukhothai Thammathirat Open University 2018

2. Community Lessons of Water-related Disaster and Water Resources Management in Ping, Wang, Yom, Nan and Upper Chao Phraya Basin. funding: Sukhothai Thammathirat Open University 2019

3. Bioactive Compounds and Cytotoxicity of Okra (*Abelmoschus esculentus* (L.) Moench). funding: Sukhothai Thammathirat Open University 20120

4. Business Elevation of High Quality Compost Fertilizer from Agricultural Wastes of Baansabuyjai Community Enterprise and Baansaraphi Community Enterprise in Samut Songkram Province. funding: National research council of Thailand 2021

Funding: This research received no external funding.

Conflicts of Interest: The authors declare no conflict of interest.

References

[1] Samran, S. Department of Agricultural Extension supported the farmer to make crop value added under Royal Coronation Ceremony of the King. Available online: https://www.technologychaoban.com /bullet-news-today/article_107930. (accessed on 11 October 2022).

[2] International Biochar Initiative. Standardized Product definition and product testing guidelines for biochar that is used in soil (online). 2016. Retrieve November 23, 2015, from https://www.biochar-international.org/wp-content/uploads/2018/04/IBI_Biochar_Standards_V2.1_Final.pdf

[3] Lehmann, J. Bio-energy in the black. *Frontiers Ecology and the Environment*. 2007, *5*(7), 381–387.
[4] Novak, J.; Sigua, G.; Watts, D.; Cantrell, K; Shumaker, P.; Szogi, A.; Spokas, Mark, G. J.; Kurt, S. *Biochars impact on water infiltration and water quality through a compacted subsoil layer*. Chemosphere. 2016, 142, 160–167.
[5] Nanthaphop, C.; Nuangjan C.; Sangmanee, K.; Wiwat S. The application of biochar with durian shell compose for soil improvement on durain producing under acidity soil. Land Development Department. 2020.
[6] Gonzagaa M.I.S.; Mackowiakb, C.; Almeidaa, A. Q.; Juniora, J.I.T.C.; Andrade, K.R. Positive and negative effects of biochar from coconut husks, orange bagasse and pine wood chips on maize (Zea mays L.) growth and nutrition. *CATENA*. 2018, 162, 414–420.
[7] Hariz, A.R.M.; Wan Azlina, W.A.K.G.; Mohd Fazly, M.; Norziana, Z.Z.; Mohd Ridzuan, M.D.; Tosiah, S.; Nurul, A.A.B. Local practices for production of rice husk biochar and coconut shell biochar: production methods, product characteristics, nutrient and field water holding capacity. *Journal of Tropical Agriculture and Food Science*. 2015, 43, 91–101.
[8] Coconut leaf nutrient levels of bearing dwarf varieties. Available online: https://journal.coconutcommunity.org. (accessed on 11 October 2022).
[9] Land Development Department. (2019). High quality organic fertilizer. Available online: http://ofs101.ldd.go.th/LDDNews/PAPR/ปุ๋ยอินทรีย์คุณภาพสูงสูตรกรมพัฒนาที่ดินโดยใช้สารเร่งพด/ปุ๋ยอินทรีย์คุณภาพสูงสูตรกรมพัฒนาที่ดินโดยใช้สารเร่ง พด.pdf. (accessed on 11 October 2022).

JSTR
ASEAN Journal of Scientific and Technological Reports

Research article

Techno-Economic Assessment of a 1 MW Solar PV Rooftop System at Thaksin University (Phatthalung Campus), Thailand

Jompob Waewsak[1,*], Rawit Khamharnphol[2], Sakrapee Khunpetch[3], Ismail Kamdar[4], Somphol Chiwamongkhonkarn[5], Chuleerat Kongruang[6], and Yves Gagnon[7]

[1] Research Center in Energy and Environment, Division of Physics, Faculty of Science, Thaksin University, Phatthalung, 93210, Thailand; jompob@tsu.ac.th
[2] Faculty of Industrial Technology, Nakhon Si Thammarat Rajabhat University, Nakhon Si Thammarat, 80280, Thailand; rawit_kam@nstru.ac.th
[3] Faculty of Industrial Technology, Nakhon Si Thammarat Rajabhat University, Nakhon Si Thammarat, 80280, Thailand; sakrapee_khu@nstru.ac.th
[4] Research Center in Energy and Environment, Division of Physics, Faculty of Science, Thaksin University, Phatthalung, 93210, Thailand; ismailkamdar1014@gmail.com
[5] Faculty of Engineering, Thaksin University, Phatthalung, 93210, Thailand; dung_ding19@hotmail.com
[6] School of Accountancy and Finance, Walailak University, Nakhon Si Thammarat, 80160, Thailand; chuleerat.ko@wu.ac.th
[7] Université de Moncton Edmundston, New Brunswick, Canada; yves.gagnon@umoncton.ca
* Correspondence: jompob@tsu.ac.th

Citation:
Waewsak, J, Khamharnphol, R, Khunpetch, S, Kamdar, I, Chaichan, W, Chiwamongkhonkarn, S, Kongruang, C, and Gagnon Y. Techno-economic assessment of a 1 MW solar PV rooftop (Phatthalung Campus), Thailand. *ASEAN J. Sci. Tech. Report.* **2023**, *26*(1), 59-75. https://doi.org/10.55164/ajstr.v26i1.248159.

Article history:
Received: January 9, 2023
Revised: February 20, 2023
Accepted: February 21, 2023
Available online: March 22, 2023

Abstract: This study presents a techno-economic assessment of a 1 MW solar photovoltaic (PV) rooftop system at Thaksin University (Phatthalung Campus) in Thailand. A detailed analysis of the solar PV rooftop system is performed with particular attention to the performance of different PV technologies and the effects of different tilt angles and orientations of the PV panels on the annual energy production, the specific production, and the performance ratio. The economic analysis was performed for four scenarios: (1) self-investment and self-consumption scheme, (2) bankable and self-consumption scheme, (3) bankable and feed-in tariff (FiT) scheme, and (4) energy service company (ESCO) scheme. The results show that the amorphous silicon/micro-crystalline silicon (a-Si/μc-Si) technology shows the lowest annual energy production and performance ratio (PR), while the copper indium disulfide (CIS) technology records the largest annual energy production and PR. The largest annual energy production and specific production were obtained with the PV panels installed at a 10° tilt angle and with the PV modules facing South (S), while the lowest annual energy production and specific production were observed with the PV panels installed at a 45° tilt angle and the PV modules facing North (N). The economic analysis results show that the best scenarios are Scenario 3 (bankable and FiT scheme) and Scenario 1 (self-investment and self-consumption scheme). The findings of this research provide valuable information for regional stakeholders and policymakers regarding investments in solar PV rooftop systems.

Keywords: Photovoltaic; Energy Yield; PV Technology; Economic Analysis; Solar PV Rooftop.

1. Introduction

The world is facing key challenges related to environmental protection, energy conservation, and sustainable energy consumption and production. The growing population and industrialization have increased the electricity demand [1-2]. Non-renewable resources such as oil, coal, and natural gas are diminishing over time and are characterized by greenhouse gas emissions. Globally, researchers are investigating alternative energy sources to meet the energy demand in an eco-friendly way [3-4]. The best alternative to non-renewable

energy sources is solar and wind energy. In 2021, the global total installed capacity of renewable energy reached 3,064 GW (IRENA) [5], out of which 843 GW was in solar photovoltaic (PV) installed capacity [6].

The International Energy Agency (IEA) has reported that solar PV systems could deliver 22% of the world's electricity by 2050. Worldwide, the potential of solar PV to be installed on a mega-scale has been enhanced by the progress in solar PV technology and rapid cost reductions. Solar PV has the potential to substantially decrease the amount of rising global CO2 emissions from fossil fuels. The carbon emission intensity is high in conventional fossil fuel-based technologies, while it is minimal in the operation of solar PV technology. Hence, solar PV technology can significantly contribute to meeting the worldwide energy demand through low-carbon power generation [7].

The average daily solar radiation is a significant factor in forecasting various applications, mainly the sizing of photovoltaic (PV) systems, building design, agrometeorology, and agriculture [8]. The performance of solar PV technology largely depends on the weather, the regional conditions and the solar cell technology [9-10]. For instance, Quansah et al. [9] studied the outdoor performance of five PV technologies, i.e., polycrystalline (p-Si), monocrystalline (m-Si), copper indium disulfide (CIS) thin-film, amorphous silicon (a-Si), and heterojunction incorporating thin (HIT) films. They evaluated that the p-Si technology is the most appropriate, while the CIS is the least appropriate in the considered site. Ali and Khan [11] conducted a techno-economic assessment of p-Si and CIS technologies. They analyzed that the CIS performs better regarding the performance ratio (PR), and they produce higher annual energy, while the p-Si shows a better-levelized cost of electricity (LCOE) and requires less area. Olarewaju et al. [12] examined fourteen PV modules to determine the best technology. They observed that the Panasonic solar PV showed the best capacity factor and performance ratio performances. Nour-eddine et al. [13] scrutinized the techno-economic performance of three PV technologies, including m-Si, p-Si, and a-Si. They found that the m-Si technology is the most suitable for performance parameters.

The energy produced by solar PV modules mainly depends on several parameters, namely the spatial layout, the tilt, and the azimuth angle [14]. Various studies focused on the optimal configuration of PV and optimal tilt angle for solar PV systems. For instance, Bakirci [15] found that the optimal tilt angle varies between 0° and 65° during the whole year in Turkey. Mamun et al. [16] investigated the effect of the tilt angle on the PV module performance on an experimental basis and confirmed that the optimum tilt angle is 15° in Malaysia. Al Garni et al. [17] analyzed the impact of the tilt and azimuth angle on a PV system in Saudi Arabia. They reported that adjusting the orientation five times per year can increase the energy yield by up to 3.63%.

Techno-economic assessments of solar PV rooftop systems have been performed in many parts of the world. For example, Christiaanse et al. [18] studied a grid-friendly solar PV rooftop system for commercial buildings in British Columbia, Canada. They applied a bi-level optimization framework and determined that the solar PV rooftop installation is profitable at a 50% cost reduction of current prices. Mangiante et al. [19] presented a novel solar PV rooftop approach in Brownsville, Texas, U.S.A. Based on the technical potential, they analyzed that residential buildings could generate up to 11% of the city's energy demand. Imam and Al-Turki [20] studied the feasibility of a 12.25 kWp solar PV system under a typical residential building in Saudi Arabia. They determined that the proposed model could fulfill 87% of the electricity demand of the residential building.

Thailand, situated close to the equator, has a high solar energy potential. Assessing the incident solar radiation over a specified region is significant to obtain the maximum potential of solar energy. The amount of available solar radiation over the earth's surface is important for numerous applications, such as the practical utilization of solar energy for electricity generation, domestic water heating, drying processes, estimation of crop productivity, environmental and agro-meteorological research as well as atmospheric physics research [21]. Thailand mainly invested in installing the utility-scale solar system in the past [22] (Tongsopit, 2015). However, the number of prosumers significantly increased in the industrial and residential sectors due to the cost reductions of solar PV systems. Thus, the role of solar PV rooftop systems in Thailand continues to increase renewable energy production in commercial and residential buildings [23](Yoomak et al., 2019).

This study presents a techno-economic assessment of a 1 MW solar PV rooftop system with an application at Thaksin University (Phatthalung Campus) in Thailand. This work aims to evaluate the performance of different PV technologies and the effects of the tilt angle and orientation on solar PV panels. Furthermore, the solar PV rooftop system is analyzed under four economic scenarios: (1) self-investment and

self-consumption scheme, (2) bankable and self-consumption scheme, (3) bankable and feed-in tariff (FiT) scheme, and (4) energy service company (ESCO) scheme, to identify the best scheme with specific application to this public university situated in southern Thailand.

2. Materials and Methods

2.1 Study area

The solar PV rooftop system is installed at 7.81 °N latitudes and 99.94 °E longitudes in the Phatthalung Campus of Thaksin University in southern Thailand. The installed capacity of the project site is 1 MW. This project aims to assess this university's potential for clean energy technologies while encouraging the surrounding communities to consider becoming self-sufficient in energy. The satellite imagery for the location of the proposed 1 MW solar PV rooftop system at the Phatthalung campus of Thaksin University is shown in Figure 1.

The monthly and daily electrical load demands of the Phatthalung Campus of Thaksin University are displayed in Figure 2 for 2019. It is noticeable from the figure that the campus monthly electrical load demand is highest in March and April, along with in July, August, and September. Also, the daily load profile shows the cyclic variation of the load demand in typical weeks, with high on-peak needs during the week and low off-peak demands during the weekends. Additionally, the highest electrical load demands are observed in the last weeks of March and in September.

2.2 Simulation of the solar PV Rooftop System

A 1 MW solar PV rooftop power generation system is assessed through the PVsyst simulation tool. This model has emerged as a convenient simulation tool for energy yield assessments and the optimal design of solar power plants [4]. The simulation uses an extensive knowledge of PV technology, meteorological, solar irradiance data, and solar PV system components [24]. PVsyst can import meteorological data from various databases, notably from the National Aeronautics and Space Administration (NASA) and Meteonorm 7.3. It intelligently evaluates the performance of grid-tied, stand-alone, pumping, and DC-grid systems. The model uses detailed hourly data, and it predicts the system output. Furthermore, PVsyst contains an inclusive solar PV system components database for PV modules and inverters [25].

The flow diagram of the PVsyst model is shown in Figure 3. The site location is specified in the first step, and the PV panels' tilt angle and the PV modules' orientation are defined. In the second step, the weather data (global horizontal irradiance (GHI) and air temperature) are accessed through the Meteonorm database and are imported into the PVsyst tool. In the third step, appropriate PV system components (PV modules and inverters) and the electrical load demand of the study area are analyzed. In the next step, the system sizing and optimization process is performed. Finally, after the execution of the simulation, various tables, graphs, and summary reports, such as the annual energy production (AEP), the performance ratio (PR), and the system losses, are generated.

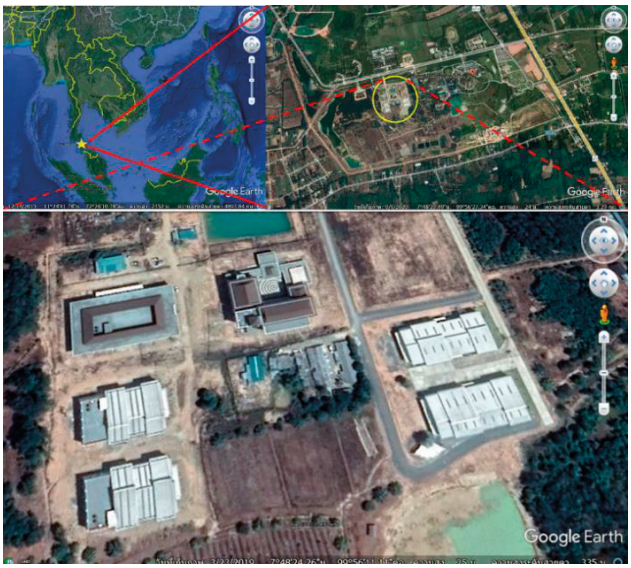

Figure 1. Satellite imagery of the study area shows the location of the proposed 1 MW solar PV rooftop installation.

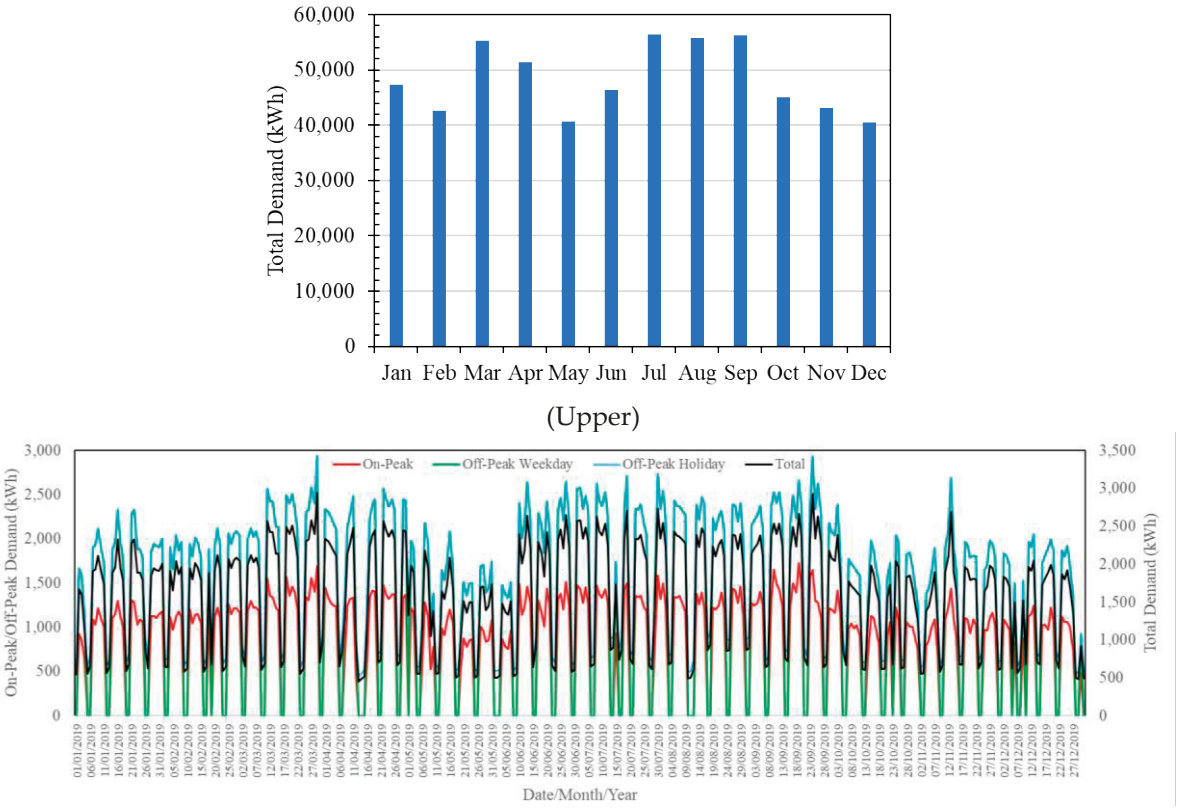

Figure 2. Monthly (upper) and daily (lower) electrical load demand of ThaksinUniversity (Phatthalung Campus) in 2019.

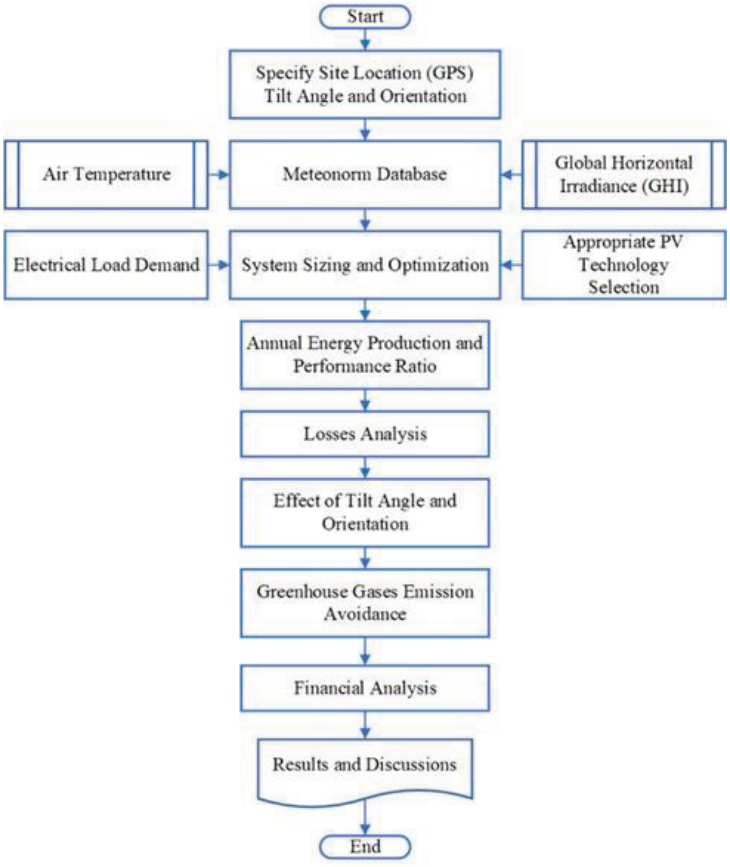

Figure 3. Flow diagram of the PVsyst model.

2.3 Climatic Data of the Study Area

Phatthalung, a province in southern Thailand on the Malay Peninsula, borders the large shallow Songkhla lake in the east. The region's climate is characterized by southwest and northeast monsoons, with hot summers [26-27]. Figure 4 displays the monthly average global horizontal irradiation (GHI) and average ambient temperature of the study area, taken from Meteonorm 7.3. The maximum average GHI is found to be 182.3 kWh/m² in March and 184.4 kWh/m² in April, while the lowest average GHI is observed in December, with a value of 110.8 kWh/m².

The average temperature varies between 26.29 °C and 28.21 °C over one year. The maximum average temperature is noticed from March to May, while the lowest average is observed in November. Furthermore, the solar GHI, global incident irradiation, and GHI clear sky data have been analyzed by the Solar and Wind Energy Research Laboratory (SWERL) at the Research Center in Energy and Environment, Thaksin University (Phatthalung Campus) and are shown in Figure 5. It is noticeable from the figure that the solar GHI, the global incident irradiation, and the GHI clear sky are characterized by two peaks, namely one peak in March-April and another peak in September. It can also be observed that these variables fluctuate greatly daily, which is due to the changing weather patterns throughout one month.

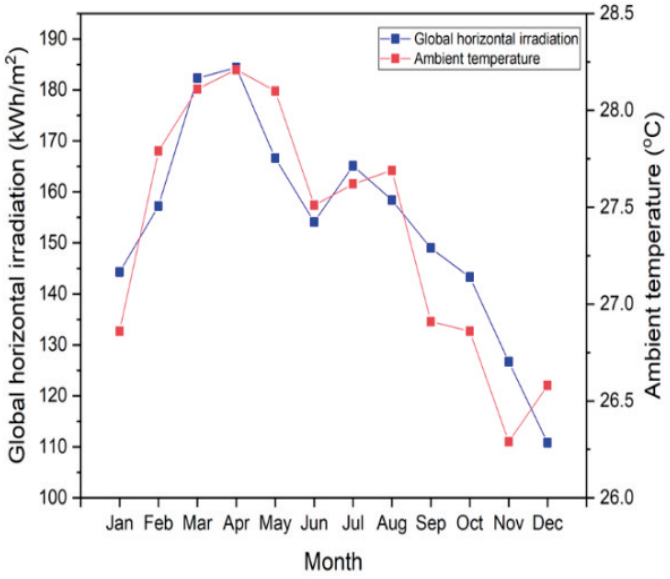

Figure 4. Monthly average global horizontal irradiation and average ambient temperature of the study area.

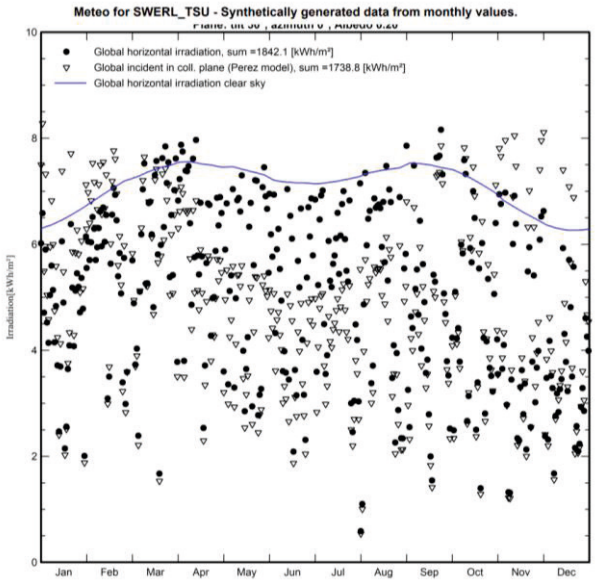

Figure 5. Variation of the solar global horizontal irradiation, global incident, and global horizontal irradiation clear sky throughout the year in the study area.

2.4 Description of the PV Technology

In this study, different PV technologies have been considered to compare and determine the optimal PV technology under the climate conditions of southern Thailand. The proposed 1 MW solar PV rooftop power generation system has the option of a variety of solar PV technologies, consisting of polycrystalline silicon (p-Si), monocrystalline silicon (m-Si), heterojunction incorporating thin (HIT) film, cadmium telluride (CdTe), amorphous silicon/micro-crystalline silicon (a-Si/μc-Si), and copper indium disulfide (CIS). The nominal power of PV modules is 400 Wp, except the cell-type CIS (thin-film) PV module, which has a 360 Wp nominal power. The PV modules would be connected with several strings in series. The technical specifications of each PV module are presented in Table 1.

Table 1. Technical specifications of the potential PV panel modules.

PV modules					
Cell-type	**Model**	**Nominal Power (Wp)**	**Total PV Modules**	**Nominal Power (STC) (Wp)**	**Modules (Strings x Series)**
p-Si	CS3W-440P SE	440	2,280	1,003	120 x 19
m-Si	LG 440 N2T-E6	440	2,280	1,003	121 x 19
HIT	REC440AA 72	440	2,272	1,000	142 x 16
CdTe	FS-6440-PA	440	2,272	1,000	568 x 4
a-Si/μc-Si	F440	440	2,280	1,003	570 x 4
CIS	CIGS-3600A1	360	2,784	1,002	232 x 12

Key: p-Si: polycrystalline silicon, m-Si: monocrystalline silicon, HIT: heterojunction incorporating thin-film, CdTe: cadmium telluride, a-Si:/μc-Si: amorphous silicon/micro-crystalline silicon, CIS: copper indium disulfide.

2.5 PV Inverter

The inverter model selected for this solar PV rooftop power generation system is the PVS800-57, manufactured by ABB. The nominal AC power of the ABB inverter is 1,000 kW, while the DC voltage ranges between 600 and 850 V. The nominal AC output voltage and the AC are 400 V and 1,445 A, respectively. The efficiency of the inverter is 98.8%. Further details of the technical specifications of the PV inverter are given in Table 2.

Table 2. Technical specifications of the PV inverter [28].

Manufacturer	**ABB**
Model	PVS800-57-1000 kW-C
DC Voltage Range	600-850 V
Max DC Voltage	1,100 V
Max DC Current	1,710 A
No. of DC Inputs	8-20 (+/-)
Efficiency	98.8%
Nominal AC Power (at 50oC)	1,000 kW
Max AC Output Power	1,200 kW
Nominal AC Current	1,445 A
Nominal AC Output Voltage	400 V
Output Frequency	50/60 Hz

2.6 Tilt Angle and Orientation of the PV modules

When exposed perpendicularly to the incoming solar irradiation, the PV modules will work most efficiently in the sunlight. However, the solar irradiance is not necessarily perpendicular to the PV panels. Therefore, the concept of tilt angle originated such that the PV modules could be positioned over the horizontal surface in an inclined manner [29]. A solar PV rooftop system's performance is determined by the PV panels' tilt angle and the azimuth angle of the PV modules [30]. This study analyzed the performance of a solar PV rooftop system at eight different tilt angles and eight different azimuth angles, as shown in Table 3 and Table 4, respectively.

Table 3. Various tilt angles for the solar rooftop PV modules.

Tilt angle	10°	15°	20°	25°	30°	35°	40°	45°

Table 4. Various azimuth angles along with the orientation for the solar rooftop PV modules.

Azimuth Angle	0°	-45°	-90°	-135°	180°	135°	90°	45°
Orientation	S	SE	E	NE	N	NW	W	SW

2.7 Cost-benefit Analysis

A cost-benefit analysis (CBA) is a technique for assessing the strengths and weaknesses of a project, such as those related to the installation or modification of energy projects [31-33]. The benefits of energy projects include positive impacts on the environment, job creation, reduced reliance on fossil fuels, and reduced oil dependence costs. Various studies have highlighted the benefits of energy projects from environmental and social perspectives [34-36]. This study determines the economic impacts from four main perspectives: (1) self-investment and self-consumption, (2) bankable and self-consumption, (3) bankable and feed-in tariffs (FiT), and (4) Energy Service Company (ESCO), with each of these schemes analyzed under the parameters and assumptions provided in Table 5. The four main financial indices are discussed below to determine a project's CBA.

2.7.1. Cost-benefit Analysis

The benefit-cost ratio (BCR) is a useful metric in decision-making to assess the benefits of a specific project. It is the ratio of the project's total benefits relative to its total costs over a specific period. The BCR identifies the rate of return to the investors in terms of net gain or loss. A project is considered economically viable if the BCR exceeds 1 [37]. The formula to calculate the BCR of a project is expressed as [38]:

$$CR = \frac{\sum_{t=0}^{T} \frac{B_t}{(1+r)^t}}{\sum_{t=0}^{T} \frac{C_t}{(1+r)^t}} \quad (1)$$

Where B_t = the project benefit in year t; time t = 0 to T years; C_t= the project costs in year t; T = the total number of years of the project life span; and r = the discount rate for the investment.

2.7.2. Net Present Value

The net present value (NPV) determines whether a project is profitable. It is defined as the difference between the present value of the benefits and the costs related to the investment. A positive NPV indicates the financial viability of a project, whereas a negative NPV implies a financial loss. The NPV can be calculated mathematically as:

$$NPV = \sum_{t=0}^{T} \frac{B_t}{(1+r)^t} - \sum_{t=0}^{T} \frac{C_t}{(1+r)^t} \quad (2)$$

2.7.3. Internal Rate of Return

A project's internal rate of return (IRR) is the interest rate that makes the NPV equal to zero. Usually, it evaluates the desirability of projects where a high IRR makes a project more desirable to undertake [39]. The IRR can be calculated as:

$$0 = \sum_{t=0}^{T} \frac{c_t}{(1+r)^t} \quad (3)$$

where c_t denotes the cash flow in the period t and r represents the internal rate of return.

2.7.4. Internal Rate of Return

The payback period (PBP) is defined as the time required to recover the initial investments in the project. Energy projects having shorter PBP are economically viable and sustainable. The payback period is calculated as:

$$PBP = \frac{Investment}{Net\ annual\ cash\ flow} \quad (4)$$

The financial metrics for a proposed 1 MW solar PV rooftop power generation system are determined using various inputs and assumptions, as mentioned in Table 5.

Table 5. Inputs and assumptions used to evaluate the 1 MW solar PV rooftop system.

No.	Parameter	Value	Unit
1	Project Lifetime	25	Year
2	On-Peak Tariff (TOU)	5.1135	THB/kWh
3	Off-Peak Tariff (TOU)	2.6037	THB/kWh
4	On-Peak/Off-Peak Ratio	15/75	%
5	FiT [45]	6.40	THB/kWh
6	Discount Tariff (ESCO)	20	%
7	Exchange Rate	34.47	THB/US$
8	Interest Rate (MRR)	5.97	%
9	Debt Ratio	70	%
10	Amortizing Repayment	7	Year
11	Discount Rate	7	%
12	Inflation Rate	5.73	%
13	Upfront Fee	1	%
14	Power Development Fund	0.01	THB/kWh
15	Salvage	3	%
16	Carbon Credit Trading (T-VER)	200	THB/tonnes CO2eq
17	Gas Emission Factor	0.5986	kWh/g CO2eq
18	Cleaning Cost (2 Time/Year)	4	US$/Panel
19	Basic Inspection for Maintenance	1,100	US$/Year
20	Egrid	1,536	MWh/Year

2.8. Levelized Cost of Electricity

The levelized cost of electricity (LCOE) is the selling price of electricity required by the system to break even at the end of its period [40]. It can be measured using the following expression:

$$LCOE = \frac{\sum_{t=1}^{n} \frac{I_t + M_t + F_t}{(1+r)^t}}{\sum_{t=1}^{n} \frac{E_t}{(1+r)^t}} \quad (5)$$

where I_t, M_t, F_t and E_t refer to the investment costs in year t, the maintenance costs in year t, the fuel expenditures in year t and the electricity generation in year t, respectively. Here, r is the discount rate, and n shows the lifespan, in years, of the solar PV rooftop system.

3. Results and Discussion

This section presents the technical and economic assessment of the proposed solar PV rooftop system using the PVsyst tool.

3.1. Technical assessment

In this subsection, the performance of six PV technologies, along with their total losses, are analyzed. The effect of the PV panels' tilt angle and the solar PV modules' orientation are studied to determine the optimal tilt angle of the PV modules and the azimuth angle.

3.1.1. Annual energy production and performance ratio

The annual energy production and the performance ratio of six PV technologies are plotted in Figure 6. It is noticeable from the figure that the a-Si/μc-Si technology shows the lowest annual energy production of about 1,370 MWh, with a PR of 78.6%. The m-Si and CdTe induce almost the same annual energy production and PR with a slight dominance of CdTe. The annual energy production and the PR for the p-Si, m-Si, and CdTe technologies are approximately 1,458 MWh and 83.65%, 1,466 MWh and 84.12%, and 1,468 MWh and 84.51%, respectively. The CIS technology has observed the highest annual energy production of 1,537 MWh, with a PR of 88.24%, followed by HIT, with a yearly energy production of 1,501 MWh and a PR of 86.41%.

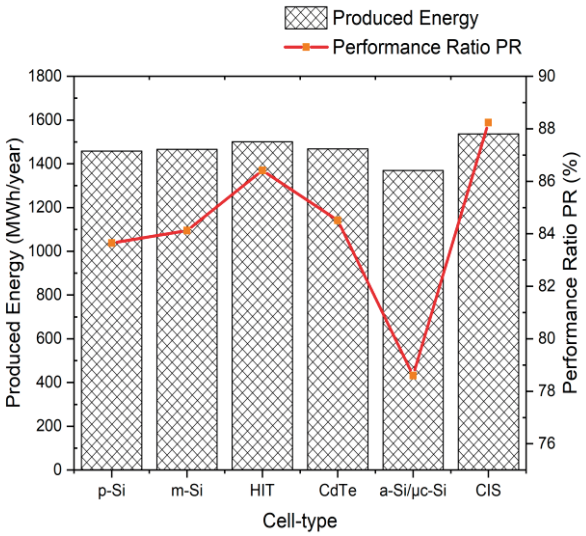

Figure 6. *Annual energy production and performance ratio of different PV technologies.*

The CIS and HIT technologies yield more annual energy output than the other PV technologies in this study. The a-Si/μc-Si technology produces the lowest annual energy output. This might be a consequence of its low conversion efficiency [41]. Similarly, the CIS technology has the highest PR, whereas the a-Si/μc-Si technology has the lowest PR. A PR above 80% is always considered desirable as it accounts for an economic gain [42]. The PR of all PV technologies is above 80%, except for the a-Si/μc-Si technology, which has a 78.6% PR value.

Figure 7 illustrates the monthly energy production of different PV technologies. The results show that all PV technologies attain the highest monthly energy production from January to April. The CIS and HIT achieved the maximum monthly energy production in March, with 156.1 MWh and 152.5 MWh values, respectively. The lowest monthly energy production for all PV technologies was observed in June and December. The a-Si/μc-Si technology has recorded the lowest monthly energy production of 95.1 MWh in June and 98 MWh in December. This implies that these months receive low solar radiation.

Based on the monthly energy production, a comparison has been performed among the six PV technologies. Over the entire period, the CIS and HIT technologies show the best performance compared to other technologies. The monthly energy production during the entire period is almost identical for the CdTe, m-Si, and P-Si. Nevertheless, the a-Si/μc-Si technology has been observed as the least interesting in monthly energy production.

3.1.2. Analysis of the losses in the PV technologies

The difference between the reference yield (Y_r) and the field yield (Y_f) of a PV system is termed as the system's total losses (L_T), which can be expressed as [43]:

$$L_T = Y_r - Y_f \tag{6}$$

The total losses for the six PV technologies considered in this study are presented in Figure 8. It is evident from the figure that the highest total losses, with a value of 4.2 kWh/kWp/day, are observed in the CIS technology, followed by the HIT, with a value of 4.11 kWh/kWp/day. The total losses recorded by the CdTe, m-Si, and p-Si are 4.02 kWh/kWp/day, 4 kWh/kWp/day, and 3.98 kWh/kWp/day, respectively. The a-Si/µc-Si technology has noticed the lowest total losses of 3.74 kWh/kWp/day.

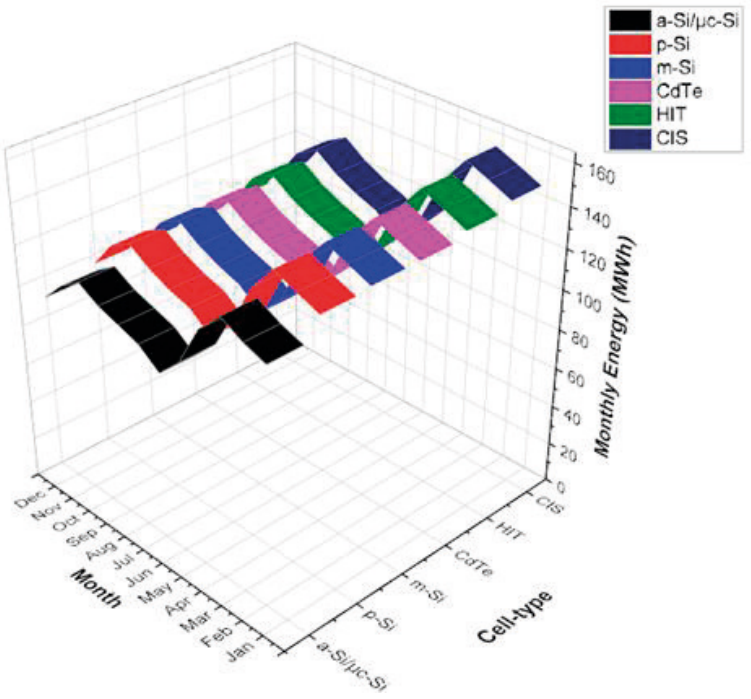

Figure 7. Monthly energy production of different PV technologies.

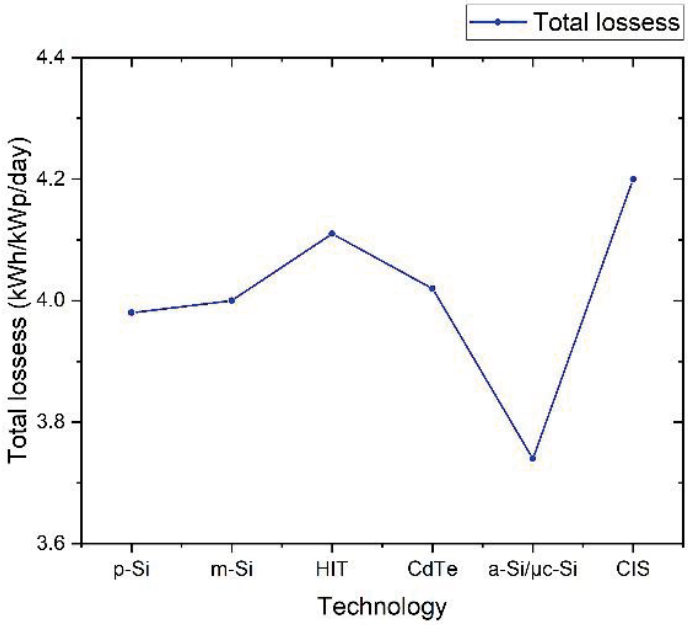

Figure 8. Total losses for six PV technologies.

3.1.3. Effect of the tilt angle of the PV panels and the orientation of PV panels

Figure 9 shows the variation of the annual energy production, specific production, and the performance ratio concerning the tilt angle, which ranges from 10° to 45°. The annual and specific energy

production declines by increasing the tilt angle. The largest annual energy production and the largest specific production have been observed at a tilt angle of 10°, with values of 1,545 MWh/year and 1,541 kWh/kWp/year, respectively. In contrast, the lowest annual energy production and the lowest specific production have been observed at a 45° tilt angle, with values of 1,304 MWh/year and 1,300 kWh/kWp/year. On the other hand, the PR increases by varying the tilt angle from 10° to 40° and slightly declines at a tilt angle of 45°.

Figure 10 shows the effect of the orientation of the solar PV panels on the annual energy production, specific production, and PR. It is clear from the figure that the installed solar PV rooftop system produces the largest annual energy production and the largest specific production, with PV modules facing south (S), southeast (SE), and southwest (SW). This is because Thailand is situated in the Northern Hemisphere. Additionally, the largest annual energy production and the largest specific production reached values of 1,456 MWh/year and 1,451 kWh/kWp/year with PV modules facing S, while the lowest annual energy production of 1,358 MWh/year and the lowest specific production of 1,353 kWh/kWp/year were noticed with PV modules facing north (N). However, the PR reaches its maximum value when the PV modules are facing the northeast (NE) and the north (N) orientations, while it shows the lowest value with the PV module facing the west (W) orientation.

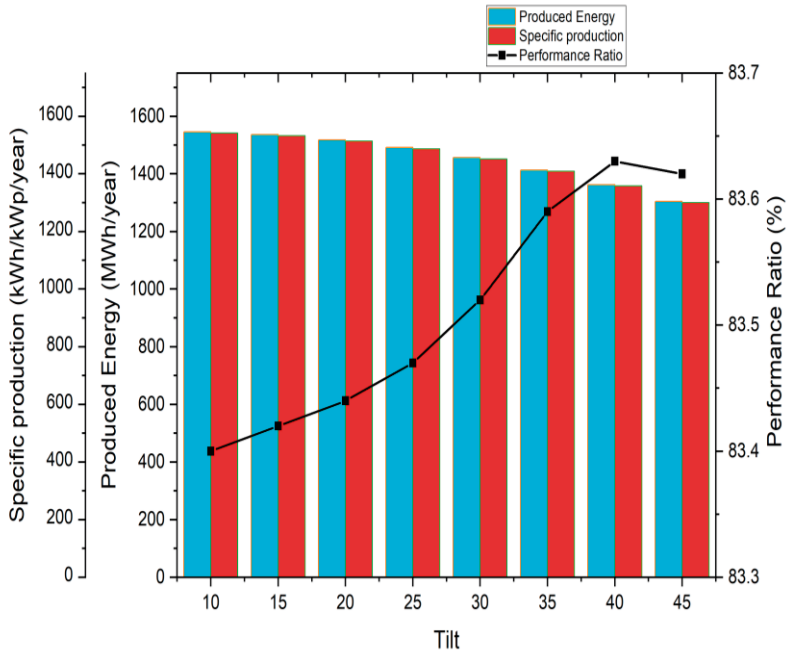

Figure 9. Effect of the tilt angle of the PV panels on the annual energy production, the specific production, and the performance ratio.

3.1.4. Optimal tilt and azimuth angles

The optimization of the tilt angle of the PV panels and the azimuth angle of the PV modules can increase the performance of the solar PV rooftop system. The optimal tilt angle of the panels versus the azimuth angle of the modules for the maximum energy injected into the grid and the maximum global incident radiation on the collector plane is shown in Figure 11 and Figure 12, respectively. It is seen from both figures that the solar PV rooftop system operates the most efficiently with a tilt angle of 10° and an azimuth angle of 0°, where it injects the maximum energy of 1,546.3 MWh into the grid with a maximum global incident radiation of 1,848.2 kWh/m^2 in the collector plane.

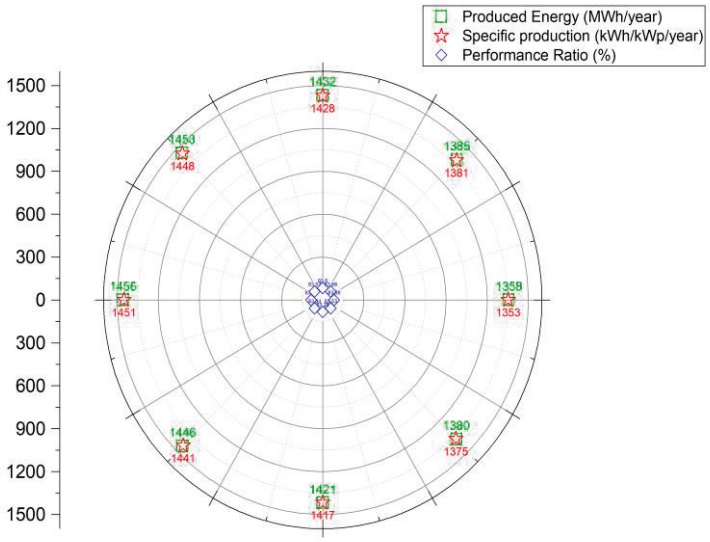

Figure 10. Effect of the orientation of the PV modules on the annual energy production, the specific production, and the performance ratio.

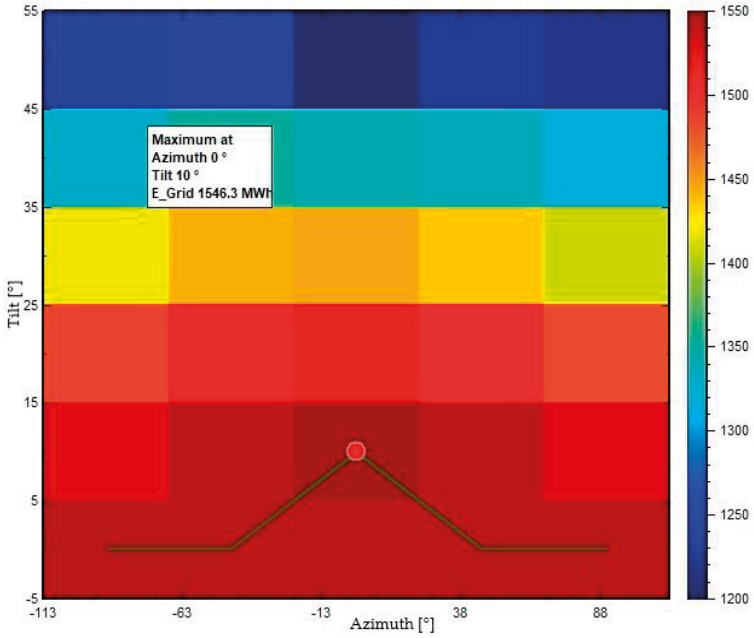

Figure 11. The optimal tilt angle of the panels and the azimuth angle of the modules for the maximum energy injected into the grid.

The appropriate design of a 1 MW Solar PV rooftop at Thaksin University (Phatthalung Campus) consists of 6 units of 80 kWac inverters, which are connected to 95 strings of PV panels, including 18 PV panels per string on one side and 4 units of 60 kWac inverters connected to 10 strings of PV panels with 14 PV panels per string on another side with the single line diagram as shown in Figure 13.

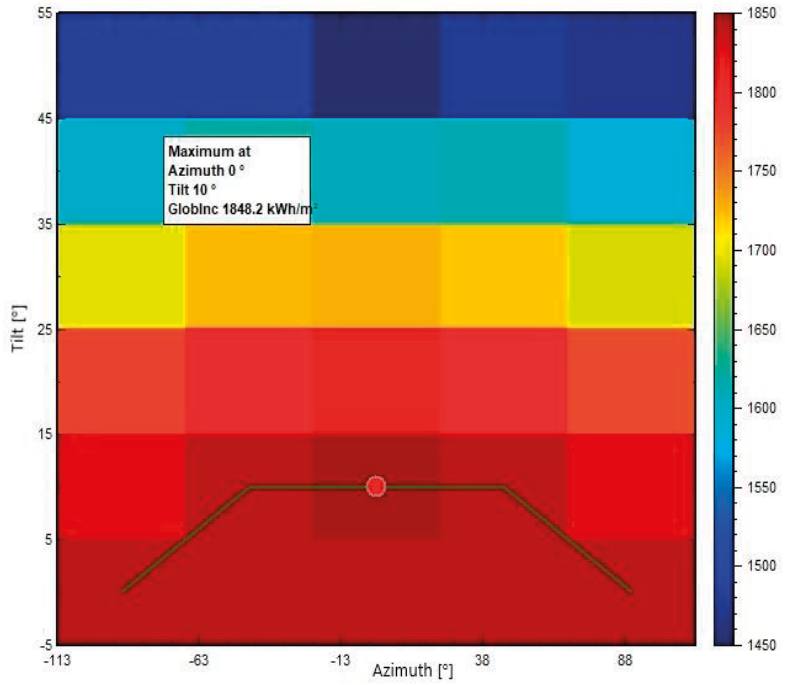

Figure 12. The optimal tilt angle of the panel and azimuth angle of modules for the maximum global incident radiation on the collector plane.

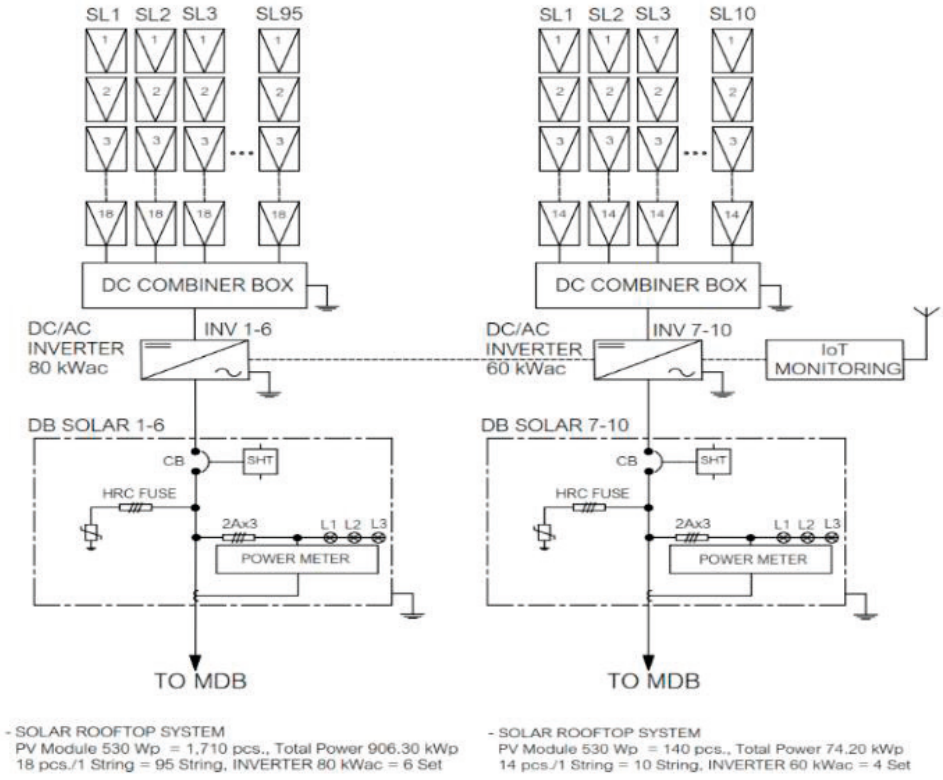

Figure 13. Single line diagram of a 1 MW solar PV rooftop at Thaksin University (Phatthalung Campus).

3.2. Economic analysis

The current study evaluates four possible economic scenarios for a 1 MW solar PV rooftop system installed at Thaksin University (Phatthalung Campus). Scenario 1 is related to a self-investment and self-consumption scheme, where the university (the project owner) would invest in the project and produce its

solar power for consumption. Both are based on bankable projects. Scenario 2 is a self-consumption scheme, while Scenario 3 is a feed-in tariff (FiT) scheme. For these two scenarios, commercial banks would invest in the project. Furthermore, the solar power produced would be utilized by the university in the case of Scenario 2, while in the case of Scenario 3, the produced energy by the solar PV rooftop system would be fed into the national grid. Scenario 4 is associated with an energy service company (ESCO) scheme, where private companies would be invited to participate in the project through a competitive bidding process. The company with the highest offer would be asked to invest in the project.

The economic indicators of every scenario are shown in Table 6. Scenario 3 (bankable and FiT scheme) offers a BCR of 3.34; an NPV of 71,963,009 THB; an IRR of 30%, and a PBP of 5 years, which makes it the best-case scenario. The PBP in this scenario is within the acceptable range of 5-7 years [43] for profitable solar PV rooftop projects [44]. Scenario 1 (self-investment and self-consumption scheme) is the second favorable case, with a BCR of 1.68; an NPV of 20,817,144 THB; an IRR of 10%; and a PBP of 9 years. On the other hand, Scenario 4 (ESCO scheme) and Scenario 2 (bankable and self-consumption scheme) are the least preferable cases, with PBP of 13 and 15 years, respectively. The LCOE calculated for all scenarios is 0.80 THB/kWh.

For comparison, the economic analysis indicates that the bankable and FiT scheme (Scenario 3) is the best model for the stakeholders, with the highest NPV and the shorter PBP. The self-investment and self-consumption scheme (Scenario 1) is the second-best model for the university itself. This model presents the project owner with an opportunity to invest, with an NPV of above 20,000,000 THB and a PBP of 9 years. On the other hand, the ESCO (Scenario 4) and the bankable and self-consumption schemes (Scenario 2) are the least interesting models due to the long PBP of 13 to 15 years.

Table 6. Economic indicators for the 1 MW solar PV rooftop system.

Sr.	Sr. Details	BCR	NPV (THB)	IRR (%)	PBP (Year)	LCOE (THB/kWh)
1	Self-investment and self-consumption	1.68	20,817,144	10	9	0.80
2	Bankable and self-consumption	1.14	4,332,252	1	15	0.80
3	Bankable and FiT	3.34	71,963,009	30	5	0.80
4	ESCO	1.34	10,512,475	5	13	0.80

Key: Sr.: scenario, BCR: benefit-cost ratio, NPV: net present value,
IRR: internal rate of return, PBP: payback period, LCOE: levelized cost of electricity, FiT: Feed-in-Tariff.

4. Conclusions

This study addresses the performance of six solar PV technologies: p-Si, m-Si, HIT, CdTe, a-Si/μc-Si, and CIS. The effect of the tilt angle of the solar PV panels and the orientation of the solar PV modules are also assessed and discussed. Further, four economic scenarios for a 1 MW solar PV rooftop system are evaluated at the Phatthalung campus of Thaksin University (Thailand).

The CIS technology recorded the highest annual energy production of 1,537 MWh and a performance ratio of 88.24%, while the a-Si/μc-Si technology showed the lowest annual energy production of 1,370 MWh and a PR of 78.6%. The CIS and HIT technologies achieved the maximum monthly energy production in March, with 156.1 MWh and 152.5 MWh values, respectively. The CIS technology detected the largest total losses, with a value of 4.2 kWh/kWp/day, while the a-Si/μc-Si noticed the lowest total losses of 3.74 kWh/kWp/day. The largest annual energy production and the largest specific production, with values of 1,545 MWh/year and 1,541 kWh/kWp/year, were respectively obtained for the PV panels positioned at a 10° tilt angle, while the lowest annual energy production and the lowest specific production, with values of 1,304 MWh/year and 1,300 kWh/kWp/year, were respectively obtained for the PV panels positioned at a 45° tilt angle. Furthermore, the largest annual energy production and specific production, with values of 1,456 MWh/year and 1,451 kWh/kWp/year, were respectively obtained with the PV modules facing South (S), while the lowest annual energy production of 1,358 MWh/year and the specific production of 1,353 kWh/kWp/year were noticed when the PV modules were facing North (N). The economic analysis shows that the bankable and FiT scheme (Scenario 3) is the best model for the stakeholders, offering the highest NPV and the shortest PBP.

Similarly, the self-investment and self-consumption scheme (Scenario 1) is the second-best model, which offers the university an NPV of above 20,000,000 THB and a PBP of 9 years.

The solar PV rooftop methodology defined in this work can be applied to other regional buildings. Future research may include the techno-economic evaluation of solar PV rooftop systems and a DC battery storage system for the university and other provincial buildings. Other technical aspects, e.g., evaluation of the thermal performance of rooftop PV and shading loss affecting overall performance, would also be recommended for further study.

Author Contributions: Conceptualization and Writing Rawit Khamharnphol: Technical Analysis and Visualization Sakrapee Khunphet: Electric and Single Line Diagram Design Ismail Khamdar: Writing and Data Analysis Somphol Chiwamongkhonkarn: Computer Simulation Chuleerat Kongruang: Economic Analysis Yves Gagnon: Validation and Editing

Funding: This research received no external funding.

Conflicts of Interest: The authors declare no conflict of interest.

References

[1] Al-Ghussain, L.; Samu, R.; Taylan, O.; Fahrioglu, M. Techno-Economic Comparative Analysis of Renewable Energy Systems: Case Study in Zimbabwe. *Inventions* 2020, *5*(3). https://doi.org/10.3390/inventions5030027.

[2] Abdin, Z.; Mérida, W. Hybrid energy systems for off-grid power supply and hydrogen production based on renewable energy: A techno-economic analysis. *Energy Conversion and Management* 2019, *196*, 1068-1079. https://doi.org/10.1016/j.enconman.2019.06.068.

[3] Dahiru, A. T.; Tan, C. W. Optimal sizing and techno-economic analysis of grid-connected nanogrid for tropical climates of the Savannah. *Sustainable Cities and Society*, 2020, *52*, 101824. https://doi.org/10.1016/j.scs.2019.101824.

[4] Ahmed, N.; Naveed Khan, A.; Ahmed, N.; Aslam, A.; Imran, K.; Sajid, M. B.; Waqas, A. Techno-economic potential assessment of mega scale grid-connected PV power plant in five climate zones of Pakistan. *Energy Conversion and Management* 2021, *237*, 114097. https://doi.org/10.1016/j.enconman.2021.114097.

[5] IRENA. Renewables Take Lion's Share of Global Power Additions in 2021. Retrieved from https://www.irena.org/News/pressreleases/2022/Apr/Renewables-Take-Lions-Share-of-Global-Power-Additions-in-2021#:~:text=By%20the%20end%20of%202021,power%20by%209.1%20per%20cent (accessed: 13 October 2022).

[6] Statistica. Solar photovoltaic capacity worldwide in 2021, by region. Retrieved from https://www.statista.com/statistics/271374/new-installed-solar-photovoltaic-capacity-worldwide-by-region/ (accessed: 20 November 2022).

[7] Lau, K. Y.; Tan, C. W.; Ching, K. Y. The implementation of grid-connected, residential rooftop photovoltaic systems under different load scenarios in Malaysia. *Journal of Cleaner Production*, 2021, *316*, 128389. https://doi.org/10.1016/j.jclepro.2021.128389

[8] Waewsak, J.; Chancham, C.; Mani, M.; Gagnon, Y. Estimation of Monthly Mean Daily Global Solar Radiation over Bangkok, Thailand Using Artificial Neural Networks. *Energy Procedia*, 2014, 57, 1160-1168.https://doi.org/10.1016/j.egypro.2014.10.103.

[9] Yazdani, H.; Yaghoubi, M. Techno-economic study of photovoltaic systems performance in Shiraz, Iran. *Renewable Energy*, 2021, *172*, 251-262. https://doi.org/10.1016/j.renene.2021.03.012.

[10] Quansah, D. A.; Adaramola, M. S.; Appiah, G. K.; Edwin, I. A. Performance analysis of different grid-connected solar photovoltaic (PV) system technologies with combined capacity of 20 kW located in humid tropical climate. *International Journal of Hydrogen Energy*, 2017, *42*(7), 4626-4635. https://doi.org/10.1016/j.ijhydene.2016.10.119.

[11] Ali, H.; Khan, H. A. Techno-economic evaluation of two 42 kWp polycrystalline-Si and CIS thin-film based PV rooftop systems in Pakistan. *Renewable Energy*, 2020, *152*, 347-357. https://doi.org/10.1016/j.renene.2019.12.144.

[12] Olarewaju, R.O.; Ogunjuyigbe, A.S.O.; Ayodele, T. R.; Yusuff, A. A.; Mosetlhe, T. C. An assessment of proposed grid integrated solar photovoltaic in different locations of Nigeria: Technical and economic perspective. *Cleaner Engineering and Technology,* 2021, *4*, 100149. https://doi.org/10.1016/j.clet.2021.100149.

[13] Nour-eddine, I. O.; Lahcen, B.; Fahd, O. H.; Amin, B.; Aziz, O. Outdoor performance analysis of different PV technologies under hot semi-arid climate. *Energy Reports,* 2020, *6*, 36-48. https://doi.org/10.1016/j.egyr.2020.08.023

[14] González-González, E.; Martín-Jiménez, J.; Sánchez-Aparicio, M.; Del Pozo, S.; Lagüela, S. Evaluating the standards for solar PV installations in the Iberian Peninsula: Analysis of tilt angles and determination of solar climate zones. *Sustainable Energy Technologies and Assessments,* 2022, *49*, 101684. https://doi.org/10.1016/j.seta.2021.101684.

[15] Bakirci, K. General models for optimum tilt angles of solar panels: Turkey case study. *Renewable and Sustainable Energy Reviews,* 2012, *16*(8), 6149-6159. https://doi.org/10.1016/j.rser.2012.07.009.

[16] Mamun, M. A. A.; Islam, M. M.; Hasanuzzaman, M.; Selvaraj, J. Effect of tilt angle on the performance and electrical parameters of a PV module: Comparative indoor and outdoor experimental investigation. *Energy and Built Environment,* 2022, *3*(3), 278-290. https://doi.org/10.1016/j.enbenv.2021.02.001.

[17] Al Garni, H. Z., Awasthi, A., & Wright, D. (2019). Optimal orientation angles for maximizing energy yield for solar PV in Saudi Arabia. *Renewable Energy, 133*, 538-550. .https://doi.org/10.1016/j.renene. 2018.10.048

[18] Christiaanse, T. V.; Loonen, R. C. G. M.; Evins, R. Techno-economic optimization for grid-friendly rooftop PV systems – A case study of commercial buildings in British Columbia. *Sustainable Energy Technologies and Assessments,* 2021, *47*, 101320. https://doi.org/10.1016/j.seta.2021.101320.

[19] Mangiante, M. J.; Whung, P.-Y.; Zhou, L.; Porter, R.; Cepada, A.; Campirano, E.; Torres, M. Economic and technical assessment of rooftop solar photovoltaic potential in Brownsville, Texas, U.S.A. *Computers, Environment and Urban Systems,* 2020, *80*, 101450. https://doi.org/10.1016/j.compenvurbsys. 2019.101450.

[20] Imam, A. A.; Al-Turki, Y. A. J. S. Techno-economic feasibility assessment of grid-connected PV systems for residential buildings in Saudi Arabia—A case study. *Sustainability,* 2019, *12*(1), 262. https://doi.org /10.3390/su12010262.

[21] Chimres, N.; Wongwises, S. Critical review of the current status of solar energy in Thailand. *Renewable and Sustainable Energy Reviews,* 2016, *58*, 198-207. https://doi.org/10.1016/j.rser.2015.11.005.

[22] Tongsopit, S. Thailand's feed-in tariff for residential rooftop solar PV systems: Progress so far. *Energy for Sustainable Development,* 2015, *29*, 127-134. https://doi.org/10.1016/j.esd.2015.10.012.

[23] Yoomak, S.; Patcharoen, T.; Ngaopitakkul, A. Performance and Economic Evaluation of Solar Rooftop Systems in Different Regions of Thailand. *Sustainability,* 2019, *11*(23), 6647. https://doi.org/10.3390 /su11236647.

[24] Boddapati, V.; Nandikatti, A. S. R.; Daniel, S. A. Techno-economic performance assessment and the effect of power evacuation curtailment of a 50 MWp grid-interactive solar power park. *Energy for Sustainable Development,* 2021, *62*, 16-28. https://doi.org/10.1016/j.esd.2021.03.005.

[25] Sekyere, C. K. K.; Davis, F.; Opoku, R.; Otoo, E.; Takyi, G.; Atepor, L. Performance evaluation of a 20 MW grid-coupled solar park located in the southern oceanic environment of Ghana. *Cleaner Engineering and Technology,* 2021, *5*, 100273. https://doi.org/10.1016/j.clet.2021.100273.

[26] Kamdar, I.; Ali, S.; Taweekun, J.; Ali, H. M. Wind Farm Site Selection Using WAsP Tool for Application in the Tropical Region. *Sustainability, 2021, 13*(24). https://doi.org/10.3390/su132413718.

[27] Waewsak, J.; Ali, S.; Gagnon, Y. Site suitability assessment of para rubberwood-based power plant in the southernmost provinces of Thailand based on a multi-criteria decision-making analysis. *Biomass and Bioenergy,* 2020, *137*, 105545. https://doi.org/10.1016/j.biombioe.2020.105545.

[28] ABB. *central inverters data sheet PVS800 - 500 to 1000 kW* Retrieved from https://cdn.enfsolar.com /Product/pdf/Inverter/5d538c5f7f8a8.pdf. (accessed: 15 October 2022).

[29] Kumar, N. M.; Das, P.; Krishna, P. R. (2017). *Estimation of grid feed in electricity from roof integrated Si-amorph PV system based on orientation, tilt and available roof surface area.* Paper presented at the 2017 International

Conference on Intelligent Computing, Instrumentation and Control Technologies (ICICICT), 588-596, https://doi.org/10.1109/ICICICT1.2017.8342629.

[30] Hafez, A. Z.; Soliman, A.; El-Metwally, K. A.; Ismail, I. M. Tilt and azimuth angles in solar energy applications – A review. *Renewable and Sustainable Energy Reviews,* 2017, *77*, 147-168. https://doi.org/10.1016/j.rser.2017.03.131.

[31] Chaianong, A.; Bangviwat, A.; Menke, C.; Darghouth, N. R. Cost–Benefit Analysis of Rooftop PV Systems on Utilities and Ratepayers in Thailand. *Energies,* 2019, *12*(12), 2265. https://doi.org/10.3390/en12122265.

[32] Pikas, E.; Kurnitski, J.; Thalfeldt, M.; Koskela, L. J. E. Cost-benefit analysis of nZEB energy efficiency strategies with on-site photovoltaic generation. *Energy,* 2017, *128*, 291-301. https://doi.org/10.1016/j.energy.2017.03.158.

[33] Leurent, M.; Da Costa, P.; Rämä, M.; Persson, U.; Jasserand, F. J. E. Cost-benefit analysis of district heating systems using heat from nuclear plants in seven European countries. *Energy,* 2018, *149*, 454-472. https://doi.org/10.1016/j.energy.2018.01.149.

[34] Kopp, R. J.; Krupnick, A. J.; Toman, M. Cost-benefit analysis and regulatory reform: an assessment of the science and the art. Retrieved from https://media.rff.org/documents/RFF-DP-97-19.pdf (accessed: 17 October 2022).

[35] Ramadhan, M.; Naseeb, A. The cost benefit analysis of implementing photovoltaic solar system in the state of Kuwait. *Renewable Energy,* 2011, *36*(4), 1272-1276. https://doi.org/10.1016/j.renene.2010.10.004.

[36] Dincer, I. Environmental impacts of energy. *Energy Policy, 1999, 27*(14), 845-854. https://doi.org/10.1016/S0301-4215(99)00068-3.

[37] Shukla, A. K.; Sudhakar, K.; Baredar, P. Simulation and performance analysis of 110 kWp grid-connected photovoltaic system for residential building in India: A comparative analysis of various PV technology. *Energy Reports,* 2016, *2*, 82-88. https://doi.org/10.1016/j.egyr.2016.04.001.

[38] Eltamaly, A. M.; Mohamed, M. A. 8 - Optimal Sizing and Designing of Hybrid Renewable Energy Systems in Smart Grid Applications. In I. Yahyaoui (Ed.), *Advances in Renewable Energies and Power Technologies*, 2018. 231-313: Elsevier.

[39] Milborrow, D. 2.15 - Wind Energy Economics. In T. M. Letcher (Ed.), *Comprehensive Renewable Energy (Second Edition)*. 2022, 463-496. Oxford: Elsevier.

[40] Papapetrou, M.; Kosmadakis, G. Chapter 9 - Resource, environmental, and economic aspects of SGHE. In A. Tamburini, A. Cipollina, & G. Micale (Eds.), *Salinity Gradient Heat Engines*. 2022, 319-353: Woodhead Publishing.

[41] Ameur, A.; Berrada, A.; Bouaichi, A.; Loudiyi, K. Long-term performance and degradation analysis of different PV modules under temperate climate. *Renewable Energy,* 2022, *188*, 37-51. https://doi.org/10.1016/j.renene.2022.02.025.

[42] Schultz, D.; Clark, W. W.; Sowell, A. Chapter 7 - Life-Cycle Analysis: The Economic Analysis of Demand-Side Programs and Projects in California. In W. W. Clark (Ed.), *Sustainable Communities Design Handbook*. 2010, 99-137. Boston: Butterworth-Heinemann.

[43] Anang, N.; Syd Nur Azman, S. N. A.; Muda, W. M. W.; Dagang, A. N.; Daud, M. Z. Performance analysis of a grid-connected rooftop solar PV system in Kuala Terengganu, Malaysia. *Energy and Buildings,* 2021, *248*, 111182. https://doi.org/10.1016/j.enbuild.2021.111182.

[44] Sewchurran, S.; Davidson, I. E. Technical and financial analysis of large-scale solar-PV in eThekwini Municipality: Residential, business and bulk customers. *Energy Reports,* 2021, *7*, 4961-4976. https://doi.org/10.1016/j.egyr.2021.07.134.

[45] Pita, P.; Tia, W.; Suksuntornsiri, P.; Limpitipanich, P.; Limmeechockchai, B. Assessment of feed-in-tariff policy in Thailand: impacts on national electricity prices. *Energy Procedia*, 2015, *79*, 581-589.

JSTR
ASEAN Journal of Scientific and Technological Reports

Research article

Effect of Pre-harvest Periods by Replacing Nutrient Solution with Tap Water on Nitrate and Quality in Hydroponic Lettuce

Eaknarin Ruangrak[1, 2*], Nurainee Salaemae[2], Somnuek Sornnok[3], and Nang Myint Phyu Sin Htwe[4]

[1] Faculty of Science and Technology, Prince of Songkla University, Pattani Campus, Pattani 94000, Thailand; eaknarin.r@psu.ac.th
[2] Faculty of Science and Technology, Prince of Songkla University, Pattani Campus, Pattani 94000, Thailand; nurainee.s@psu.ac.th
[3] Faculty of Science and Technology, Prince of Songkla University, Pattani Campus, Pattani 94000, Thailand; somnuk.so@psu.ac.th
[4] Faculty of Science and Technology, Prince of Songkla University, Pattani Campus, Pattani 94000, Thailand; nmphyusinhtwe@gmail.com
* Correspondence: eaknarin.r@psu.ac.th

Citation:
Ruangrak, E.; Salaemae, N.; Sornnok, S.; Htwe, NMPS. Effect of pre-harvest periods by replacing nutrient solution with tap water on nitrate and quality in hydroponic lettuce. *ASEAN J. Sci. Tech. Report.* **2023**, *26*(1), 76-83. https://doi.org/10.55164/ajstr.v26i1.247666.

Article history:
Received: November 3, 2022
Revised: February 24, 2023
Accepted: February 28, 2023
Available online: March 21, 2023

Abstract: Lettuce (*Lactuca sativa* L.) is a high-value nutritional food for human consumption, rich in minerals and vitamins. However, people are still concerned about the residues of nitrate content in hydroponic lettuce. Pre-harvesting by replacing nutrient solution with tap water is one of several factors that can help to reduce nitrate content and improve the quality of hydroponic lettuce. Therefore, this study focused on the effect of pre-harvest periods by replacing nutrient solution with tap water on nitrate and quality in hydroponic lettuce. This experiment was performed by replacing nutrient solution with tap water in a hydroponic system for 0 h, 24 h, 48 h, and 72 h before harvesting the lettuce product. Nitrate, vitamin C, phenolic, and soluble sugar contents were determined. The results showed that nitrate content was lowest under pre-harvest conditions for 72 h (19 mg/g dry weight, 63% reduction), but it was not significantly different for 48 h (20 mg/g dry weight, 61% reduction). The vitamin C content was significantly decreased after pre-harvesting for 72 h (5.3 μg/100 g, 30% reduction). The soluble sugar content was significantly increased and reached its highest content after pre-harvest for 48 h (3.3 mg/100 g, 105% increase), but there was no significant difference at 72 h (3.2 mg/100 g, 98% increase). Although the phenolic content decreased slightly, there was no significant difference among the treatments. In conclusion, nitrate contents were reduced the lowest, and soluble sugar contents were increased the highest after pre-harvest for 48 h. Vitamin C and phenolic contents were slightly decreased after pre-harvest periods by replacing the nutrient solution with tap water.

Keywords: Green Oak Lettuce; Nitrate; Phytochemicals; Hydroponic System; Water Flow; Pre-harvest

1. Introduction

A hydroponic system is a suitable farming technology to produce fresh leafy vegetables rapidly, and it also has the potential to reduce the environmental impact of food production worldwide. A hydroponic farm has an efficient water and fertilizer system, pays lower labor costs, and promotes plant growth. Furthermore, vegetables grown in a hydroponic system are less likely to be contaminated with *Escherichia coli* and *Salmonella* spp [1]. Therefore, customers feel comfortable consuming raw vegetable products from a hydroponic farm as it offers sustainable, healthy food production and maintains a clean environment without heavy chemicals.

Lettuce (*Lactuca sativa* L.) has a high nutritional value for human consumption. Lettuce is rich in minerals and vitamins. Aćamović-Djoković et al. [2] reported that the vitamin C content of lettuce ranges from 3.50 to 9.60 mg/100 g of fresh weight. However, lettuce is not always good for consumer health, and several people are concerned about excessive nitrate content or nitrate residue, especially in hydroponic lettuce production. Hydroponic vegetables have the potential to accumulate high nitrate concentrations that are a risk to human health as they can produce carcinogenic N-nitroso compounds that cause gastrointestinal cancer [3-4]. The European Commission Regulation (No. 194/97, 1997) [5] suggests that the maximum nitrate concentration should not exceed 3.65 mg/kg of body weight daily. For example, 60 kg of body weight should not consume more than 219 mg per day.

Nitrate is one of the nitrogen sources that plays an essential role as a plant nutrient for the main constituents of chlorophyll, protein, and genetic material [6]. Plants take nitrate via the root hair, xylem, mesophyll cells, and cell walls. Then nitrate is stored in the cell and reduced into nitrite, ammonium, glutamine, and other amino acids [7]. After assimilating nitrate into glutamine acid, it is safe for human health. However, during the transportation of nitrate from the root to the leaf cells, nitrate is specially retained in the xylem vessels of the root, stem, petiole, and leaf veins. This nitrate molecule is still harmful to human health [8].

Pre-harvest is a practical method that can help to improve the quality and shelf-life of vegetables and reduce their risk before harvest [9–11]. For example, Gil [9] studied pre-harvest related to agricultural practices, including type and rate of fertilization, irrigation, and salinity, which affect fresh-cut quality, and found that pre-harvest factors increased the quality of fresh-cut lettuce and baby leaves. Arturas et al. [12] reported that pre-harvest with supplemental solid-state lighting on lettuce cultivars can improve the antioxidant properties of lettuce. Wanlai et al. [13] also studied the effect of pre-harvest illumination with a red and blue light ratio. They found that nitrate content was reduced and soluble sugar content was dramatically increased in lettuce under pre-harvest continuous illumination. Guffanti et al. [14] have reported that nitrate content has reduced and antioxidant activity has increased after exposure to light and replacing the nutrient solution with tap water before harvest in a vertical farm. Moreover, several research studies related light pre-harvest in lettuce [15–17]. However, there is less knowledge of pre-harvest periods by replacing nutrient solution with tap water, which can reduce nitrate and other synthetic fertilizers in the xylem of plants by replacing water in a hydroponic system. Therefore, this study focused on the effect of pre-harvest periods by replacing nutrient solution with tap water on nitrate and quality in hydroponic lettuce.

2. Materials and Methods

2.1 Plant materials and growth conditions

The green oak lettuce (*Lactuca sativa* L.) was used as plant material, and a nutrient film technique (NFT) hydroponic system was applied for cultivation. The seeds were sown on the wet tissue paper in the box and left at room temperature for three days. Then the seeds with a radicle of about 10 mm were transplanted into polyfoam cubes (2.5x2.5x2.5 cm), and placed in the nursery greenhouse for 2 weeks. Afterward, the seedlings were transplanted into the NFT system for this experiment. All the plants were grown under a 50% aluminum net shade with a temperature of 24 to 32 °C and a relative humidity of 62% to 92%. Modified Hoagland and Arnon [18] nutrient solution was used as a hydroponic nutrient solution with an electrical conductivity (EC) of 1.8 mS/cm and pH 5.5- 6.5 were adjusted once a week. Briefly, the nutrient stock composition was prepared as follows: In solution stock A, it contained; potassium nitrate (KNO_3, 780 g/10 L), mono ammonium phosphate ($NH_4H_2PO_4$, 130 g/10 L), magnesium sulfate ($MgSO_4 \cdot 7H_2O$, 500 g/10 L), manganese EDTA (MnEDTA, 8 g/10 L), monopotassium phosphate (KH_2PO_4, 100 g/10 L), and microelements (Boron EDTA, MnEDTA, MgO, CuEDTA, MoEDTA, and FeEDTA, 10 g/10 L). The stock B solution was comprised of calcium nitrate ($Ca(NO_3)_2 \cdot 4H_2O$, 1000 g/10 L) and iron chelate (FeEDTA, 10 g/10 L). This experiment was performed at the Department of Agricultural and Fisheries Science, Faculty of Science and Technology, Prince of Songkla University, Pattani Campus (latitude 6.882424 and longitude 101.235334).

2.2 Treatment and experimental design

This study focused on the effect of pre-harvest periods by replacing nutrient solution with tap water on nitrate and quality in hydroponic lettuce. Thus, lettuce plants experimented with 30 days after transplanting into the NFT system. The experiment was comprised of four treatments with different pre-harvest periods by

replacing nutrient solution with tap water, including (1) 0 h (harvested before replacing nutrient solution with tap water, control treatment), (2) 24 h (harvested after replacing nutrient solution with tap water for 24 h), 48 h (harvested after replacing nutrient solution with tap water for 48 h), and 72 h (harvested after replacing nutrient solution with tap water for 72 h). A completely randomized design (CRD) with three replications was used in this experiment.

2.3 Determination of nitrate content

The samples of lettuce leaves were collected, washed with running tap water, and washed with distilled water three times. After that, the samples were dried at 65 °C for 24 h and then finely grounded. Next, 1 g of the samples were weighed, suspended in 10 mL of distilled water, stood at 45 °C for 1 h, and filtered through No. 40 Whatman filter paper. A 50 mL tube with 0.4 mL of 5% (w/v) salicylic acid was used, and 0.1 mL of the extraction was added. After that, the samples were left at room temperature for 20 min. 9.5 mL of a 2N sodium hydroxide (NaOH) solution was added to the samples. The absorbance was immediately applied at 412 nm (Biochrom, Libra S12, England) for determination [19].

2.4 Determination of soluble sugar content

The determination of soluble sugar content was done by Yemn and Willis method [20]. Lettuce leaves were dried at 65 °C for 48 h before being ground thoroughly. 50 mg of the dry sample was mixed in 4 mL of 80% ethanol, homogenized, transferred into test tubes, and then boiled in a water bath for 15 min. After that, the samples were centrifuged at 3,000 rpm for 15 min. The supernatant was removed. 2 mL of 80 % ethanol was added and recentrifuged. This step was repeated two times. The supernatant was collected and the final volume was 10 mL. After that, 0.2 mL of the aliquot was pipetted into test tubes and evaporated to dryness. The sample was left out until it was cold. The residue of each sample was added to 1 mL of distilled water and well dissolved. Then, 4 mL of anthrone reagent (0.2 g anthrone in 100 mL (H_2SO_4)) was added to the solution, then boiled in a water bath for 10 min. After cooling, soluble sugar contents were determined at 620 nm against blank.

2.5 Determination of vitamin C content

The modified Jagota and Dani method [21] was applied for vitamin C determination. Fresh samples were used, cut into small pieces, and weighed 7 g. Then, the samples were homogenized and suspended in 30 mL of oxalic acid (0.5% w/v). These homogenous mixtures were filtered through No. 40 Whatman filter paper, followed by adding 4 mL of 10% Trichloroacetic acid into 1 mL of the homogenous mixture, which was then shaken well and immediately placed on ice for 5 min. The mixture was centrifuged at 8,000 rpm for 5 min. Then, 0.2 mL of 0.2 M Folin-Ciocalteu's reagent was added to 3 mL of supernatant, and the mixture was left at room temperature for 60 min. The samples were measured at an absorbance of 760 nm with a spectrophotometer (Biochrom, Libra S12, England).

2.6 Determination of phenolic content

As in a previous study, total phenolic contents were determined using Folin–Ciocalteu's method [22], modified for the 96-well plate assay [23]. Fresh lettuce leaves were washed with tap water and repeated with distilled water. Then, the sample was cut into small pieces and ground into a fine paste. The sample was weighed at 5 g into a Duran bottle, and then 10 mL of 70% EtOH (v/v) was added and shaken for 1 h on a shaker plate. After that, sample extracts were filtered and rinsed into 1.5 mL microtubes and stored at -20 °C in the dark until further analysis. Folin–Ciocalteu's reagent (25 µL, 50% v/v) was added to 10 µL of extract (1 mg/mL, w/v) in a well of a 96-well plate. After 5 min of incubation at room temperature, 25 µL of 20% (w/v) sodium carbonate was added to the mixture, followed by distilled water to a final volume of 200 µL per well plate. After 30 min of incubation at room temperature, the absorbance was read at 760 nm against a blank using a Multiskan EX microplate reader (Thermo Fisher Scientific, Finland). A standard curve was plotted using gallic acid [24].

2.7 Statistical analysis

This study's statistics were carried out using a CRD. Data analysis was done using the MS Excel program and one-way analysis of variance (ANOVA) (version 7.0). Treatment means underwent Least Significant Difference (LSD) analysis with a 95% confidence level.

3. Results and Discussion

3.1. Nitrate content

In a hydroponic vegetable farm, nitrates are assimilated through the root hair, xylem, and mesophyll cells, as they can pass through the cell wall via transporters. The result of hydroponic lettuce grown under the pre-harvest condition of replacing nutrient solution with tap water showed that nitrate content was decreased by 19 to 63% when compared with 0 h (51 mg/g dry weight, control treatment) (Fig. 1). The treatment of replacing nutrient solution with tap water for 72 h (19 mg/g dry weight, 63% reduction) showed the lowest nitrate content, followed by treatments of 48 h (20 mg/g dry weight, 61% reduction), and 24 h (41 mg/g dry weight, 19% reduction). However, the treatments between 72 h and 48 h did not show a statistically significant difference. Furthermore, the treatments at 0 h and 24 h did not show a significant difference from each other (Fig. 1). The results of this study are consistent with Guffanti et al. [25], who reported that reducing the concentration of the nutrient solution by adding water or completely substituting the nutrient solution with water in the last days before harvest can help reduce the amount of nitrate in leaves. The nitrate content was decreased by more than half of what it was at 48 h and 72 h, whereas that at 24 h treatment was not significantly reduced. The statistic suggested that pre-harvest treatment by replacing nutrient solution with tap water for 48 h was enough to decrease nitrate content. It is proposed that tap water clean up the residual nitrate in the xylem vessels of the roots, stems, and leaves of hydroponic green oak lettuce within 48 h. On the other hand, the electrons from the photosynthetic process play a key role in reducing nitrate assimilation to glutamate acid in plant cells, which could be another reason for less nitrate accumulation after pre-preharvest for 48 h [26]. However, Qiu et al. [8] have reported that during nitrate assimilation to glutamate acid in lettuce plants, some nitrate residue is in the xylem vessels of the root, stem, petiole, and leaf veins. This experiment was designed by replacing the nutrient solution with tap water to clean up the xylem vessels of the roots, stems, and leaves of hydroponic green oak lettuce. Furthermore, these results are similar to those of Guffanti et al. [25], Wanlai et al. [13], and Cometti et al. [27].

3.2. Vitamin C content

Plant vitamin C has an important antioxidant function and is a major source in the human diet. The hydroponic lettuce grown under the pre-harvest treatment of replacing nutrient solution with tap water for 72 h (5.3 μg/100 g, 30% reduction) showed the lowest content of vitamin C, followed by treatments of 48 h (6.3 μg/100 g, 16% reduction), and 24 h (7.2 μg/g dry weight, 4% reduction) (Fig. 2). The vitamin C content was decreased by 4 to 30% when compared with 0 h (7.6 μg/100 g, control treatment). The amount of vitamin C gradually reduced as the treatment duration increased, implying that vitamin C is most likely used during pre-harvest periods to convert H_2O_2 to H_2O [28,29]. H_2O_2 can cause the ROS reaction, activating the plant cells' stress defense mechanism. Vitamin C can reduce and control the appropriate H_2O_2 content in plant cells [28,29]. Vitamin C biosynthesis begins with the photosynthesis system that produces D-glucose-6-P, and vitamin C is stimulated in the mitochondria, then released and accumulated in the cytosol. This experiment showed that vitamin C content decreased after pre-harvesting when the nutrient solution was replaced with tap water. The reason is probably, the vitamin C content is accumulated in the cytosol before the pre-harvest experiment. Following the investigation, lettuce may use vitamin C to reduce H_2O_2 to H_2O [28-29], where H_2O_2 is normally induced by pre-harvest stress [30].

3.3. Phenolic content

The accumulation of phenolic content in plants indicates plant response to abiotic and biotic stresses. The phenolic content was not significantly different among the different time intervals under pre-harvest of replacing nutrient solution with tap water and control treatment. The treatment of replacing the nutrient solution with tap water for 24 h (125 μg/100 g, 13% reduction) showed the lowest phenolic content. It was followed by both treatments of 48 h and 72 h (both 134 μg/100 g, 6% reduction) (Fig. 3). The phenolic content was decreased by 6 to 13% when compared with 0 h (143 μg/100 g, control treatment). Still, there were no statistically significant differences among treatments. This result was consistent with lettuce and rocket plants grown in a vertical farm in a controlled environment hydroponic system [25]. As a result, this result indicates that pre-harvest nutrient solution replacement with tap water within 72 h was not stressful and had no adverse effect on crop quality. Phenolic biosynthesis in plants is triggered by H_2O_2 [30]. However, H_2O_2 was probably reduced by vitamin C as vitamin C in this experiment was decreased for use in the reduction of H_2O_2.

3.4. Soluble sugar content

Soluble sugars are highly sensitive to environmental stresses and act as nutrient and metabolite signaling molecules that affect plant cellular modification levels [31]. In the present study, we measured the soluble sugar of hydroponic lettuce grown under the pre-harvest condition of replacing the nutrient solution with tap water. The soluble sugar content ranged from 1.6 to 3.3 mg/100 g among treatments (Fig. 4). It significantly increased by 86 to 105% compared to 0 h (1.6 mg/100 g, control treatment). The treatment of replacing nutrient solution with tap water for 48 h (3.3 mg/100 g, 105% increase) showed the highest content, followed by treatments of 72 h (3.2 mg/100 g, 98% increase) and 24 h (3.0 mg/100 g, 86% increase). However, soluble sugar content did not significantly differ between treatments lasting 48 h and 72 h. This study showed that soluble sugar content is significantly increased after replacing nutrient solution with tap water in the uncontrolled environment of a hydroponic farm. It could be possible that energy sources for photosynthesis, such as ATP and $NAPH_2$, are not necessary for nutrient uptake, transportation, and stimulation of the nitrate molecule to glutamine acid. Instead, this energy was accumulated and may be changed to produce soluble sugar [26, 31]. This result was in contrast with the vertical farming technique of a hydroponic system, in which total sugar content did not significantly differ after replacing the nutrient solution with tap water [25].

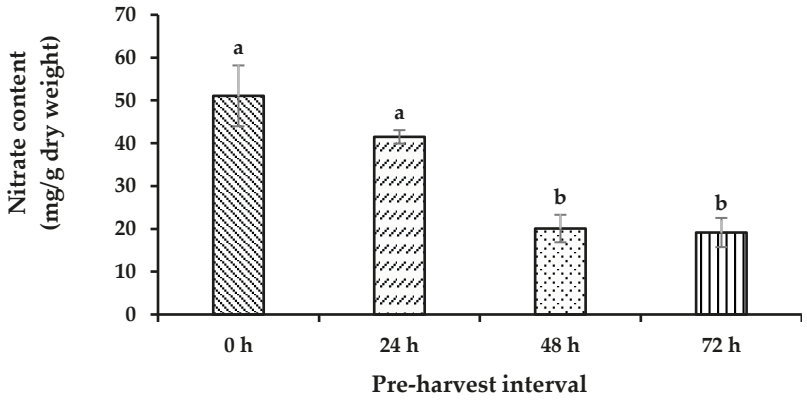

Figure 1. The effect of pre-harvest periods caused by replacing nutrient solution with tap water on nitrate content in hydroponic lettuce. The error bars display the standard error over three replications. The means indicated by the different letters are substantially different at $p < 0.05$, according to the least significant difference.

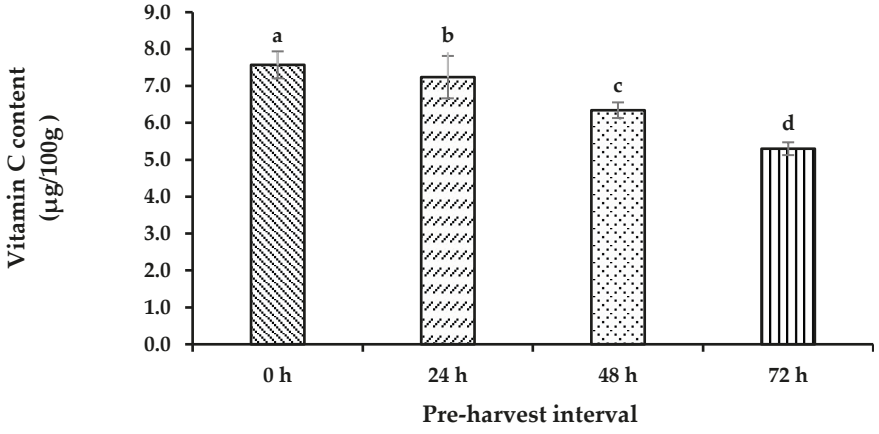

Figure 2. The effect of pre-harvest periods caused by replacing nutrient solution with tap water on vitamin C content in hydroponic lettuce. The error bars display the standard error over three replications. The means indicated by the different letters are substantially different at $p < 0.05$, according to the least significant difference.

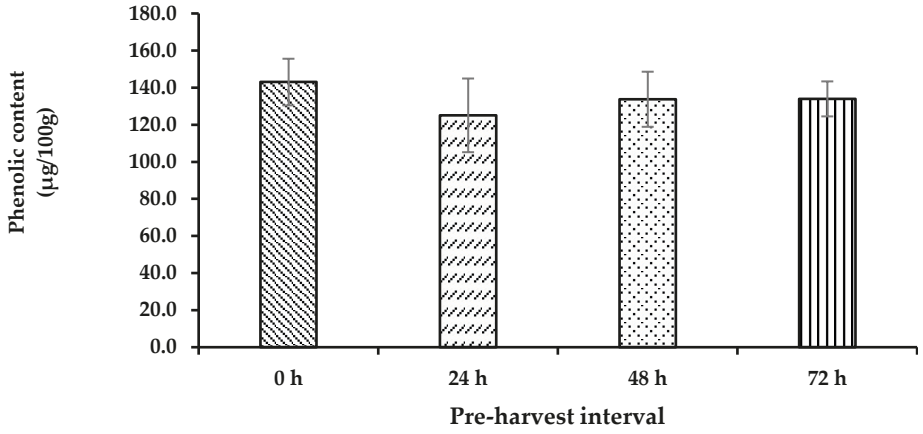

Figure 3. The effect of pre-harvest periods caused by replacing nutrient solution with tap water on phenolic content in hydroponic lettuce. The error bars display the standard error over three replications. The means indicated by the different letters are substantially different at $p < 0.05$, according to the least significant difference.

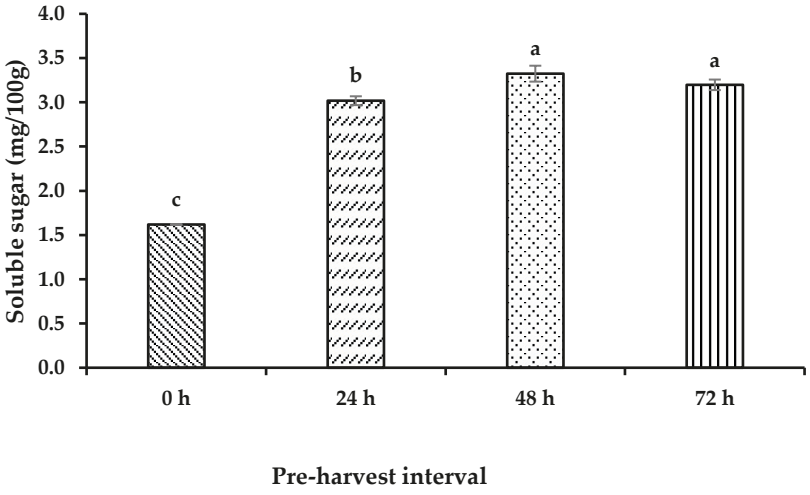

Figure 4. The effect of pre-harvest periods caused by replacing nutrient solution with tap water on soluble sugar content in hydroponic lettuce. The error bars display the standard error over three replications. The means indicated by the different letters are substantially different at $p < 0.05$, according to the least significant difference.

4. Conclusions

This study focused on the effect of pre-harvest periods by replacing nutrient solution with tap water on nitrate and quality in hydroponic lettuce. The results suggested that nitrate contents were reduced the lowest and soluble sugar contents were increased the highest after pre-harvest for 48 h. Vitamin C and phenolic contents were slightly decreased after pre-harvest periods by replacing the nutrient solution with tap water.

5. Acknowledgements

The authors thank the Urban Agriculture Technology Research Group team at the Department of Agricultural and Fisheries Science, Faculty of Science and Technology, Prince of Songkla University, Pattani Campus, for helping in this work.

Author Contributions: E.R., conceptualization, methodology, software, formal analysis, investigation, data curation, writing—original draft preparation; N. S., proofreading, format form; S. S., proofreading, visualization; N. M.P.S.H., writing—review and editing, visualization

Funding: This research was funded by the Faculty of Science and Technology, Prince of Songkla University (grant number SAT6104067S, reference No. 21915)

Conflicts of Interest: The authors declare no conflict of interest.

References

[1] Weller, D.L.; Saylor, L.; Turkon, P. Total coliform and generic E. coli levels, and salmonella presence in eight experimental aquaponics and hydroponics systems: A brief report highlighting exploratory data. *Horticulturae* 2020, *6*, 42, https://doi.org/10.3390/horticulturae6030042.

[2] Aćamović-Djoković, G.; Pavlović, R.; Mladenović, J.; Djurić, M. Vitamin C content of different types of lettuce varieties. *Acta Agric. Serbica* 2011, *17*, 83–89.

[3] Hmelak Gorenjak, A. Nitrate in vegetables and their impact on human health. A review. *Acta Aliment.* 2013, *42*(2), 158–172, https://doi.org/10.1556/AAlim.42.2013.2.4.

[4] The nitrate content in some green leafy vegetables with different cultivation methods in Thailand | Thai journal of public health available online: https://he02.tci-thaijo.org/index.php/jph/article/view/133167 (accessed on 21 February 2023).

[5] Bell, R.; Davies, R.; Howard, E. The changing structure of food retailing in europe: The implications for strategy. *Long Range Plann.* 1997, *30*, 853–861, https://doi.org/10.1016/S0024-6301(97)00071-X.

[6] Htwe, N.M.P.S.; Ruangrak, E. A review of sensing, uptake, and environmental factors influencing nitrate accumulation in crops. *J. Plant Nutr.* 2021, *44*, 1054–1065, https://doi.org/10.1080/01904167.2021.1871757.

[7] Stitt, M. Nitrate regulation of metabolism and growth. *Curr. Opin. Plant Biol.* 1999, *2*, 178–186, https://doi.org/10.1016/S1369-5266(99)80033-8.

[8] Qiu, W.; Wang, Z.; Huang, C.; Chen, B.; Yang, R. Nitrate accumulation in leafy vegetables and its relationship with water. *J. Soil Sci. Plant Nutr.* 2014, *14*, 761–768, https://doi.org/10.4067/S0718-95162014005000061.

[9] Gil, M.I. Preharvest factors and fresh-cut quality of leafy vegetables. *Acta Hortic.* 2016, 57–64, https://doi.org/10.17660/ActaHortic.2016.1141.6.

[10] Hooks, T.; Sun, L.; Kong, Y.; Masabni, J.; Niu, G. Short-term pre-harvest supplemental lighting with different light emitting diodes improves greenhouse lettuce quality. *Horticulturae* 2022, *8*, 435, https://doi.org/10.3390/horticulturae8050435.

[11] Tyagi, D. Impact of pre-harvest environmental gactors on the survival of enterohemorrhagic *E. coli* and salmonella on lettuce. Degree of Master of Science, North Dakota State University of Agriculture and Applied Science, Fargo, Noth Dakota, America, November 2014.

[12] Zukauskas, A.; Bliznikas, Z.; Breivė, K.; Novičkovas, A.; Samuolienė, G.; Urbonavičiūtė, A.; Brazaitytė, A.; Jankauskienė, J.; Duchovskis, P. Effect of supplementary pre-harvest LED lighting on the antioxidant properties of lettuce cultivars. *Acta Hortic.* 2011, 87–90, https://doi.org/10.17660/ActaHortic.2011.907.8.

[13] Zhou, W.; Wenke, L.; Qichang, Y. Reducing nitrate content in lettuce by pre-harvest continuous light delivered by red and blue light-emitting diodes. *J. Plant Nutr.* 2013, *36*, https://doi.org/10.1080/01904167.2012.748069.

[14] Lastra, O.C. Derivative spectrophotometric determination of nitrate in plant issue. *J. AOAC Int.* 2003, *86*, 1101–1105, https://doi.org/10.1093/jaoac/86.6.1101.

[15] Min, Q.; Marcelis, L.F.M.; Nicole, C.C.S.; Woltering, E.J. High light intensity applied shortly before harvest improves lettuce nutritional quality and extends the shelf life. *Front. Plant Sci.* 2021, *12*, 615355, https://doi.org/10.3389/fpls.2021.615355.
[16] Vàsquez, H.; Ouhibi, C.; Lizzi, Y.; Azzouz, N.; Forges, M.; Bardin, M.; Nicot, P.; Urban, L.; Aarrouf, J. Pre-harvest hormetic doses of UV-C radiation can decrease susceptibility of lettuce leaves (Lactuca Sativa L.) to botrytis cinerea L. *Sci. Hortic.* 2017, *222*, 32–39, https://doi.org/10.1016/j.scienta.2017.04.017.
[17] Woltering, E.J.; Witkowska, I.M. Effects of pre- and postharvest ighting on quality and shelf life of fresh-out lettuce. *Acta Hortic.* 2016, 357–366, https://doi.org/10.17660/ActaHortic.2016.1134.47.
[18] Sirinupong, M. *Practical for Soilless Culture in Thailand*; 4th ed.; Flam-up Design Press, Bangkok, Thailand, 2017, 43-62.
[19] Lastra, O.C. Derivative spectrophotometric determination of nitrate in plant tissue. *J. AOAC Int.* 2003, *86*, 1101–1105.
[20] Yemm, E.W.; Willis, A.J. The estimation of carbohydrates in plant extracts by anthrone. *Biochem. J.* 1954, *57*, 508–514, https://doi.org/10.1042/bj0570508.
[21] Jagota, S.K.; Dani, H.M. A new colorimetric technique for the estimation of vitamin C using folin phenol reagent. *Anal. Biochem.* 1982, *127*, 178–182, https://doi.org/10.1016/0003-2697(82)90162-2.
[22] Singleton, V.L.; Orthofer, R.; Lamuela-Raventós, R.M. Analysis of total phenols and other oxidation substrates and antioxidants by means of folin-ciocalteu reagent. *Methods Enzymol.* 1999, https://doi.org /10.1016/s0076-6879(99)99017-1.
[23] Dicko, M.H.; Hilhorst, R.; Gruppen, H.; Traore, A.S.; Laane, C.; van Berkel, W.J.H.; Voragen, A.G.J. Comparison of content in phenolic compounds, polyphenol oxidase, and peroxidase in grains of fifty sorghum varieties from burkina faso. *J. Agric. Food Chem.* 2002, *50*, 3780–3788, https://doi.org/10.1021 /jf011642o.
[24] Eldeen, I.M.S.; Seow, E.-M.; Abdullah, R.; Sulaiman, S.F. In vitro antibacterial, antioxidant, total phenolic contents and anti-HIV-1 reverse transcriptase activities of extracts of seven phyllanthus sp. *South Afr. J. Bot.* 2011, *77*, 75–79, https://doi.org/10.1016/j.sajb.2010.05.009.
[25] Guffanti, D.; Cocetta, G.; Franchetti, B.M.; Ferrante, A. The effect of flushing on the nitrate content and postharvest quality of lettuce (Lactuca Sativa L. Var. Acephala) and rocket (Eruca Sativa Mill.) grown in a vertical farm. *Horticulturae* 2022, *8*, 604, https://doi.org/10.3390/horticulturae8070604.
[26] Sanz-Luque, E.; Chamizo-Ampudia, A.; Llamas, A.; Galvan, A.; Fernandez, E. Understanding nitrate assimilation and its regulation in microalgae. *Front. Plant Sci.* 2015, *6*, 899, https://doi.org/10.3389/fpls. 2015.00899.
[27] Cometti, N.N.; Martins, M.Q.; Bremenkamp, C.A.; Nunes, J.A. Nitrate concentration in lettuce leaves depending on photosynthetic photon flux and nitrate concentration in the nutrient solution. *Hortic. Bras.* 2011, *29*, 548–553, https://doi.org/10.1590/S0102-05362011000400018.
[28] Rosado-Souza, L.; Fernie, A.R.; Aarabi, F. Ascorbate and thiamin: metabolic modulators in plant acclimation responses. *Plants* 2020, *9*, 101, https://doi.org/10.3390/plants9010101.
[29] Paciolla, C.; Fortunato, S.; Dipierro, N.; Paradiso, A.; De Leonardis, S.; Mastropasqua, L.; de Pinto, M.C. Vitamin C in plants: from functions to biofortification. *Antioxidants* 2019, *8*, 519, https://doi.org/10.3390 /antiox8110519.
[30] Wang, W.; Zhang, C.; Shang, M.; Lv, H.; Liang, B.; Li, J.; Zhou, W. Hydrogen peroxide regulates the biosynthesis of phenolic compounds and antioxidant quality enhancement in lettuce under low nitrogen condition. *Food Chem. X* 2022, *16*, 100481, https://doi.org/10.1016/j.fochx.2022.100481.
[31] Rosa, M.; Prado, C.; Podazza, G.; Interdonato, R.; González, J.A.; Hilal, M.; Prado, F.E. Soluble sugars-metabolism, sensing and abiotic stress. *Plant Signal. Behav.* 2009, *4*, 388–393.

JSTR
ASEAN Journal of Scientific and Technological Reports

Article type

Type of the Paper (Article, Review, Communication, etc.) *about 8,000 words maximum*

Title (Palatino Linotype 18 pt, bold)

Firstname Lastname[1], Firstname Lastname[2] and Firstname Lastname[2*]

[1] Affiliation 1; e-mail@e-mail.com
[2] Affiliation 2; e-mail@e-mail.com
* Correspondence: e-mail@e-mail.com; (one corresponding authors, add author initials)

Citation:
Lastname, F.; Lastname, F.; Lastname, F. Title. *ASEAN J. Sci. Tech. Report.* **2023**, *26*(X), xx-xx. https://doi.org/10.55164./ajstr.vxxix.xxxxxx

Article history:
Received: date
Revised: date
Accepted: date
Available online: date

Abstract: A single paragraph of about 400 words maximum. Self-contained and concisely describe the reason for the work, methodology, results, and conclusions. Uncommon abbreviations should be spelled out at first use. We strongly encourage authors to use the following style of structured abstracts, but without headings: (1) Background: Place the question addressed in a broad context and highlight the purpose of the study; (2) Methods: briefly describe the main methods or treatments applied; (3) Results: summarize the article's main findings; (4) Conclusions: indicate the main conclusions or interpretations.

Keywords: keyword 1; keyword 2; keyword 3 (List three to ten pertinent keywords specific to the article yet reasonably common within the subject discipline.)

1. Introduction

The introduction should briefly place the study in a broad context and highlight why it is crucial. It should define the purpose of the work and its significance. The current state of the research field should be carefully reviewed and critical publications cited. Please highlight controversial and diverging hypotheses when necessary. Finally, briefly mention the main aim of the work. References should be numbered in order of appearance and indicated by a numeral or numerals in square brackets—e.g., [1] or [2,3], or [4–6]. See the end of the document for further details on references.

2. Materials and Methods

The materials and methods should be described with sufficient details to allow others to replicate and build on the published results. Please note that your manuscript's publication implicates that you must make all materials, data, computer code, and protocols associated with the publication available to readers. Please disclose at the submission stage any restrictions on the availability of materials or information. New methods and protocols should be described in detail, while well-established methods can be briefly described and appropriately cited.

Interventional studies involving animals or humans, and other studies that require ethical approval, must list the authority that provided approval and the corresponding ethical approval code.

2.1 Subsection

2.1.1. Subsubsection

3. Results and Discussion

This section may be divided by subheadings. It should provide a concise and precise description of the experimental results, their interpretation, as well as the experimental conclusions that can be drawn.Authors should discuss the results and how they can be interpreted from previous studies and the working hypotheses. The findings and their implications should be discussed in the broadest context possible. Future research directions may also be highlighted.

3.1. Subsection

3.1.1. Subsubsection

3.2. Figures, Tables, and Schemes

All figures and tables should be cited in the main text as Figure 1, Table 1, etc.

Figure 1. This is a figure. Schemes follow the same formatting.

Table 1. This is a table. Tables should be placed in the main text near the first time they are cited.

Title 1	Title 2	Title 3
entry 1	data	data
entry 2	data	data [1]

[1] Table may have a footer.

3.3. Formatting of Mathematical Components

This is example 1 of an equation:

$$a = 1, \tag{1}$$

The text following an equation need not be a new paragraph. Please punctuate equations as regular text. This is example 2 of an equation:

$$a = b + c + d + e + f + g + h + i + j + k + l + m + n + o + p + q + r + s + t + u \tag{2}$$

The text following an equation need not be a new paragraph. Please punctuate equations as regular text. The text continues here.

4. Conclusions

Concisely restate the hypothesis and most important findings. Summarize the significant findings, contributions to existing knowledge, and limitations. What are the future directions? Conclusions MUST be well stated, linked to original research question & limited to supporting results.

5. Acknowledgements

Should not be used to acknowledge funders – funding will be entered as a separate. As a matter of courtesy, we suggest you inform anyone whom you acknowledge.

Author Contributions: For research articles with several authors, a short paragraph specifying their individual contributions must be provided. The following statements should be used "Conceptualization, X.X. and Y.Y.; methodology, X.X.; software, X.X.; validation, X.X., Y.Y. and Z.Z.; formal analysis, X.X.; investigation, X.X.; resources, X.X.; data curation, X.X.; writing—original draft preparation, X.X.; writing—review and editing, X.X.; visualization, X.X.; supervision, X.X.; project administration, X.X.; funding acquisition, Y.Y. All authors have read and agreed to the published version of the manuscript." Please turn to the CRediT taxonomy for the term explanation. Authorship must be limited to those who have contributed substantially to the work reported.

Funding: Please add: "This research received no external funding" or "This research was funded by NAME OF FUNDER, grant number XXX" and "The APC was funded by XXX". Check carefully that the details given are accurate and use the standard spelling of funding agency names at https://search.crossref.org/funding. Any errors may affect your future funding.

Conflicts of Interest: Declare conflicts of interest or state "The authors declare no conflict of interest." Authors must identify and declare any personal circumstances or interest that may be perceived as inappropriately influencing the representation or interpretation of reported research results. Any role of the funders in the design of the study; in the collection, analyses or interpretation of data; in the writing of the manuscript, or in the decision to publish the results must be declared in this section. If there is no role, please state "The funders had no role in the design of the study; in the collection, analyses, or interpretation of data; in the writing of the manuscript, or in the decision to publish the results".

References

References must be numbered in order of appearance in the text (including citations in tables and legends) and listed individually at the end of the manuscript. We recommend preparing the references with a bibliography software package, such as EndNote, ReferenceManager to avoid typing mistakes and duplicated references. Include the digital object identifier (DOI) for all references where available.

Citations and references in the Supplementary Materials are permitted provided that they also appear in the reference list here.

In the text, reference numbers should be placed in square brackets [ ] and placed before the punctuation; for example [1], [1–3] or [1,3]. For embedded citations in the text with pagination, use both parentheses and brackets to indicate the reference number and page numbers; for example [5] (p. 100), or [6] (pp. 101–105).

[1] Author 1, A.B.; Author 2, C.D. Title of the article. *Abbreviated Journal Name* Year, *Volume*, page range.

[2] Author 1, A.; Author 2, B. Title of the chapter. In *Book Title*, 2nd ed.; Editor 1, A., Editor 2, B., Eds.; Publisher: Publisher Location, Country, 2007; Volume 3, pp. 154–196.

[3] Author 1, A.; Author 2, B. *Book Title*, 3rd ed.; Publisher: Publisher Location, Country, 2008; pp. 154–196.

[4] Author 1, A.B.; Author 2, C. Title of Unpublished Work. *Abbreviated Journal Name* stage of publication (under review; accepted; in press).
[5] Author 1, A.B. (University, City, State, Country); Author 2, C. (Institute, City, State, Country). Personal communication, 2012.
[6] Author 1, A.B.; Author 2, C.D.; Author 3, E.F. Title of Presentation. In Title of the Collected Work (if available), Proceedings of the Name of the Conference, Location of Conference, Country, Date of Conference; Editor 1, Editor 2, Eds. (if available); Publisher: City, Country, Year (if available); Abstract Number (optional), Pagination (optional).
[7] Author 1, A.B. Title of Thesis. Level of Thesis, Degree-Granting University, Location of University, Date of Completion.
[8] Title of Site. Available online: URL (accessed on Day Month Year).

Reviewers sugestion

1. Name, Address, e-mail
2. Name, Address, e-mail
3. Name, Address, e-mail
4. Name, Address, e-mail

URL link:

Notes for Authors >>
https://drive.google.com/file/d/1r0zegnIVeQqe4iLQyT1xDEIinNggINPD/view?usp=sharing
https://drive.google.com/file/d/1r0zegnIVeQqe4iLQyT1xDEIinNggINPD/view?usp=sharing

Online Submissions >> https://ph02.tci-thaijo.org/index.php/tsujournal/user/register

Current Issue >> https://ph02.tci-thaijo.org/index.php/tsujournal/issue/view/16516

AJSTR Publication Ethics and Malpractice >> https://ph02.tci-thaijo.org/index.php/tsujournal/ethics

Journal Title Abbreviations >> http://library.caltech.edu/reference/abbreviations


JSTR
ASEAN Journal of Scientific
and Technological Reports

ASEAN Journal of Scientific and Technological Reports

สถาบันวิจัยและพัฒนา มหาวิทยาลัยทักษิณ
222 หมู่ 2 ต.บ้านพร้าว อ.ป่าพะยอม จ.พัทลุง 93210
โทรศัพท์ 074-609-600 ต่อ 7242 โทรศัพท์ 074-609-655
E-mail Address: tsujournal@tsu.ac.th, aseanjstr@tsu.ac.th